Investigation on radio channel over the air emulation by multi-probe setup

Mounia Belhabib

ANNÉE 2017

UNIVERSITÉ DE RENNES 1

UNIVERSITE BRETAGNE LOIRE

THÈSE / UNIVERSITÉ DE RENNES 1
sous le sceau de l'Université Bretagne Loire

pour le grade de

DOCTEUR DE L'UNIVERSITÉ DE RENNES 1

Mention : Traitement du Signal et Télécommunications

Ecole doctorale MATISSE

présentée par

Mounia Belhabib

Préparée à l'unité de recherche 6164 IETR et CEA-Leti
Institut d'Electronique et de Télécommunications de Rennes

Investigation on Radio Channel Over-the-Air Emulation by Multi-probe Setup

Thèse soutenue à Grenoble
le 09/11/2017

devant le jury composé de :

Ghaïs El Zein
Professeur à l'université de Rennes 1 *Examinateur*

Yannis Pousset
Professeur à l'université de Poitiers *Rapporteur*

Marion Berbineau
Directrice de Recherche à l'IFFSTAR *Rapportrice*

Philippe Boutier
Ingénieur de recherche, Renault SAS *Examinateur*

Raffaelle D'Errico
Ingénieur de recherche HDR au CEA *Examinateur*

Bernard Uguen
Professeur à l'université de Rennes 1 *Examinateur*

Remerciements

Les travaux présentés dans ce manuscrit ont été effectués au centre de recherche CEA, au sein de l'équipe LAPCI « Laboratoire d'Antennes et Propagation & Couplage Inductifs, dirigé par Monsieur *Raffaele d'Erricco.* Ma profonde gratitude lui est adressée. J'ai beaucoup appris pendant son encadrement, la rigueur et l'esprit d'analyse. Mes remerciements vont à Monsieur *Bernard Uguen*, Professeur à l'Université de Rennes 1 de diriger cette thèse et de ses précieux conseils. . Beaucoup de votre temps m'a été consacré. Vos conseils et vos idées m'ont permis d'arriver à ce stade, MERCI.

.

Ma profonde gratitude à Monsieur *Ghaïs El Zein*, Professeur à l'Université de Rennes 1 pour avoir accepté de présider le jury de thèse, mes remerciements à Mr *Yannis Pousset,* Professeur à l'Université de Poitiers et à Madame *Marion Berbineau*, Directrice de Recherche à l'IFFSTAR pour avoir accepté d'être rapporteurs. Mes sincères remerciements vont à Mr *Philippe Boutier*, Ingénieur à la société RENAULT, pour avoir accepté et pour m'avoir fait l'honneur d'être membre de jury.

Mes chaleureux remerciements à mes collègues qui m'ont soutenu dans la réalisation expérimentale, tous sans exception. Un grand merci à *Sattar, Camille , Nabil, Lotfi……...*

Merci à mes parents, à mes frères qui m'ont soutenu pendant ces années et merci à tous ceux qui ont contribué de loin ou de près à la réussite de ce travail.

Merci

Résumé

La nécessité d'une transmission sans fils des données à des débits élevés, à la fois fiables et avec de faible latence a donné lieu à ces dernières années à une succession de normes sans fil, allant de 3G-4G, WLAN à la cinquième génération (5G) des réseaux mobiles. Dans ce contexte, les équipementiers, ainsi que les opérateurs, doivent élaborer des méthodes d'essai standard précises et efficaces pour évaluer les performances des systèmes et des terminaux. Les méthodologies de test en direct par voie aérienne ("Over-The-Air") (OTA) visent à reproduire des environnements multi-trajets radio en laboratoire de manière répétable et contrôlable, en évitant les coûteuses mesures in-situ.

L'objectif de cette thèse est de proposer une nouvelle méthodologie d'essai OTA, afin de reproduire la propagation des canaux radio, sur une large bande et d'évaluer les performances des systèmes sans fil dans des environnements réels.

La thèse débute en présentant les bases de la chaîne radio et de certains modèles de chaînes présentés dans la littérature. Ensuite, un examen critique des méthodologies OTA existantes dans la littérature est fourni. Parmi les différentes méthodologies, nous avons opté pour l'approche de la chambre anéchoïde multi-sonde, qui consiste à déployer un certain nombre de sondes autour d'un équipement radio sous test et à les alimenter avec un émulateur d’évanouissements (fading). Cette méthodologie fournit une reproduction précise des caractéristiques des canaux spatiaux, qui sont nécessaires pour évaluer la performance des terminaux multi-antennes dans des environnements réels. L'avantage le plus important de cette méthodologie est la capacité d'imiter différents modèles de canaux en termes de résolution spatiale, d’évanouissements angulaire et temporel.

Un outil de simulation a été développé pour étudier et déterminer les caractéristiques de l'installation OTA pour différents types de canaux d’intérêt. En particulier, le nombre et la mise en place des antennes nécessaires et la taille de l'installation ont été étudiés en fonction de la taille électrique du dispositif testé. Sur la base des études de dimensionnement, une configuration OTA expérimentale a été réalisée pour reproduire les caractéristiques des canaux dans l'espace tridimensionnel pour une plage de fréquences de 2 à 6 GHz.

Abstract

The need for high data-rate, reliable and low latency transmission in wireless communication systems motivated a multitude of wireless standards, spanning from 3G-4G, WLAN to the upcoming fifth generation (5G) of mobile networks. In this context, technology providers, as well as operators, need to develop accurate and cost effective standard test methods, to evaluate devices performance. Over-The-Air (OTA) test methodologies aim to reproduce radio multipath environments in laboratory in repeatable and controllable manner, avoiding costly field test.

The focus of this thesis is to propose a new OTA test methodology, in order to emulate radio channel propagation, over a wide band, and to evaluate the performance of the wireless systems in real environments.

We start our study by introducing the basics of radio channel and some channel models presented in literature. Then a critical review of existing OTA methodologies in literature is provided. Among the different methodologies we opted for the multi-probe anechoic chamber approach, which consists into deploying a number of probes around a device, and feed them with fading emulator. This methodology provides an accurate reproduction of spatial channel characteristics, which are needed to assess the performance of multi-antenna terminals in real environments. The most important advantage of this methodology is the capability to emulate different channel model in term of spatial resolution, angular and temporal fading.

A simulation tool was developed to investigate and determine the OTA setup under different channel condition. In particular the number and emplacement of antennas needed and the size of the setup were investigated as a function of the electrical size of the device under test. Based on the dimensioning studies, an experimental OTA setup was realized to reproduce the channel characteristics in the three dimensional space for a frequency range from 2 to 6 GHz.

Contents

List of Acronyms

3GPP	Third Generation Partnership Project
5G	Five Generation
ACF	Autocorrelation Function
AOA	Angles of Arrivals
AS	Azimuth Spread
BB	Baseband
BC	Broadcast Channel
C2C	Car to-Car
BER	Bit Error Rate
CIR	Channel Impulse Response
CE	Channel Emulator
COST	Cooperation in Science and Technology
CTIA	Cellular Telecommunication Industrial Association
DOA	Angles of Departures
DUT	Device Under Test
EIRP	Effective Isotropic Radiated Power
EIS	Effective Isotropic Sensitivity
EOA	Elevation of Arrivals
ES	Elevation Spread
FFT	Fast Fourier Transform
FF	Far-Field
FOM	Figures of Merit
GSCM	Geometry-based Stochastic Channel Model
IEEE	Institute of Electrical and Electronics Engineers
I/O	Input/output
LOS	Line-Of-Sight
LTE	Long Term Evolution [Standard]
MERP	Mean Effective Radiated Power
MERS	Mean Effective Radiated Sensitivity
MIMAX	Advanced MIMO systems for Maximum reliability and performance
MIMO	Multiple-Input Multiple- Output
MISO	Multiple-Input Single-Output
MPC	Multipath Component
MS	Mobile Station
NLOS	Non Line-Of-Sight
OTA	Over The Air
PA	Power Amplifier
PAS	Power Angular Spectrum
PC	Personal Computer
Pdf	Probability Density Function
PDP	Power Delay Profile
PFS	Pre-faded Signal Synthesis

PWS	Plane Wave Synthesis
RAN WG4	Radio Access Network Work Group 4
RC	Reverberation Chamber
RF	Radio frequency
RMS	Root Mean Square
RX	Receiver
SCM	Spatial Channel Model
SCME	Spatial Channel Model Extension
SIMO	Single-Input Multiple-Output
SISO	Single-Input Single-Output
SINR	Signal to Interference plus Noise Ratio
SISO	Single-Input Single-Output
SNR	Signal to Noise Ratio
TX	Transmitter
UWB	Ultra-Wide Band
V2V	Vehicle to vehicle
VNA	Vector Network Analyzer
WCDMA	Wideband Code Division Multiple Access
WIMAX	Worldwide Interoperability for Microwave Access
WINNER	Wireless World Initiative New Radio
WSN	Wireless Sensor Networks
WSS	Wide-Sense Stationary [process]
WSSUS	Wide-Sense Stationary Uncorrelated Scattering
XPD	Cross-Polarization Discrimination
XPR	Cross Polarization Ratio

List of Figures

List of Tables

Chapter 1

1 Introduction

1.1 Motivation

In the last decades, wireless telecommunications did not cease to evolve. On the one hand a wide variety of advanced technologies have greatly facilitated our daily lives, on the other hands the user needs stimulated an explosive growth of these technologies.
In the years 2000 the third generation (3G) of mobile phone network, which is based mainly based on Universal Mobile Telecommunications System (UMTS) and CDMA2000 technology, has been deployed to provide up to 42 Mbit/s data rate. However, the demands of users on the quality and efficiency of networks make challenges to invent new systems.
As a result, the fourth generation (4G) mobile radio system is developed. The prime objective of 4G mobile system is to achieve a fully integrated digital communication that offers voice, data, and multimedia, and to provide enhanced peak data rate of 100 Mbit/s. The Long Term Evolution (LTE) standard was first proposed by 3GPPP to fulfill the 4G requirements. Finally, only in 2010, the International Telecommunication Union (ITU) recognized the LTE Advanced (LTE-A) as 4G technology. The 3GPP rel.11 foresees bandwidth from 1.4 MHz to 20 MHz, and 64 QAM modulation providing up to 450 Mbit/s downlink data rate. One of the key-technologies employed is Multiple Input Multiple Output (MIMO) approaches, exploiting multi-antenna system.

Nowadays the focus of the research and development is on the fifth generation (5G) of wireless communication, which is expected to answer to a wide number of use cases requirement, spanning from the Internet of Things (IoT) to high-data rate and low-latency communication. It promises significant gains in wireless network capacity and data rates up to 20 Gbits/s. Different technologies are aimed for the development of 5G, including massive MIMO and millimeter wave. However the first technologies deployed are expected to work for frequency below 6 GHz. Also vehicle-to-everything (V2X) communications are expected to gain an important role in the next years. Here the data volume is relatively low, and the foreseen standard is an evolution of Wireless Local Area Network (WLAN) based on IEE 802.11(p) working at frequencies around 5.9 GHz.

In each one of the above mentioned wireless technologies, the performance are intrinsically limited by the radio channel characteristics. The propagation environment often presents multipath fading that could alter the communication quality. To counteract fading effect, one of the techniques used is the diversity of antennas. This technique consists to place several antennas at both ends of the radio link.

For the operators and manufacturers of mobile industry there is a need to evaluate, by standardized measurements, the performance of such advanced systems. This evaluation must be carried out in realistic way in different representative environment such as indoor or outdoor. However, the field tests in the application environments are tedious and costly. For this reason, the so called Over-The-Air (OTA) channel emulation technique appears as a reasonable solution, for reproduce repeatability and reliability realistic fading conditions.

OTA test methodologies aim to recreate in a laboratory the multipath environment, to characterize and evaluated wireless devices. It can include the actual interaction of the antennas, radio frequency front ends and baseband processing elements. OTA is the best way to evaluate the performance as experienced by the user equipment. OTA testing terminal has attracted great attention by the research community in the last years [3]. However a great number of questions are still open to reproduce accurately the radio channel.

1.2 Outline of the thesis and contributions

The ultimate goal of this work is to investigate an OTA test methodology to reproduce realistic multi-path propagation channels. This methodology is based on multi-probe approach where a number of antennas are placed around the device under test (DUT) in an anechoic chamber. This work is mainly focused on frequency below 6 GHz, being the main wireless communication standard in this frequency range.

The objective is to provide an experimental setup, which is able to be adapted to the different needs in terms of application, hence propagation channel. For this reason the OTA setup must be wideband, and ensuring the reproduction of multipath channel in a three dimensions (3D) environment, in both vertical and horizontal polarization. A synopsis of the manuscript is graphically represented in Figure 1-1.

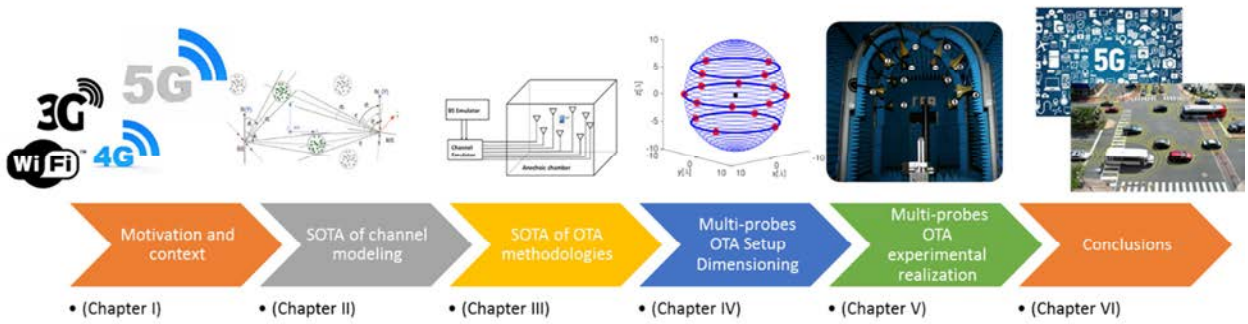

Figure 1-1 Synopsis of the thesis manuscript

Chapter 2 presents the state of the art of basic concepts of channel propagation by recalling the phenomena generated by the interactions of the electromagnetic signal with the environment. Different channel modeling approaches are presented. In particular mathematical representation and classical stochastic description of the channel are provided. An overview of some standardized channel models of interest is also presented.

Chapter 3 introduces OTA systems and their potential for the evaluation of the communication systems. A review of different OTA methodologies proposed in the literature, and various measurement systems to assess the performance of systems are discussed. The analysis is focused on multi-probes methodology that has been retained to achieve the project objective. In this kind of setup, two methods of OTA channel emulation are presented: the so called "Prefaded Signals Synthesis" (PFS) and "Planar Wave Synthesis" (PWS) techniques.

Chapter 4 is dedicated to the dimensioning of OTA setup. The analysis is based on an OTA simulator in Matlab. This physical dimensioning is based on criteria of far field and correlation characteristics of the emulated channel. We start by simulating a two dimensional (2D) OTA system to determine the number of antennas, and the radius of the OTA system as a function of the device size under measurement, its orientation, frequency band and the channel propagation model. Simulation results are presented in the case of a uniform channel model and a single cluster. Based on the PFS technique, a weighting OTA antennas method is adopted. The objective of this method consists of calculating the excitation of the transmitting antennas, which minimizes the error between the desired correlation and the emulated correlation. Dimensional study is extended to 3D OTA system in order to take into account of both azimuth and elevation angular distribution in the channel

Chapter 5 introduces the experimental OTA setup realized in the anechoic chamber at CEA LETI. The setup intends to reproduce 3D channel over a wideband from 2 to 6 GHz. A series of measurements has been carried out in order to validate its performance under different configurations and scenarios.

Finally, **Chapter 6** throws the conclusions of this work and proposed some perspectives for future research work.

Chapter 2

2 State of the Art of Channel Modeling for Wireless Devices Testing

2.1 Introduction

During the channel propagation between a transmitter and a receiver. A several distinct multi-path component are present. This fact is due to reflections and diffractions surrounding environment. The received signal is composed from the multiples paths with specific directions and delays. This last phenomenon is more commonly called fading; it can significantly affect the performance of mobile systems communications.

This chapter reviews wireless channel characterization. Firstly, it describes the general description of propagation principles, and then a multipath environment is described, where channel parameters as delay spread and coherence time are introduced. Secondly, the multipath channel is modeled as a multi-dependent random Wide/Sense Stationary (WSS) process. The MIMO channel and its intrinsic characteristics are reviewed. Different channels models are presented. The GSCMs channel models are discussed and different standards channels models are presented to determine the distribution of PAS in this channel.

This chapter is organized as follows: Section 2.2 describes the general principles of propagation principles, and then in section 2.3 a multipath environment is described and presents multipath channel modeling, highlighting the most important phenomena to be considered throughout in wireless communication. A mathematical representation of channel propagation and the MIMO systems, focusing on their spatial proprieties, is given in section 2.5. Section 2.6 studies different classification of channel models. The geometrical stochastic channel models are presented in section 2.7. Finally, in Section 2.8, the main conclusions are summarized.

2.2 Radio channel basic

2.2.1 Definition of radio channel propagation

The concept of radio channel refers to the transfer function between a transmitter and receiver. It is composed of two termination antennas and a propagation environment where takes place various electromagnetic phenomena such as reflection, refraction, diffraction, diffusion. It is a common practice in the field to make a clear distinction between the propagation channel (which relates a vector electric field at the transmitter side to another electric field at the receiver side) and the transmission channel which is scalar and relates a transmit signal to a received signal see Figure 2-1.

Figure 2-1 Illustration of the channel.

2.2.2 Free-Space Propagation and Antenna Gain

When an electromagnetic wave propagates through free space, i.e. the environment around the transmitter and the receiver is uncluttered; the wave is attenuated as the distance increases. The free space path loss between the transmitter and the receiver is given by the Friis formula as follows. Consider a transmitter radiating a power P_{tx} with an antenna gain of G_{tx}. Hence at a distance of d from the transmitter, the received power is given by the expression

$$P_{rx}\ (d) = P_{tx}G_{tx}G_{rx}\left(\frac{\lambda}{4\pi d}\right)^2 \quad (2.1)$$

Where λ refers to the wavelength.

From the expression for the received power, the free space path loss can be computed as the ratio of the received power to that of the transmitted power and is usually expressed in decibels. If we take apart the effect of both transmitting and receiving antenna gains, the free space path loss is expressed as:

$$PL = \left(\frac{\lambda}{4\pi d}\right)^2 \quad (2.2)$$

2.3 Multipath propagation channel

In a real environment, the transmission of a signal is usually composed of a direct path and many other propagation paths. These paths vary in number and depend on the interaction between the electromagnetic wave and obstacles surrounding environments. The signal obtained at the level of the receiver antenna corresponds to a recombination of these waves, which arrive at the receiver with different delays. Inside the buildings, the path of direct visibility Line of Sight, (LOS), is not always available. In this case, the paths which are not in visibility or Non Line of Sight (NLOS) allow the communication. Figure 2-2 illustrates the concept of multi-path propagation, as well as the main encountered propagations phenomena.

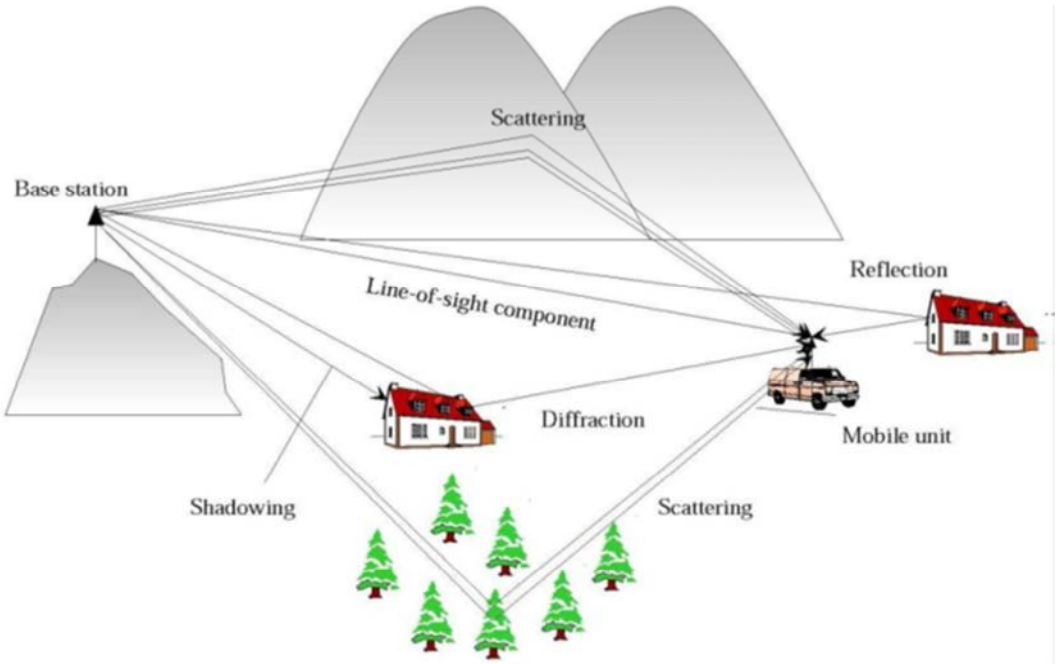

Figure 2-2 Principle of multipath propagation. Source [2]

The electromagnetic wave when propagating in a cluttered space experiences various well known physical effects which modifies on a well-established manner the amplitude and phase of the propagating signal. There are mostly the reflection and the refraction effect when considering the interaction with surfaces, respectively going backward or forward the interface. In NLOS an important effect especially in urban environment for UHF and VHF is the diffraction which corresponds to the ability of a wave to go into shadow regions where the geometrical optics field is zero. And there is also the important effect of diffusion which corresponds to the effect on the field of rough surfaces which spread the radiated energy in large regions of the angular domain.

2.4 Variation of channel propagation, large and small scale fading

There are two types of fading, large-scale fading and small-scale fading.

Large-scale fading corresponds to a loss or large fluctuation of the received signal due to shadowing by obstacles present in the propagation environment. If a receiver is moving at a constant distance from the transmitter, and suddenly goes behind a building, the received power drops. This kind of channel variation is called shadowing. In practice, shadowing is determined by considering the statistical property of the channel power around the path loss curve. This type of channel variations can be determined and characterized with extensive measurement campaigns. Several models exist to describe the shadowing variations[6].

Small-scale fading corresponds to a random recombination of multipath and is characterized by a rapid fluctuation on a shorter temporal scale. The variation of the received signal level depends on the relationships of the relative phases among the number of signals reflected from the local scatterers. Each of the multiple signal paths may also undergo changes that depend on the speeds of the mobile station and surrounding objects. In summary, small-scale fading is attributed to multi-path propagation, mobile speed, speed of surrounding objects, and transmission bandwidth of signal [7].

2.5 Representation of radio channel propagation

2.5.1 Mathematic formulation

The complex baseband impulse response h(t) radio channel is usually described [3][4] by its links the input baseband signal at the transmitter with the output baseband signal at the receiver.

$$y(t) = h(t) * x(t) + n(t) \qquad (2.6)$$

Where x(t) and y(t) are the transmitted and the received complex signal, respectively, and n(t) represents the additive noise at the receiver. The operator * is the convolution operator. In the frequency domain this expression becomes:

$$Y(f) = H(f)X(f) + N(f) \qquad (2.7)$$

Where Y(f), H(f), X(f) and N(f) are the Fourier transforms of y, h, x and n respectively. The channel transfer function does not consist of a single propagation path. When an antenna is excited, it transmits electromagnetic waves in multiple directions. Each of these waves interacts differently with the environment, and reaches the receiver with a certain delay (which may be different between different waves).

The impulse response is thus composed of the sum of multiple propagation paths. Note that the properties of an antenna are dependent on the direction in which the wave is transmitted. Each propagation path is thus composed of:

- The effects of the transmit antenna in the direction of emission of the propagation path.
- The effects of the propagation channel on the propagation path.
- The effects of the receive antenna in the direction of arrival of the propagation path.

The channel of a narrowband system is reduced generally to a single tap and the delay spread is in that case not a relevant parameter while in the case of a wideband system the delay spread becomes a key parameter of the radio channel. There exist four system functions to describe the behavior of the channel [8]:

- The time variant impulse response.
- The time-variant transfer function.
- The Doppler-variant impulse response.
- The Doppler-variant transfer function.

Time-variant impulse response

The radio propagation channel can be represented by a time variant impulse response h (t, τ) and the received signal y(t) is the convolution of the transmit signal x (t) with the time-variant impulse response h (t, τ):

$$y(t) = \int_{-\infty}^{\infty} x(t-\tau)\, h(t,\tau) d\tau \qquad (2.8)$$

2.5.2 Characterization of deterministic channels

Time-variant transfer function Bello formulas [9]

Applying the Fourier transform to the time-variant impulse response h (t, τ) with respect to the variable τ leads to the time-variant transfer function H(t, f).

(2.9)

$$H(t,f) = \int_{-\infty}^{\infty} h(t,\tau)\, exp(-j2\pi f\tau) d\tau$$

The relationship between the spectrums transmit signal X (f) and the received signal y (t) is given by:

$$y(t) = \int_{-\infty}^{\infty} X(f)H(t,f)\, exp(j2\pi ft) df \qquad (2.10)$$

Doppler-variant impulse response

Similarly, applying the Fourier transform to the time-variant impulse response h (t, τ) with respect to the variable t leads to the Doppler-variant impulse response s (ν, τ)

$$s(\nu,\tau) = \int_{-\infty}^{\infty} h(t,\tau)\, exp(-j2\pi\upsilon t) dt \qquad (2.11)$$

The Doppler-variant impulse response s (ν, τ) describes the spreading effect of the radio channel to the transmit signal in both the delay and Doppler domains.

Doppler-variant transfer function

Finally, applying the Fourier transform to the Doppler-variant impulse response s (ν, τ) with respect to τ leads to the Doppler-variant transfer function:

$$B(\nu, f) = \int_{-\infty}^{\infty} s(\nu, \tau) exp(-j2\pi f\tau) d\tau \tag{2.12}$$

The interrelations among the above four system functions are shown in Figure 2-3, where the symbols $\mathcal{F}$ and $\mathcal{F}^{-1}$ denote the Fourier transform and the inverse Fourier transform, respectively [9].

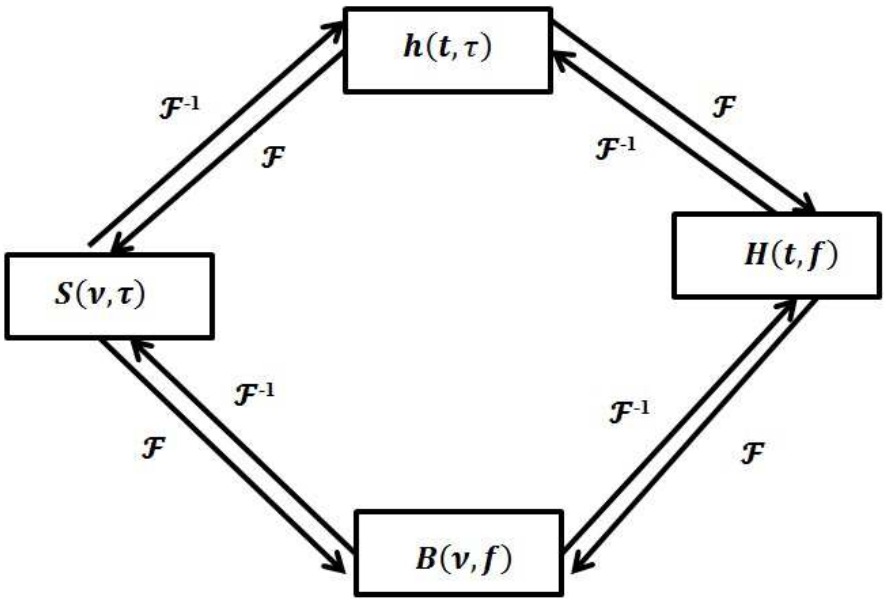

Figure 2-3 Interrelations among h-functions for WSSUS channels.

2.5.3 Characterization of randomly time-variant linear channels

As mentioned previously, in practice a radio is a random process. We thus interpret them as randomly time-variant linear systems. A complete description of such radio channels requires a joint multidimensional PDF of all the system functions which is in practice too complicated to obtain. Hence, a less accurate but more realistic approach which is frequently used is based on a second-order description, i.e. the autocorrelation function of various system functions [10].

Here, we still use the h (t, τ), H (t, f), s (ν, τ) and B (ν, f) to represent the randomly time-variant impulse response, the randomly time-variant transfer function, the randomly Doppler-variant impulse response and the randomly Doppler-variant transfer function, respectively, for notational simplicity. The autocorrelation functions of the four system functions for the randomly time-variant linear systems are defined as follows:

$$R_h(t, t', \tau, \tau') = \mathrm{E}\{h^*(t, \tau)h(t', \tau')\} \quad (2.13)$$

$$R_H(t, t', f, f') = \mathrm{E}\{H^*(t, f)H(t', f')\} \quad (2.14)$$

$$R_s(\nu, \nu', \tau, \tau') = \mathrm{E}\{s^*(\nu, \tau)s(\nu', \tau')\} \quad (2.15)$$

$$R_B(\nu, \nu', f, f') = \mathrm{E}\{B^*(\nu, f)B(\nu', f')\} \quad (2.16)$$

At that stage, the autocorrelation functions depend on four variables. Hence, the Wide-Sense Stationary Uncorrelated Scattering (WSSUS) assumption is usually made to further simplify the autocorrelation functions. Under the assumption of the WSSUS, the autocorrelation functions of the four system functions satisfy the following relationships:

$$R_h(t, t + \Delta t, \tau, \tau') = P_h(\Delta t, \tau)\delta(\tau - \tau') \quad (2.17)$$

$$R_H(t, t + \Delta t, f, f + \Delta f) = R_H(\Delta t, \Delta f) \quad (2.18)$$

$$R_s(\nu, \nu' + \Delta t, \tau, \tau') = P_s(\nu, \tau)\delta(\nu - \nu')\delta(\tau - \tau') \quad (2.19)$$

$$R_B(v, v', f, f + \Delta f) = P_B(v, \Delta f)\delta(v - v') \quad (2.20)$$

Now the P-functions depend only on two variables, which greatly simplify the analysis. The = $P_h(\Delta t, \tau)$ is called the **delay cross power spectral density**; the $R_H(\Delta t, \Delta f)$ is called the **time frequency correlation function**; the $Ps(v, \tau)$ is called the **scattering function** and the $P_B(v, \Delta f)$ is called **the Doppler cross power spectral density.** They are connected to each other by the Fourier transform. Their interrelations are shown in Figure 2-4.

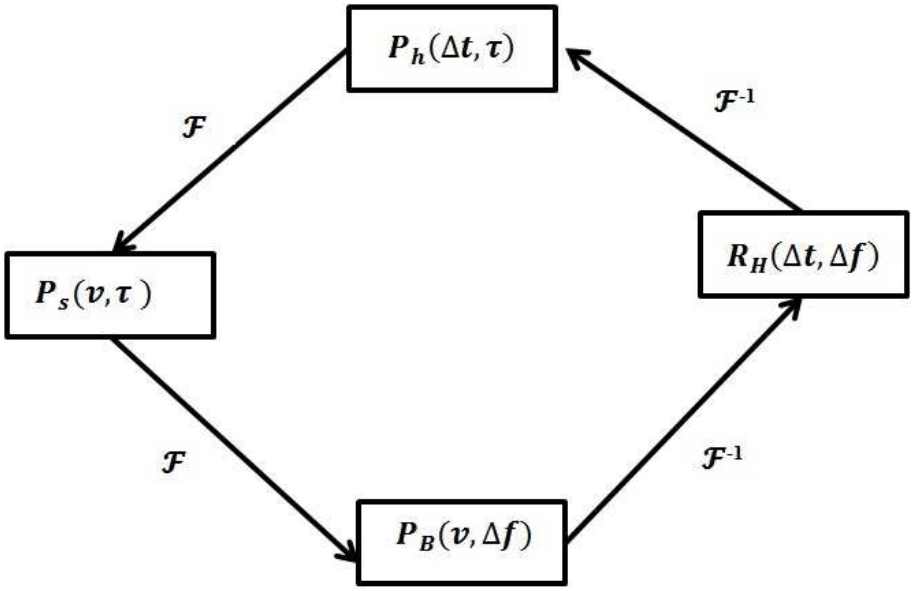

Figure 2-4 Interrelations among P-functions for WSSUS channels.

With the autocorrelation functions of the system functions in time variant linear channels, it is possible to obtain the autocorrelation function of the received signal y (t) given the autocorrelation function of the transmit signal x (t). In the following it is shown how the autocorrelation functions of the received signal are related to those of the system functions. Here, we just take the randomly time-variant impulse response h (t, τ) system function as an example. For other system functions, they can be derived in a similar way. From (2.12), we know that the autocorrelation function of the received signal $y(t)$ can be expressed as $R_y(t, t)$.

$$\begin{aligned} R_y(t, t') &= \mathrm{E}\{y^*(t)y(t)\} \\ &= \mathrm{E}\left\{\int_{-\infty}^{\infty}\int_{-\infty}^{\infty} x^*(t-\tau)x(t'-\tau')h^*(t-\tau)h(t'-\tau')\right\} \\ &= \int_{-\infty}^{\infty}\int_{-\infty}^{\infty} x^*(t-\tau)x(t'-\tau')E\{h^*(t-\tau)h(t'-\tau')\} \end{aligned} \quad (2.21)$$

$$\int_{-\infty}^{\infty} \int_{-\infty}^{\infty} x^*(t-\tau)x(t'-\tau')R_h(t,t',\tau,\tau')d\tau d\tau'$$

This shows that the autocorrelation function of the received signal can be determined by the auto correlation functions of the system functions of radio channels. For WSSUS channels, we have $R_h(t,\ t',\tau,\tau') = P_h(\Delta t,\tau)\delta(\tau - \tau')$, where:

$\Delta t = t' - t$ So (2.20) becomes

$$R_y(t,t+\Delta t) = \int_{-\infty}^{\infty} x^*(t-\tau)\, x(t+\Delta t-\tau)P_h(\Delta t,\tau)d\tau \qquad (2.22)$$

For the case $\Delta t = 0$, it becomes:

$$R_y(t,\tau) = \int_{-\infty}^{\infty} |x(t-\tau)|^2 P_h(\Delta t,\tau)d\tau \qquad (2.23)$$

Where $P_h(\tau) = P_h(0,\tau)$ is known as the Power Delay Profile (PDP). The equation (2.23) means that for WSSUS channels, the autocorrelation function of the received signal is determined by the Power Delay Profile $P_h(\tau)$of the radio channels. If ergodicity holds, the PDP can be obtained from the time-variant impulse response according to

$$P_h(\tau) = lim_{T\to\infty} \frac{1}{2T} \int_{-T}^{T} |h(t,\tau)|^2 dt \qquad (2.24)$$

2.5.4 Statistical Channel Metrics

This chapter focuses mainly on the characteristics of channel radio propagation, where the Doppler shift is negligible, so we are more interested in two of the autocorrelation functions of the system functions for randomly time-variant linear channels: the delay cross power spectral density $P_h(t, \tau)$ and the time frequency correlation function $R_H(\Delta t, \Delta f)$. For the time frequency correlation function $R_H\ (\Delta t, \Delta f)$, when Δt = 0:

$$R_H(0, \Delta f) = R_H(\Delta f) \tag{2.25}$$

The $R_H(\Delta f)$ is called the Frequency Correlation Function (FCF). When = Δf = 0,

$$R_H(\Delta t, 0) = R_H(\Delta t) \tag{2.26}$$

The $R_H(\Delta t)$ is called the Time Correlation Function (TCF). From Figure, it is easy to show that the PDP P_h (τ) and the FCF R_H(f) are a Fourier transform pair. Two useful statistical parameters associated to $P_h(\tau)$ are the mean delay $\tau_m$and the root mean square delay τ_{rms}: For the time frequency correlation function R_H (Δt, Cf), there are also two statistical parameters associated to it: the coherence bandwidth B_c and the coherence time T_c.

The coherence bandwidth B_c is the minimum value of Δf for which R_H (Δf) equals some predefined values, e.g. 0.5 or 0.9. It is a parameter used to indicate how large is the bandwidth which corresponds to the signals still strongly correlated. Similarly, the coherence time Tc is the minimum value for which $R_H(\Delta t)$ equals some predefined values. It is a measure of how long is the duration during which the two signals are still strongly correlated.

When considering wideband system, the delay spread is of great importance for communication systems. For a system with infinite bandwidth, the power delay profile (PDP) is defined as:

$$P(\tau) = E\{|h(\tau)|^2\} \quad (2.27)$$

Where τ represents the delay. In that case, the total power, the mean delay (or average delay) and the delay spread of the channel are given by 135[3][6][7]

$$P_T = \int P(\tau)\, d\tau \quad (2.28)$$

$$\tau_m = \frac{1}{P_T}\int P(\tau)\tau d\tau \quad (2.29)$$

$$\sigma_\tau = \sqrt{\frac{1}{P_T}\int P(\tau)\tau^2 d\tau - \tau_m^2} \quad (2.30)$$

The delay spread is a measure of the dispersion of the impulse response's power. The higher the delay spread of a channel is, the lower the coherence bandwidth of the channel.

2.5.5 MIMO channel models

A MIMO system is a wireless communication system that is equipped with multiple antennas at both end of the link. Compared to conventional single-antenna systems, MIMO systems enable many significant advantages in terms of e.g. link reliability and data transfer. The most fundamental difference between the operation of a single antenna system and a MIMO system is grounded on the way they treat multi-path propagation. MIMO technology has also been recently adopted by several standards, namely by the 3GPP LTE, LTEA, and it is seen more important in spectral efficiency for 5G deployment in 2020 [11].

A schematic illustration of the operation of a generic MIMO system is shown in Figure 2-5. The transmit signal is fed as a digital bit stream to the TX, where the stream is reprocessed before feeding it to the antenna ports. At the RX, the received signal needs to be post-processed in order to decode the original signal that was transmitted. The performance of a MIMO system depends on the quality of the signal processing algorithms at the TX and RX. However, the signal processing algorithms are not developed only based on the envisioned performance target i.e. link reliability, capacity enhancement, etc., but also the characteristics of the radio channel in which the system needs to operate play an essential role.

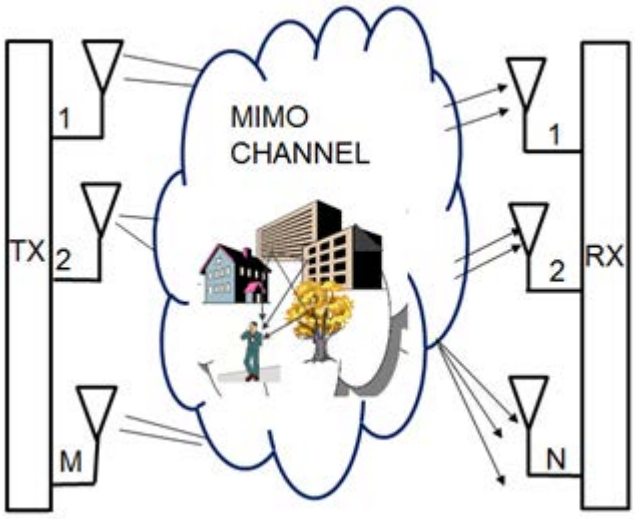

Figure 2-5 Illustration of MIMO system.

The radio channel is often represented as a time varying function $h(t,\tau)$ which includes the effect of the transmit antenna and the receive antenna as:

$$h(t,\tau) = \iint g_{tx}(\phi_T)\, F(t,\tau,\phi_R,\phi_T) g_{rx}(\phi_R)\, d\phi_T d\phi_R \qquad (2.31)$$

Where ϕ_T represents the angle (and therefore the direction) where the transmitting antenna radiates, ϕ_R represents the incoming angle of the receiving position, and $g_{rx}(\phi_R)$ and $g_{tx}(\phi_T)$ are the complex gains of the antennas. Then the integral sums the radiation of the whole system over all the possible directions. Assuming a finite *K* number of paths, transforms the integral in a summation, with the consequent reduction in complexity.

$$h(t,\tau) = \sum_{i=1}^{K} g_{tx}(\phi_T) F(t,\tau,\phi_R,\phi_T) g_{rx}(\phi_R) \qquad (2.32)$$

The impulse response described is applicable to single polarized antennas. A more general case is when both transmitting and receiving antennas are dual polarized. Then we can write matrix impulse responses with all the possible combinations between polarizations.

$$\mathrm{h}(\mathrm{t},\tau) = \begin{bmatrix} h_{vv}(t,\tau) & h_{v\mathrm{h}}(t,\tau) \\ h_{hv}(t,\tau) & h_{h\mathrm{h}}(t,\tau) \end{bmatrix} \quad (2.33)$$

Everything we have seen so far is valid for the case where there only is one antenna in the transmitting part, and other one is reception (SISO). However, to describe the full MIMO channel, we need to characterize the impulse response of all possible combinations of antennas. Thus, for the general case of M transmitters and N receiving antennas, the MIMO channel is characterized by an M*N dimension matrix, which includes all double-directional impulse response for all the single antenna combinations.

$$\mathrm{h}(\mathrm{t},\tau) = \begin{bmatrix} h_{11}(t,\tau) & \cdots & h_{1M}(t,\tau) \\ \vdots & \ddots & \vdots \\ h_{N1}(t,\tau) & \cdots & h_{NM}(t,\tau) \end{bmatrix} \quad (2.34)$$

Where $h_{nm}(t,\tau)$ represents the time-variant impulse response between the inputs of the mth transmit antenna and the output of the nth receive antenna. If polarization diversity is present on the antennas, then the impulse response $h_{nm}(t,\tau)$ must be subsided by the 2* 2 matrix defined in (Eq. 2.33).

2.6 Channels models

A remarkable study on the different channel models is presented in [13]. According to this study, channel models can be separated in two main categories, depending on whether they include or not the antenna properties of the system. Below it is shortly described each of these two categories:

2.6.1 Physical channel models

These models characterize the propagation environment from an electromagnetic point of view. To this end, by propagation theory of electromagnetic waves, the bidirectional propagation channel that connects the position of the transmitter and receiver is described. Thus, parameters inherent to the physical channel are evaluated (regardless of the transmitter receiver systems) as i.e. the complex amplitude, Delay Spread, AoA or DoA. This type of channel models is independent of parameters such as antenna radiation pattern, number of antennas and polarization... channel models based on ray tracing, or extension of Saleh-Valenzuela, are examples of this type of models.

Analytical channel models, approach the problem from another perspective. What they do is to characterize the transfer function between the transmitters and receivers antennas, individually. Thus, the analysis is not in terms of electromagnetic wave propagation.

On the contrary it produces a matrix of MIMO impulse responses that take into account all possible combinations of antennas. Other authors propose to perform this characterization of the channel matrix using the correlation between the difference antennas.

Apart from the models listed in the above categories, some international organization have proposed a number of channel models for the purpose of comparing different wireless system in order to define some reproducible conditions. These models are based on field measurements made in real environments such as streets, indoors and rural environments the objective of this type of models is to clearly define a reference environment where wireless devices can be tested the same way in different laboratories with different methodologies.

2.6.2 Deterministic channels models

Deterministic models are used for site-specific channel modeling; they consist of an environment model and a wave propagation model. The environment model describes position, geometry, material composition and surface properties of the wave propagation relevant objects and obstacles (e.g. trees, houses, vehicles, walls, etc.). In practical applications an analytic solution of the Maxwell equations, due to the computation time, is not possible. Deterministic models can provide very accurate and meaningful interpretation of the channel for a given location and environment only if an accurate description of the environment is available. To consider the uncertainties in the channel, the deterministic methods sometimes include a statistical component called diffuse scattering [14]. There are several deterministic modeling methods such as the difference time-domain (FDTD) [15] method, the finite-element method (FEM) and so-called ray tracing (RT) [16].

2.6.2.1 Ray tracing model

Ray tracing is a technique which have been used for long in computer graphics, when tracing light waves emitted from a light source. The idea is to trace radio waves in the same way, from a transmitter to a receiver. Once all possible paths have been identified, electromagnetic techniques are applied to the rays to compute interesting parameters, such as signal strength. The electrical lengths of the different ray paths give the amplitudes and phases of the component waves. The signals are also affected in amplitude and phase when being transmitted, reflected or diffracted on obstacles during propagation. Those effects are accounted for in the calculations. The ray tracing [10] model is an image-based model which assumes all objects in the propagation environments are potential reflectors.

But ray tracing has the disadvantage that its computational time grows exponentially with the order of calculated reflections. Both in the ray launching and ray tracing models, the strengths of reflected rays and refracted rays are computed according to the geometrical optics. The diffracted rays are computed according to e.g. UTD theory. For ray launching and ray tracing, the complexity of the propagation environments has a strong impact on their computational load since more obstacles lead to more reflections and diffractions etc.

2.6.2.1 FDTD model

Here, the FDTD model means the conventional FDTD model. The FDTD model [17] [10][18] is a numerical solution of Maxwell's equations. Since Maxwell's equations were first published in 1861[19] they have been considered as the most accurate and elegant description about how electric field and magnetic field interact with each other and how electromagnetic waves propagate [20]. The idea is that we replace the set of partial differential equations of Maxwell's equations by a set of finite difference equations and then this set of finite-difference equations can be solved iteratively based on the space-time grid.

2.6.3 Stochastic channel model

Stochastic channel models are those whose results are random each time, but their statistical characteristics, e.g. Probability Density Function (PDF) follow a certain law. In general, stochastic models use one or more random variables to model the random aspects of radio channels. Stochastic models are usually used to model all kinds of fading's, e.g. the large scale fading and the small scale fading, since fading are with the nature of randomness[21][22].

2.6.3.1 Rayleigh fading model

The most typical statistical behavior that we can find in real multi-path environments, especially in urban and indoor cases, is that one where both real and imaginary part follows a Gaussian distribution. Therefore, it is possible to mathematically demonstrate that the variable of amplitude follows a Rayleigh distribution (its square follows an exponential distribution) while the random phase is uniform:

$$P_{\alpha}(\alpha) = \frac{2\alpha}{\Omega} exp\left(-\frac{\alpha^2}{\Omega}\right) \qquad \alpha \geq 0 \tag{2.35}$$

Where $\Omega = \alpha^2$ is the average power of the fading.

2.6.3.2 Rice fading model

The Rice distribution is also known as the Nakagami-n distribution. Unlike the Rayleigh fading model, the Rice fading model is usually used to model the multipath fading when there is a path much stronger than the others typically in case of direct LOS path. In LOS scenarios, the received signal amplitude α is distributed according to the Rice distribution.

$$P_\alpha(\alpha) = \frac{2(1+n^2)}{\Omega} exp\left(-\frac{(1+n^2)}{\Omega}\right) I_0\left(2n\alpha\sqrt{\frac{1+n^2}{\Omega}}\right) \quad \alpha \geq 0 \qquad (2.36)$$

Where n is the Nakagami-n fading parameter ranging from 0 to ∞. This parameter n is related to the well-known Rice K factor by $K = n^2$ which is defined as the ratio of the power of the LOS component to all the NLOS components (usually called diffuse components). It is of importance to note that in the extreme case when the LOS component tends to 0, e.g. K and n → 0, the Rice distribution reduces to the Rayleigh distribution. And when K and n → ∞, the Rice distribution approaches to the Gaussian distribution.

2.6.3.3 Nakagami-m fading model

The Nakagami-m fading distribution is given as follows [23]

$$P_\alpha(\alpha) = \frac{2m^m}{\Omega^m} \frac{\alpha^{2m-1}}{\mathrm{T}(m)} exp\left(\frac{-m\alpha^2}{\Omega}\right) \quad \alpha \geq 0 \qquad (2.37)$$

Where m is called the m parameter of the Nakagami-m fading and T (·) is the gamma function. The Nakagami-m distribution includes the Rayleigh distribution when m = 1 and the one-sided Gaussian distribution when m = 1, 2 as special cases. When m → ∞, the Nakagami-m fading channel approaches to a non-fading Additive White Gaussian Noise (AWGN) channel. When m > 1, we have a one-to-one mapping between the Nakagami-m distribution and the Rice distribution by their parameters:

$$m = \frac{(1+k)^2}{1+2K}, \qquad K \geq 0 \qquad \text{(Eq. 2.38)}$$

Where K is the Rice K factor. Hence, the Nakagami-m fading model can describe a very wide range of multipath fading. Nakagami and Rician distributions are quite similar in shape, but the main difference they present in Nakagami model fits better some Ultra-Wide Band (UWB) channel, while Rician model is more appropriate for environments with LOS [24].

2.7 Geometrical stochastic channel model

When we evaluate the performance of devices, it is useful to evaluate them over at least a minimum number of channel realizations. These could be generated by deterministic propagation models described in the previous section; however, their high computational cost prohibits the intensive link or system level simulations required during testing. Thus, procedure with a lower computational complexity that could emulate a whole class of radio-propagation environments is preferred [25]. These requirements have led to (GSCMs), where the multipath often tend to appear as clusters, i.e. groups of closely rays that have propagated along a similar path. In the GSCMs the underlying idea is to theoretically create the radio channel in delay and directional domains by placing clusters in the simulation environment to emulate the physical scattering objects of real environments. The characteristics of the clusters are modeled based on channel measurements, and naturally, the accuracy of a cluster-based channel model always is indispensably dependent on the quality of the cluster parameters [26].

2.7.1 3GPP Spatial Channel Model (SCM)

The SCM was designed for evaluating multiple-antenna systems and algorithms. The model was developed within a combined 3GPP 3GPP2 ad-hoc group to address the need for a precise channel model able to facilitate fair comparisons of various MIMO proposals. The model uses a system-level approach to simulate performance across the range of conditions expected in a cellular system [27][28]. This ensures that multiple antenna algorithms are not only optimized for a few test conditions, but across the system as a whole. In the following sections, the concepts of spatial channel modeling are introduced and explained.

- **Link-level model**

Since only one snapshot of the channel characteristics can be captured by the link-level channel model, link-level simulations are not enough for understanding the typical behavior of the system and evaluating the system-level performance, such as average system throughput and outage rate. In fact, the link-level simulation is used for the purpose of calibration, which compares the performance results from different implementations of the given algorithm [28].

- **System level model**

The system level model is a multi-link physical model intended for performance evaluation in which each link represents a cell or a sector within a cell. Figure 2-6 illustrates a system-level simulation in which an MS receives interference from adjacent sectors of adjacent cells.

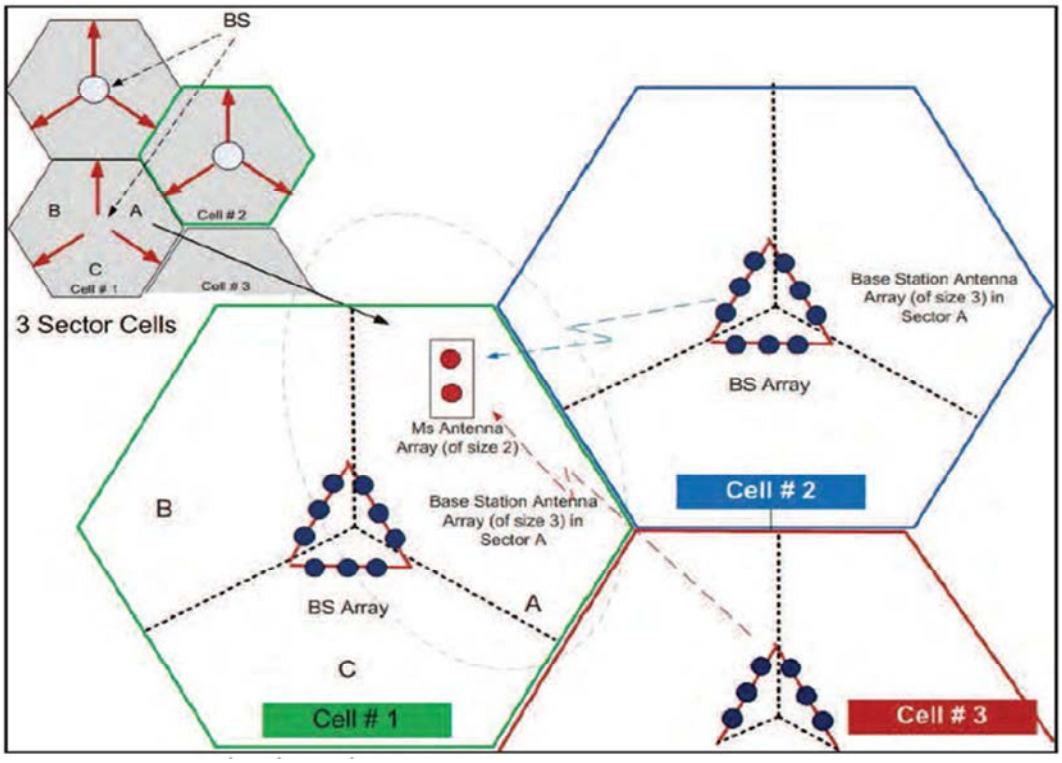

Figure 2-6 SCM system level simulation. Source [31].

Each link comprises an MS and BS MIMO antenna array. Propagation occurs via multipath and sub-paths. The excess delays of sub-paths are closely clustered around the delay of their (parent) multipath. This is assumed to originate from an environment with closely spaced clusters of scatterers.

The SCM distinguishes between three different environments:

- **Urban macro-cell**: Simulates the scenario where a user is in a very reflective (urban) environment, but where there is a certain distance to the BS.

- **Suburban macro-cell**: This model has a reduced delay spread and is used for modeling lower density environments.

- **Urban micro-cell**: simulates the case where a user is in a reflective scenario and is being serviced by a BS located within walking distance of it (typical of micro-cell).

SCM models are used so that the system simulation is performed as a sequence of drop, where a drop is a run of the channel model during a very short time. The duration is short enough, so that it can be assumed that the AS, mean AoA, DS and shadowing are constant throughout the drop. These models have both a geometric and a stochastic component. The geometric component contains the position of DUT with respect to the BS, the orientation of the antennas and the direction of motion, are calculated randomly at the beginning of each drop. The three models consist of 6 main multipath components.

The angular dispersion implementation is performed by introducing 20 sub-paths for each of the 6 main components, with the same delay, but different DoA. The per-path power azimuth spectrum (PAS) is a description of the power and angle distribution, and is typically assumed to follow a Laplacian distribution. This is a two sided exponential, which is an isosceles triangle when plotted in dB The center of the distribution is at zero degrees relative to the average AoA or AoD, as shown in Figure 2-7.

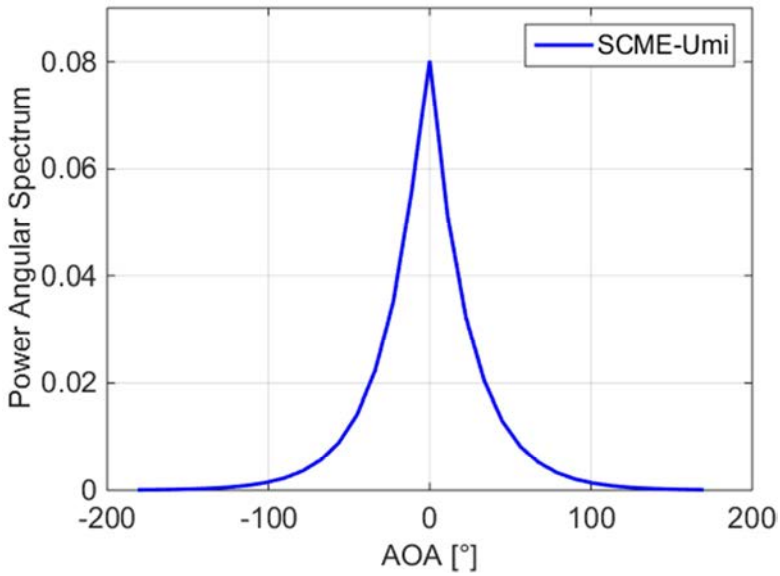

Figure 2-7 PAS path in SCM channel model

Figure 2-8 illustrates the sub-path spacing in degrees relative to the path AoD at the BS. Since the BS antennas are somewhat isolated from the clutter, the angle spread (AS) is quite small. The AS is 35 degrees as defined by the model, with 20 sub-paths of equal power and a non-linear spacing as shown to approximate the Laplacian PAS.

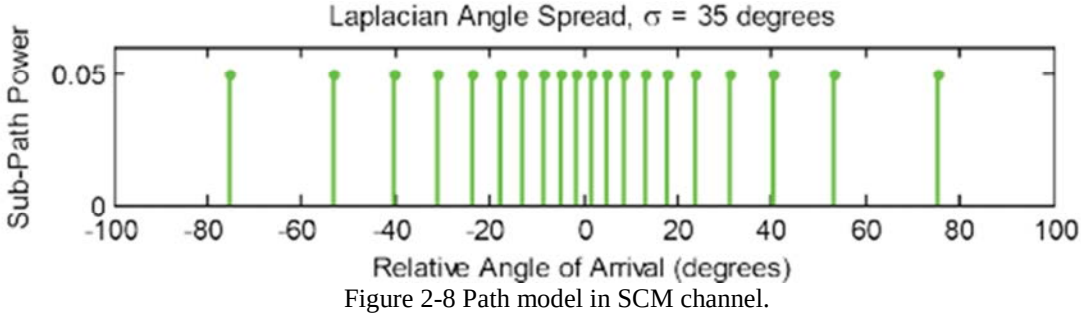

Figure 2-8 Path model in SCM channel.

This model has two drawbacks. Firstly, it is not supposed to work for higher bandwidth than 5 MHz, so it is not suitable for the new coming 4G, LTE standards, which use 20 MHz, secondly the SCM model was designed for a CDMA systems working at 2 GHz, so its accuracy is not guaranteed for other frequency band.

2.7.2 Extended 3GPP Spatial Channel Model (SCME)

The SCME [30] model proposed the extensions of some of the parameters proposed by the SCM model, maintaining the basic idea of the original model. With the arrival of the 5G standards, an extension of the channel bandwidth applicability is required to the channel model. The SCME model proposes to add intra-paths DS following a one-sided exponential function. This approach is based in the methodology proposed by Saleh and Valenzuela [27] for the modeling of indoor environments.

Another important extension included in the SCME model is the calculation of the path loss, in order to extend the frequency applicability to 5 GHz band. The SCM path loss, model is based on the Cost-Hata-Model for Suburban and Urban Macro and the COST-Walfish-Ikegami-Model (COST-WI). Instead, the SCME model proposes the use of the COST-WI model approximation for all the scenarios, due to its distance range (0.02-5 km) is more appropriate to the current standards use. (The Hata Model was calculated for GSM with a distance range of up to 20 Km/s). The proposed parameters for the different scenarios are:

- BS antenna height: Macro 32 m, Micro 10 m.
- Building height: Urban 12 m, Suburban 9 m.
- Building to building distance: 50 m, street width: 25 m.
- DUT antenna height: 1.5 m.
- Orientation: 30 ° for all paths.
- “Macro” scenarios: medium sized city / suburban centers.
- “Micro” scenarios: metropolitan.

Finally, an important characteristic proposed by the SCME model is the incorporation of a fixed set of delay taps and angular parameters, instead of the stochastic FDP estimation proposed in the original SCM. This extension is especially important for some methodologies, since it allows an important reduction in the complexity of the equipment. Proposed values are shown in Table 2-1.

Table 2-1 Parameters of Tap delay line parameters SCME scenarios. Source [(3GPP document TR 37.976)]

Scenario		Suburban		UrbanMacro		Urban Micro	
Power delay parameters relative paths power(dB)/delay(us)	1	0	0	0	0	0	0
	2	-2.6682	0.1408	-2.22.4	0.3600	-1.2661	0.2840
	3	-6.2147	0.0626	-1.7184	0.2527	-2.7201	0.2047
	4	-10.4132	0.4015	-5.1896	1.0387	-4.2973	0.6623
	5	-16.4735	1.3820	-9.0516	2.7300	-6.0140	0.8066
	6	-22.1898	2.8280	-12.5013	4.5977	-8.4306	0.9227
Resulting Total DS		0.231		0.841		0.294	
		2.35		2.35		5.35	
Angular parameters: AoA (deg) AoD (deg)	2	156.1507	-101.33	65.7489	81.9720	0.69666	6.6100
	3	-13.72020	-290086	45.645480	11.87878	13.2268	14.1360
	4	39.3383	1109758	14.5707	-136.8071	1460669	50.8297
	5	91.1897	115.508	17.7.08	-96.2155	30.5485	38.3972
	6	4.7669	118.068	107.0643	139.077	1.0587	40.2849
Resulting totral AS at BS MS (deg)		4.70, 64.78		7.87,62.35		15.76,62.19	18.21 67.80

2.7.3 WINNER Channel model

2.7.3.1 Generic WINNER model

Based on the stochastic geometry approach, the WINNER model [31] allows creating an arbitrary radio channel model. The model depends on the antenna pattern and the spatial distribution of scatterers. As well as in the SCM models, the channel parameters are determined stochastically, based on statistical distributions extracted from channel measurement.

The WINNER channel model [81] is built from measurement results. It describes the channel propagation as sum of the different paths regrouped into clusters. The clusters are the same properties in term of power but different delays. Clusters consist of the paths having interacted with obstacles in a diffuse zone. In the terminology proposed in this document the cluster is a propagation path diffused in space, either only in angle or both in delay and angle domains. Elements of the MIMO channel, i.e. antenna arrays at both link ends and propagation paths, are illustrated in Figure 2-9. It shows a set of clusters that constitute the channel propagation. The number of clusters in each path is between 8 and 20 depending on the scenario.

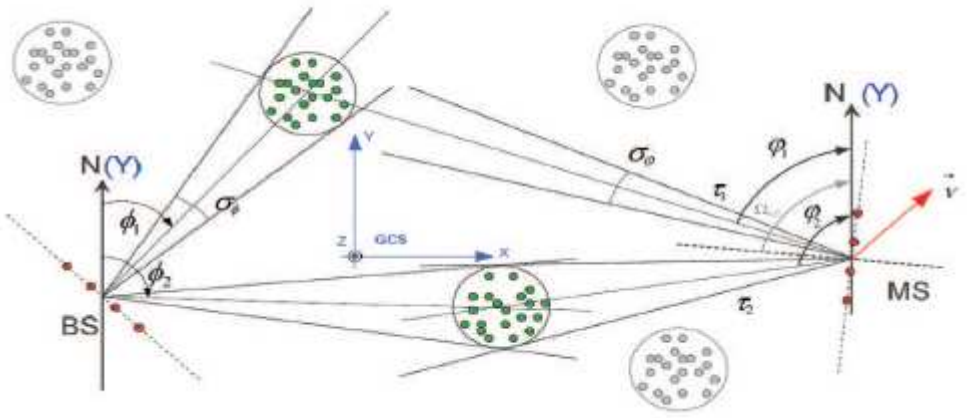

Figure 2-9 WINNER channel model.

Transfer matrix of the MIMO channel is composed the summation of N clusters:

$$H(t;\tau) = \sum_{n=1}^{N} H_n\,(t;\tau) \tag{2.37}$$

It is composed of antenna array response matrices F_{tx} for the transmitter, F_{rx} for the receiver and the propagation channel response matrix h_n for cluster n as follows:

$$H_n(t;\tau) = \iint F_{tx}(\varphi)\, h_n(t;\tau;\phi;\varphi) F_{rx}^{T}(\phi) d\phi d\varphi \tag{2.38}$$

The channel from Tx antenna element s to Rx element u for cluster n is:

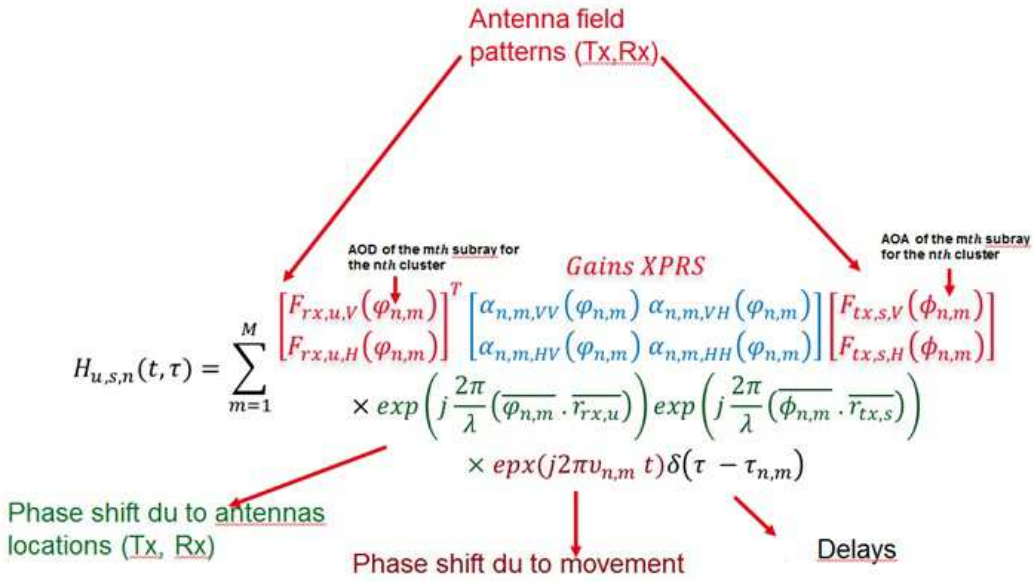

(2.39)

Where $F_{rx,u,V}$ and $F_{rx,u,H}$ are the antenna element u field patterns for vertical and horizontal polarizations respectively. $\alpha_{n,m,VV}$ and $\alpha_{n,m,VH}$ are the complex gains for vertical to vertical-to-horizontal polarizations of ray n,m respectively. Further λ_0 is the wave length of the carrier frequency.

$\bar{\phi}_{n,m}$ is AoD unit vector, $\bar{r}_{rx,u}$ and $\bar{r}_{tx,s}$ are the location vectors of elements s and u respectively, and $v_{n,m}$ is the Doppler frequency component of ray n,m. If the radio channel is modeled as dynamic, all the above mentioned small scale parameters are function of time t.

In the phase I of the WINNER [32] project, they proposed a generic model based on the same principles than SCM models, but extending the bandwidth and the number of scenarios (six in total). The model implements a ray-based double-directional model multi-link independent of the antenna, which makes the model scalable and capable of modeling MIMO channels. The model was taken from a measurement campaign at 2 and 5 GHz The following propagation models were defined:

- Typical urban micro-cell.
- Indoor.
- Sub-urban macro-cell.
- Rural macro -cell.
- Stationary feeder link.

In phase II of the WINNER [33] project, they made some extensions to the original WINNER models. One of the most important is the extension of the frequency range used so that channel models are applicable in the range 2-6 GHz. There were also added more scenarios, based on measurement campaigns, for a total of 13. The covered propagation scenarios are:

- A1 Indoor office
- A2 Indoor to outdoor
- B1 Urban micro-cell
- B2 Bad Urban micro-cell
- B3 Indoor hotspot
- B4 Outdoor to indoor
- B5 Stationary Feeder
- C1 Suburban macro-cell
- C2 Urban macro-cell
- C3 Bad urban macro-cell
- C4 Urban macro outdoor to indoor
- D1 Rural macro-cell
- D2 Moving networks

In the WINNER II a set of multidimensional channel models are developed. Also it adds features such as the extension of the AoA in elevation plane. This family of models can be applied to any wireless system operating in the frequency bands covered by the 2-6 GHz range, with up to 100 MHz bandwidth. They are based on more generic channel modeling approach, which means the possibility to vary number of antennas, the antenna configurations, geometry and the beam antenna pattern without changing the basic propagation model. We describe in the following the procedure for generation of channel coefficients.

- **Set the environment, and antenna array parameters**

a) Choose one of the scenario
b) Give the number of BS and MS
c) Give the locations of BS and MS, and relative directions of departures and arrival
d) Give BS and MS antenna field patterns and array geometry
e) Give speed and direction of motion of MS
f) Give system center frequency

- **Small scale parameters**

a) Generate the delays τ
b) Delays are drawn randomly from the delay distribution. With exponential delay distribution:

$$\boldsymbol{\tau_n}' = -r_\tau \boldsymbol{\sigma_\tau} ln(X_n) \quad (2.40)$$

Wherer_τ : delay distribution proportionality factor and σ_τ : Delay spread and $X_n \sim Uni(0,1)$

- **Generate the clusters powers P**

Cluster power is calculated a single slop exponential power delay profile as:

$$P_n{}' = exp\left(\frac{-\tau_n}{\sigma_\tau}\right) 10^{\left(\frac{-Z_n}{10}\right)} \quad (2.41)$$

Where $Z_n \sim N(0,\zeta)$ and ζ the per cluster shadowing in [dB]:

$$P_n = \frac{P_n{}'}{\sum_{n=1}^{N} P_n{}'} \quad (2.42)$$

- **Generate the azimuth arrival angles φ and azimuth departure angles ϕ**

In the generic model of the WINNER the PAS is modeled as Wrapped Gaussian, the AoAs are determined by inverse Gaussian function with input parametersP_n**:**

$$\varphi_n{}' = \frac{2\sigma_{AOA} - \sqrt{-ln\left(\frac{P_n}{max(P_n)}\right)}}{C} \tag{2.43}$$

Where $\sigma_{AOA} = \frac{\sigma_\varphi}{1,4}$: Standard deviation of arrival angles, and C: scaling factor related to the total number of cluster ratio:

$$\varphi_n = X_n \ \varphi_n{}' \ + Y_n \ + \varphi_{Los} \tag{2.44}$$

Where

$$X_n \sim Uni(-1,1) \tag{2.45}$$

$$Y_n \sim N(0, \frac{\sigma_{AOA}}{5}) \tag{2.46}$$

The procedure developed above depicts the complexity of the generic model, to determine channel parameters. Due, this WINNER project has been developed a new feature version of generic model called Cluster Delay Line (CDL) model.

2.7.3.2 Cluster Delay Line model (CDL)

CDL model is composed of a number of separate delayed clusters. Each cluster has a number of multipath components that have the same known delay values but differ in known angle of departure and known angle of arrival. The cluster angle-spread may be different from that of BS to that of the MS. The offset angles represent the Laplacian PAS of each cluster. The average power, mean AoA, mean AoD of clusters, angle-spread at BS and angle-spread at MS of each cluster. An example of the CDL model for Outdoor to Indoor channel developed in WINNER II project is developed in Table 2-2.

Table 2-2 Parameters of WINNER II scenarios (3GPP document TR 37.976)

Modified WINNER II Outdoor –to-Indoor								
Cluster	Dealy [ns]			Power [dB]			AoD [°]	AoA°
1	0	5	10	-3	-5.2	-7	0	0
2	0			-8.7			32	101.5
3	5			-3.7			-21	66.2
4	10			-11.9			37	-118.7
5	35			-16.2			-43	138.5
6	35			-6.9			-28	-90.4
7	65	70	75	-3.9	-6.1	-7.9	-49	32.7
8	120			-10.3			-34	10.5
9	125			-20.7			-49	156.6
10	195			-16			43	-157.7
11	250			-21			49	-157.7
12	3058			-22.9			51	-164.7
Dealy spread [ns]								5/25
Cluster AS AoD/AS AoA [°]								Laplacian
Total AS AoD / AS AoA [°]								28.6/56
Mobile speed [Km/h]/ Direction of travel [°]								3/120
XPR								9 dB
Mid paths Share Cluster parameter values for								AoD, AOA,AS

2.7.3.1 3D Extension of WINNER II Channel model (WINNER+)

Current popular (GSCM), e.g. [81] are in practice 2-dimensional because the addition of the third dimension, elevation, is assumed to make the models much more complex than the 2D ones. At the moment the situation is changing and there seems to be remarkable interest in 3D channel models.

The extension methodology has been largely specified for WINNER II channel models in a proprietary work published. The focus is the extended of the (2D) implementation of channel to 3D channel model [82]. The 3D implementation can be found in [81]. 3D GSCM channel model is generalized from a 2D model by generating for each ray an elevation component. The procedure has been described in [83], where there is a detailed description, how a 3D implementation is created from the existing WINNER II implementation.

Therefore the details have not been described in this chapter. In this section the PAS of elevation has been described .In the terminology of WINNER+, the values of elevation is illustrated in Table 2-3.

Table 2-3 Elevation parameters for five propagation scenarios [84].

Elevation parameters									
Scenario	Indoor (A1)		O2I (B4)	Umi (B1)		Uma(C2)		SMa (C1)	
Condition	LOS	NLOS	NLOS	LOS	NLOS	LOS	NLOS	LOS	NLOS
ESA[°]	8.7	12.6	10.2	4	7.5	9	18	12	10
MEA [°]	1.6	1.6	1.2	2	2	6	10	5.5	7
CESA [°]	3	3	3	7	7	7	7	7	7

CESA : Composite Elevation spread Angle

2.7.3.1 Comparison of geometrical channels models

The multi-probe OTA system in this thesis aims to evaluate the performance of devices of ultra-wide band, thus supported bandwidth of up 2 GHz is required. The WINNER model satisfies this requirement. The SCM is not suitable, due its 5 MHz bandwidth. The comparison parameters of these models are shown in Table 2-4.

Table 2-4 Comparaison of parameters.

Parameter	SCM	SCME	WINNERII	WINNER+
Max. bandwidth [MHz]	5	100	100**	100***
Frequency range [GHz]	2	2-5	2-6	2-6
No.of scenarios	3	3	12	12
No.of clusters	6	6	8-20	8-20
Distribution of PAS	Wrapped Gaussian[83]	Laplacian	Laplacian	3D channel models

* Artificial extension from 5 MHz bandwidth.

**Based on 100 MHz measurements.

Currently, the SCME has been considered as the first channel model for OTA testing devices by the COST2100 community. However, SCME model is built for testing devices in frequencies between 2 and 5 GHz, and the numbers of scenarios are not sufficient for advanced simulations. Due to these reasons, we use a simplification of CDL model of WINNER II in this thesis, which the objective is to emulate one single cluster individually based on the PAS. In order to preserve the delay information developed in WINNER CDL model.

2.8 Conclusion

This chapter described the fundamentals of propagation channel and different modeling approaches. We started with the characterization of deterministic channels whose behavior can be determined by any one of their four system functions. However, a realistic radio channel is a kind of random process whose characteristics cannot be completely determined in a deterministic manner. Thus a statistical modeling of the channel was introduced, together with the autocorrelation functions and popular fading models such as Rayleigh and Rician.

MIMO channels have been also described, with a focus on the spatial characteristics. Finally, we have introduced some popular Geometrical Stochastic Channel, e.g. SCM or WINEER, which are based on the cluster concept to describe propagation environment. In particular WINNER-like models, and its extension for 3D channel description in the 2-6 GHz band was retained.

Chapter 3

3 Over-The-Air (OTA) Test Methodologies

3.1 Introduction

The proper development and testing of wireless devices systems lie in detailed channel knowledge. As stated in chapter 2, multipath propagation in different environments may be modeled theoretically, in a deterministic or stochastic way. These models can truly reflect real propagation, but still lack of experimental work to support and complement the channel modeling process. Because of this, the assessment of devices in real channels is of paramount importance. To that end, the acquisition of equipment for evaluating devices under real conditions is the starting point of experimental evaluation and characterization. In the past years, wireless test beds and prototypes have received much interest from research community. Wireless devices need pass some evaluations showing that the performances reach the minimum requirements considered to address a specific market. For this reason, various experiment methods to which wireless devices are subjected before reaching the final consumer and several measurements techniques proposed for the characterization and qualification of systems are necessary. Those methods are called Over -The-Air (OTA) methodologies.

After an initial request by 3GPP RAN4 directed to COST 2100 to collect proposals for MIMO OTA measurement methods in 2008 [25], several MIMO OTA test methods have been proposed by participants of COST 2100, 3GPP RAN4 and CTIA. The proposals differ significantly in terms of measurement setup and equipment because each approach is trying to solve the issue from a different perspective. After some effort of consolidation and development, four forms of proposed methods have been accepted by 3GPP RAN4 for further investigation [34] and also under discussion in CTIA.

At the beginning, in section 3.2, the first OTA testing for device with single antenna systems was standardized by the CTIA ten years ago. Section 3.3 presents a critical review of different OTA methodologies; reverberation chamber, two stage methods and anechoic chamber method. The questions raised in analyzing these methodologies will be discussed and answered in section 3.3. The selected studies are discussed in section 3.4. Although multi-probe method is comparatively costly, from technical points of view it appears to be the most flexible one for wireless performance evaluation.

The focus of this chapter is on multi-probe anechoic chamber approach. Section 3.4 is devoted to describe the setup of the multi-probe method. Having defined the intended field several emulation techniques are discussed to emulate such field, the two most commonly used techniques are the prefaded signal synthesis (PFS) and plane-wave field synthesis (PWS). Their advantages and disadvantages are discussed. Section 3.5.2 presents multi-probes OTA methodologies and their characteristics. Finally, section 3.6 concludes this chapter.

3.2 Single-Input-Single-Output (SISO) OTA Tests Methodologies

OTA testing solutions create an environment where signals are transmitted to verify the performance of a product and accurately distinguish a poorly performing device from a good device. OTA test methods evaluate the wireless device end to end. If the device has a single antenna mode, it can be evaluated using traditional SISO OTA measurements methods. In all other cases, new test methodologies metrics are required to correctly characterize the device under test.

The first SISO OTA specification developed by The Cellular Telecommunications Industry Association (CTIA) released in 2001 and later by 3GPP [34]. It defines the general requirement for equipment configurations, laboratory techniques, test methodologies, and evaluation criteria that must be met in order to ensure the accurate, repeatable, and uniform testing of wireless devices. Proposed metrics for device radiation performance evaluation are Total Radiated Power (TRP) and Total Isotropic Sensitivity (TIS). TRP metric is a metric that provides information about radiated RF performance of the DUT.

The TRP metric is calculated by computing the average of the radiated power over a sphere centered on the device under test (DUT). The TIS metric is the average over the same sphere of the minimum received power to achieve a particular bit error rate. This DUT receiver measurement is made while the DUT is transmitting at maximum power so that any radiated effects that might cause self-blocking or desensitization of the DUT receiver are fully captured. Most of the work in this field was then concentrated on defining the right measurement procedure, the uncertainty of the technique and the minimum. DUT performance demanded. The maximum uncertainty allowed is defined in [35] and showed in Table 3-1.

Table 3-1 Uncertainty maximum limits (dB) for different configuration for TRP and TIS. Source [35].

Test Configuration	TRP	TIS
Free Space	2	2.3
Beside Head	2.1	2.3
Beside Head and Hand	2.4	2.6
Hand Right	2.2	2.4

As shown in Table 3-1, measurements of TIS and TRP can be done in four different use cases. These different cases simulate the most common scenarios where the DU is supposed to work, including the effect that user presence has over the device performance. The four typical measurement scenarios are:

- Free-Space: Where the DUT is placed on a support made of low dielectric material in order to avoid any effect from the close environment. This case is not realistic, but it is very useful as a reference case for inter-comparison purposes.
- Head Phantom Only: Where the DUT is placed against a head phantom.
- Head and Hand Phantom: where the DUT is placed in a hand phantom, against a head phantom. This position is commonly known as "talk") position and it gives an accurate idea about the device performance in a realistic case.
- Hand phantom only: where the DUT is placed in a hand phantom. This scenario (using one or two hands) is commonly known as "browse" mode and it simulates the situation where the user is using the device to send and receive data (SMS, Internet data...).

Figure 3-1 shows an illustration of the first SISO OTA testing in anechoic chamber, which consists of the measurements of total radiated power for transmit performance and total sensitivity for receive performance. It was selected as the FoMs for such OTA testing. This method was also adopted by the 3GPP. It consists in measuring a simple 3D radiation pattern measurement of the antenna by using the own RF transceiver section as an internal signal source, and by establishing a radio link with a base station (BS) emulator.

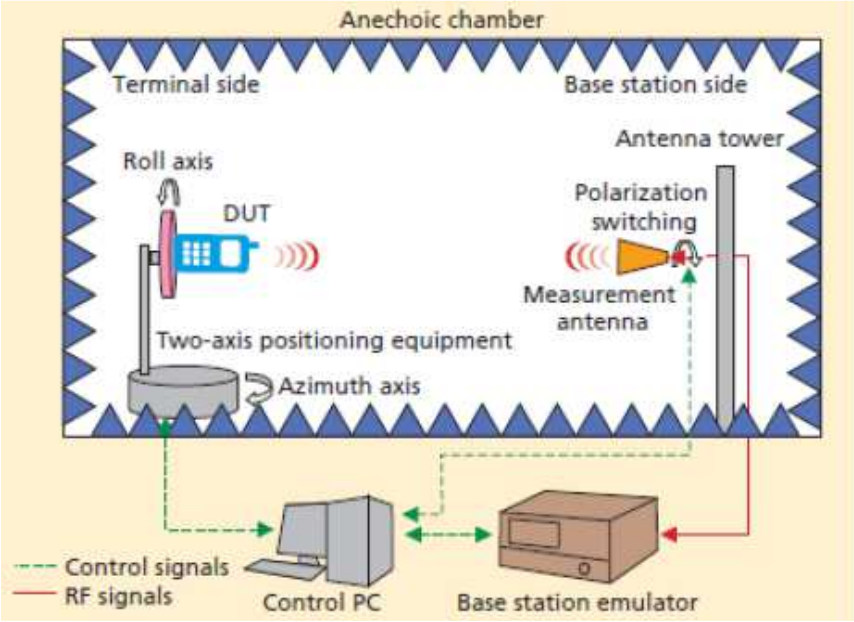

Figure 3-1 An illustration of the SISO OTA test facility in an anechoic chamber. Source [34].

With the emergence of MIMO technology, and in particular in the cellular telecommunication, the methods developed for SISO OTA could not be sufficient to measure the performance of MIMO devices.

This led in late 2007 to the formation of a reverberation chamber subgroup within CTIA to study the feasibility of extending reverberation chambers for MIMO OTA methodologies. In April 2009, CTIA developed an anechoic chamber subgroup to study the development of MIMO measurements in anechoic chambers. In 2009, the study of MIMO OTA was appeared in the COST action 2100 and in March 2009, 3GPP approved the study item “Measurement of radiated performance for MIMO and multi-antenna reception for HSPA and LTE terminals” in [85] in March 2011, the two CTIA groups were merged to create the MIMO OTA subgroup (MOSG), and finally, in February 2012, 3GPP approved the work item “Verification of radiated multi-antenna reception performance of UEs in LTE/UMTS” [86] to create a formal test specification for MIMO OTA. The major difference between SISO and MIMO performance is the radio propagation channel. For SISO, the DUT performance is independent of the channel, which is defined as isotropic and with no channel fading.

3.3 Multiple-Input-Multiple-Output (MIMO) OTA Tests Methodologies

OTA becomes very important for testing MIMO systems or products in real conditions. Ranging devices as good fair or poor w.r.t is a common practice in the industry. One distinguishes three categories of method for such MIMO OTA characterization:

- Reverberation chamber based method.
- Two-stage method.
- Anechoic chamber based multi-probes OTA method.

3.3.1 Reverberation chamber

The Reverberation Chamber is a metallic cavity or cavities that can emulate an isotropic multi-path environment which represents a reference environment for systems designed to work during fading; similar to how the free space "anechoic" reference environment is used for tests of Line-Of-Sight systems. The Rayleigh environment in a reverberation chamber is well known as a good reference for urban and indoor environments, but does not well represent rural and suburban environments.

A typical mode stirred reverberation chamber (MSRC), also referred as Reverberation Chamber (RC), consists of a closed metal cavity equipped with movable metal blades that act as field mixers (commonly called stirrers) and a turntable that rotates the DUT. A description is provided in Figure 3-2[36]. The independent movement of the stirrers and the rotation of the sample, allow to dynamically changing the boundary conditions of the electromagnetic field generated inside the cavity.

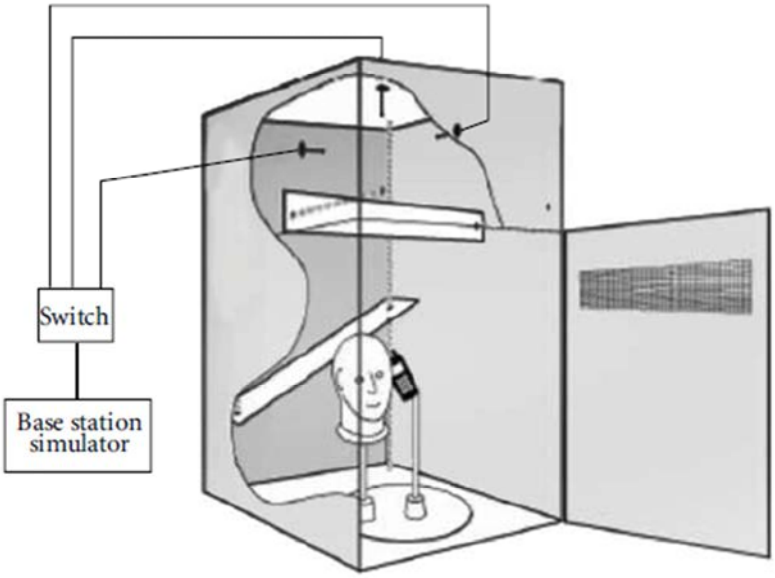

Figure 3-2 Reverberation chamber setup for devices testing with single cavity.

In a perfectly agitated MSRC, the real and imaginary parts of the rectangular components of electric and magnetic fields follow Gaussian distributions with identical paths variance. Thus, the amplitude of the electric and magnetic fields measured in a perfectly stirred follows a Rayleigh probability density function (PDF), while the phase is uniformly distributed. This type of distribution is very similar to the multipath field distribution found in urban environments for mobile communication systems. The naturally emulated Rayleigh environment in a MSRC is well known as a good reference for urban and indoor multipath environments, but does not reflect the reality of other propagation environments. Limits to emulate arbitrary channel models in a typical MSRC can be summarize as:

- Delay Spread (DS) cannot be arbitrarily set.
- Doppler is limited by the relatively slow motion of the stirrers.

On the other hand, there are some important advantages that have made this methodology become an emerging technique during the last few years.

- Cost effective solution: the number of probe antennas used in a MSRC is much lower than in other solutions (as those based in anechoic chamber).
- Measurement time: due to the capability of MSRC to emulate a 3-D environment (instead of 2-D environments generated with other methodologies), the measurement time with this technique is lower than in other techniques and can be even suitable to be included in production lines.

The extension of this methodology is one of the most promised techniques, which consist on adding more than one metal cavity so the fields do not necessarily have to be constrained to a single cavity. In consequence, MSRCs may contain more than one metal cavity that could be coupled through a variety of means, including wave guides, slots or metal plates, as it is shown in Figure 3-3.

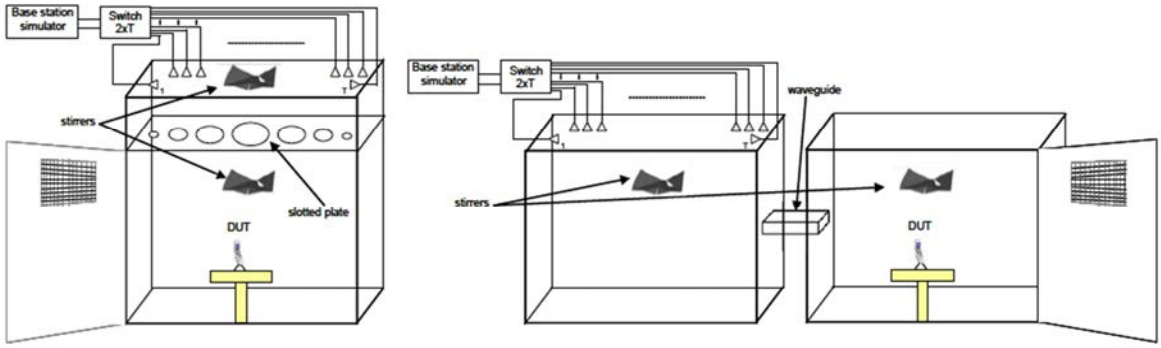

Figure 3-3 Mode-stirred chambers with multiple cavities. Source [38]

Solution that has been proposed to overcome that limitation, consist of cascading a MIMO CE and the MSRC. Using that setup, the properties of an arbitrary channel can be set in the channel emulator, extending the channel model emulation capabilities of a typical MSRC. However, the channel models parameters are changed by the innate response of the MSRC, and therefore the signal properties inside the MSRC is not exactly the same than those set in the channel emulator as seen in Figure 3-4.

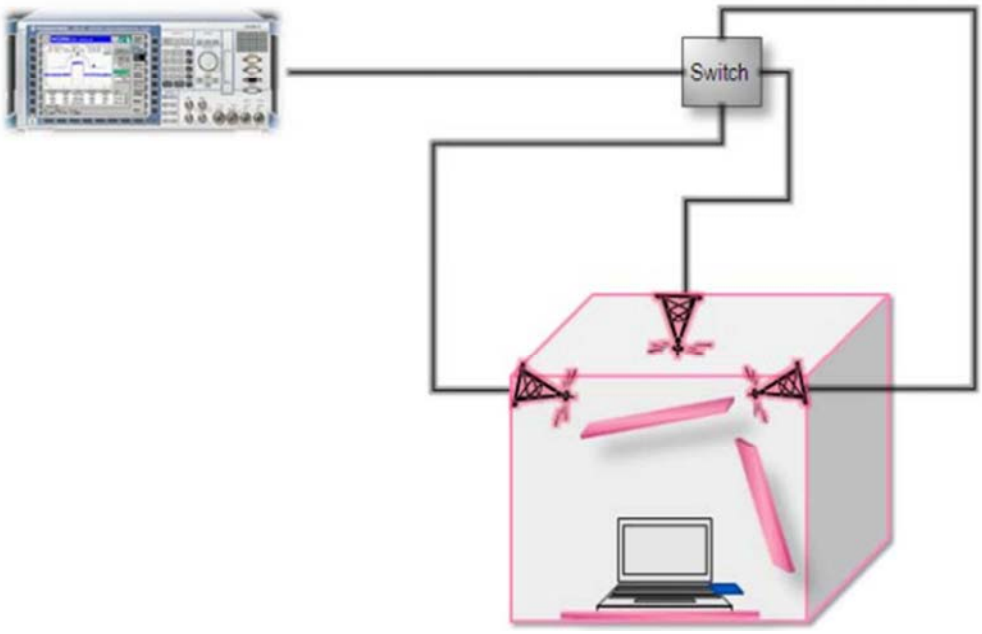

Figure 3-4 Test bench configuration for testing in reverberation chamber. Source [38]

Several works provide interesting results for the RC methods. In [87], the joint research effort of OTA in Sweden and UPCT in Spain show that it is possible for a multicavity RC to emulate different channel models with diverse levels of correlation using a novel sample-selection technique. The 3GPP MIMO OTA Work Item in progress highlighted [88], a recent contribution by EMITE. The new figures of merit, which are a statistical analysis of measured throughput, are presented in this issue by Marin-Soler et al [89]. These figures can indeed be very useful for determining the final goal of distinguishing between good and bad MIMO devices with a large set of measured throughput data obtained for a specific device following the 3GPP/CTIA test plans. The differences between test methods observed during measurement campaigns can be mitigated for RCs by the novel calibration method presented by Garcia-Fernandez et al. [90]. The ability of RCs to emulate the time domain aspects of 3GPP SCME channel models is demonstrated by Arsalane et al [91]. The work by Hansen [92] concentrates on demonstrating the ability of RCs to evaluate antenna correlations in an isotropic environment to those obtained from the classical definition.

3.3.2 Two stages method

The two stages method consists on the measurements of far field antenna radiation patter therefore the method divides the MIMO OTA tests in two separate measurements. Firstly, the MIMO antenna radiation pattern is measured inside an anechoic chamber. Secondly, a commercial channel emulator is used to mathematically convolve the measured antenna characteristic with the chosen OTA channel model for real time emulation.

In [86] authors explains how to experiment this methodology in the anechoic chamber. They demonstrated that the first stage consists of the characterization of the three dimensional antenna radiation patterns of all the antennas in the DUT, using an anechoic chamber. The setup needed to perform this part of the measurement is defined in the 3GPP document TS 34.114. The measurements are started by placing the DUT in the anechoic chamber in the far zone radiation pattern. The measurements were conducted in two polarizations θ and ϕ as shown in Figure 3-5. The user influence can be included in this stage, by repeating the antenna radiation pattern characterization including head and hand phantoms.

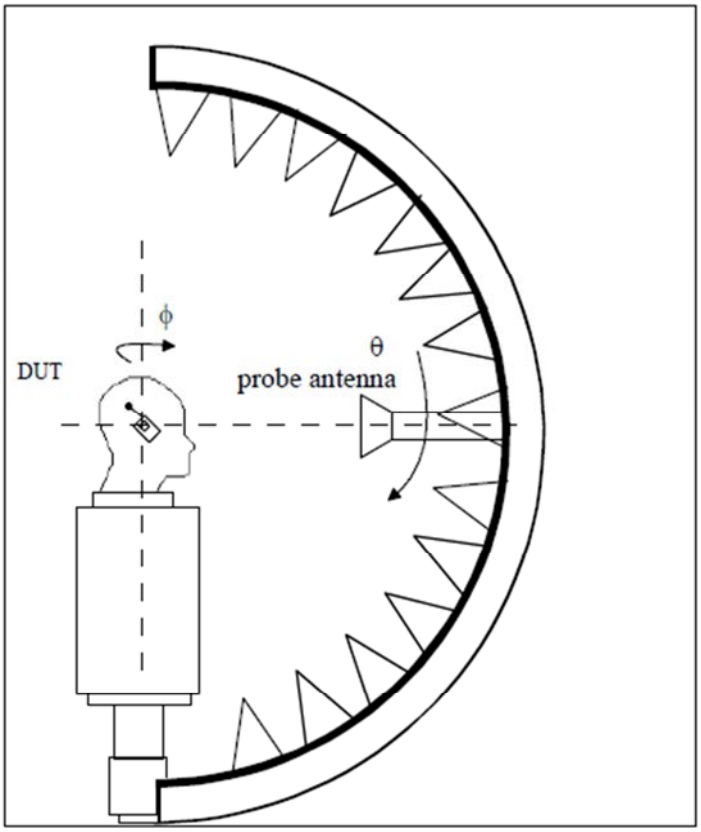

Figure 3-5 The coordinate system used in the measurements.

The second stage of this method consists on performing the desired FoM conducted measurements. To establish the communication, the BSE is connected to the MIMO CE (emulating the compound channel, including both the MIMO antenna effect and the multipath channel effect) and then to the MIMO DUT's temporary antenna ports via approved RF cables, as it is showed in Figure 3-6. By controlling the power settings of the channel emulator and also the integrated channel model, the end-to end throughput with the MIMO antenna radiation influence can be measured [38].

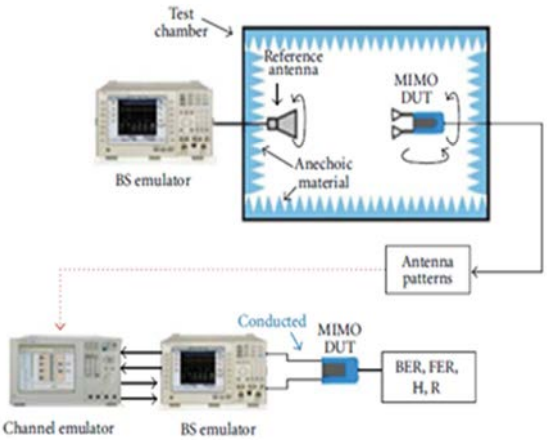

Figure 3-6 Proposed two-stage test methodology for MIMO OTA test. Source [38]

3.3.2.1 Radiated test method

This method is illustrated in Figure 3-7. It is using two probe antennas and one azimuth positioner in order to cover a large number of different angle of-arrival constellations. The two signals from the base station emulator are routed directly to the probe antennas with the chosen polarization. In the radiated test the constellations are categorized as spatial constellations, i.e., the azimuth orientation of the DUT and the elevation.

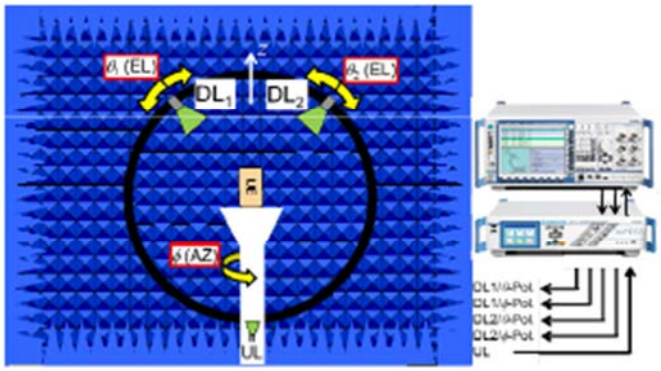

Figure 3-7 radiated test example. Source [40].

3.3.3 Multi-probe and fading emulator

This type of OTA test methodology groups a number of slightly different methodologies, but all of them include an anechoic chamber and several antennas that surround the DUT. These techniques are commonly referred as anechoic chamber based methodologies [39]. These methodologies consist of a large number of probe antennas placed inside an anechoic chamber transmitting with temporal and spatial characteristics for testing multiple antenna devices. Probe antennas are positioned around the DUT in such a way that it is possible to change the receiving spatial profile of Angle of Arrival (AoA) and consequently the Angle Spread (AS) at the DUT position. A schematic representation of the setup of a typical multi-probe method for MIMO OTA testing facility is illustrated in Figure 3-8.

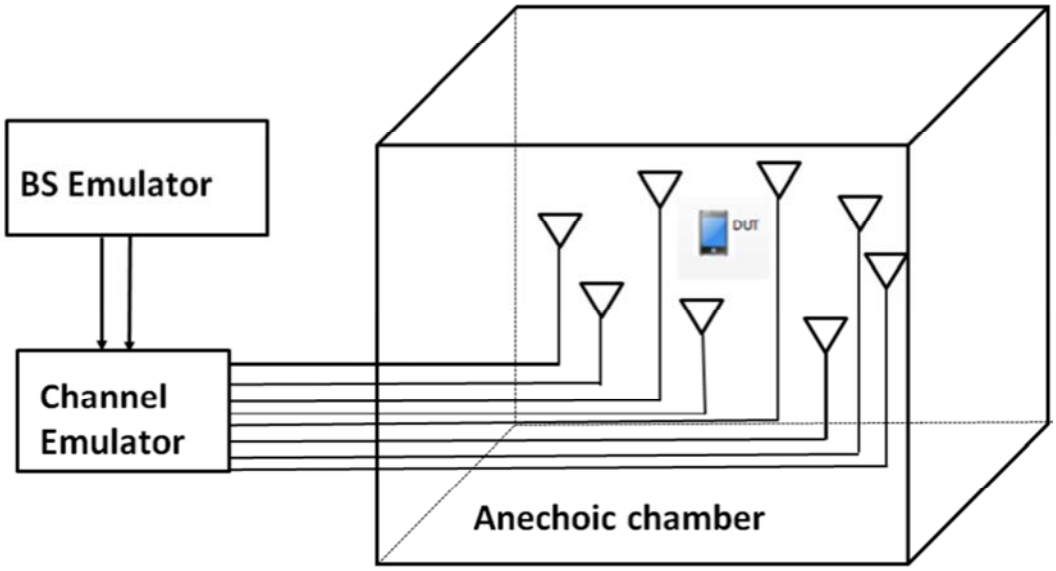

Figure 3-8 Illustration of a Multi-Probe MIMO OTA Testing. Source [38]

The contributions related to the anechoic chamber are very interesting. Khatun et al [93] clarify the very important issue of the required number of probes for synthesizing the desired fields inside a multi-probe system. The work by Kyosti et al. [94] show that the creation of a propagation environment inside an anechoic chamber with the ring of probes method requires a mapping of the original channel modeling on to the OTA antennas, with the geometric description being a prerequisite for the original channel model. In the following, we discussed some recent experimental realization for OTA test setups.

3.3.3.1 Sakata system fading emulator

The spatial fading emulator presented by Tokyo Institute of Technology and Panasonic [39] has been further developed in parallel at SP and Sony Ericson. Various aspects and measurements have been presented in COST 2100 Transmit Diversity (TD) s (see Figure 3-9). It is shown for the SFE has 62 dipoles antennas in 31 pairs dual polarized. Phase shifters, power dividers and attenuators, operating in the RF band, it has been shown that a realistic fading channel environment can be emulated reduce the influence from the measurement equipment.

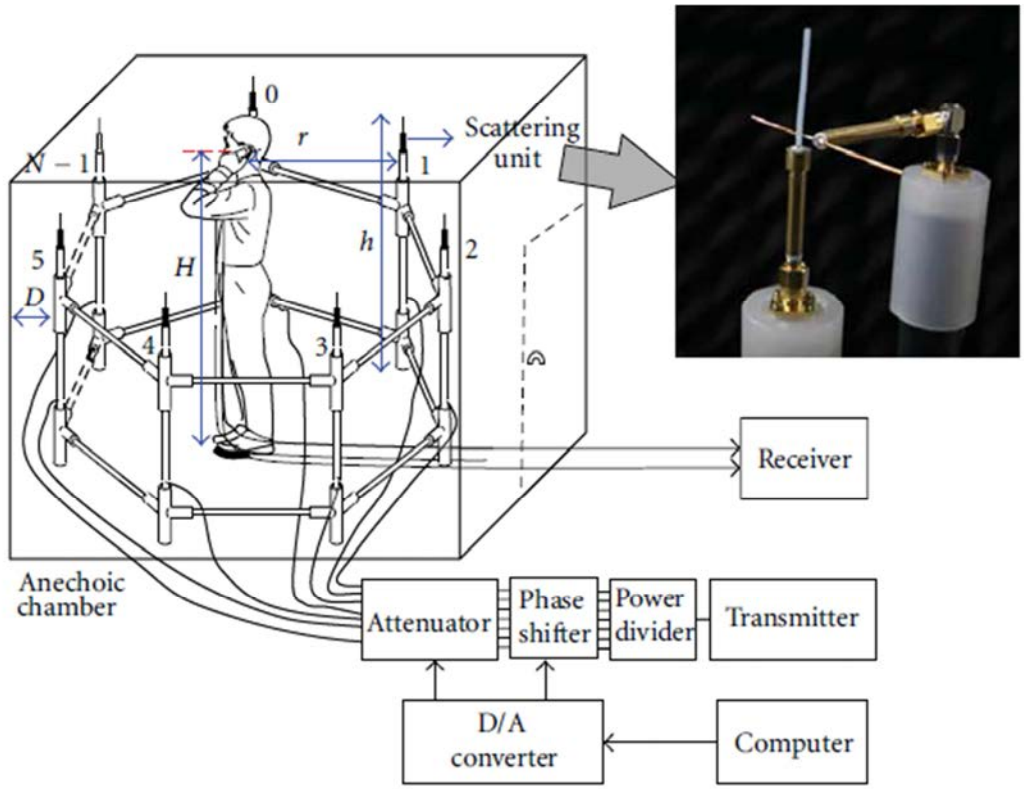

Figure 3-9 Spatial Fading Emulator Test Setup. Source [39].

The antenna probe consists of two antennas:

- A half-wavelength dipole set vertically.
- A horizontally-located half-wavelength dipole. This configuration can reproduce a cross polarization power ratio, XPR, of incoming wave. A measurement of the RF-controlled spatial fading emulator is carried out using the following procedure. The calibration procedure can be performed by using an electrical-controlled RF switch. Thus, the calibration of the emulator can be done automatically. Once the calibration is finished, the attenuators value can be modified in order to produce a special distribution of the incoming wave and to make a Cross polarization Power Ratio (XPR). Moreover, an initial phase can be imposed to each antenna probe to create a multipath fading channel.

3.3.3.2 SATIMO

Figure 3-10 shows SATIMO configuration [40]: 15 probes antennas are located on a circle with 45 cm radius. Only 8 probes are used since the multi-channel fading emulator used could only accommodate 8 outputs. Antennas are spaced 45° apart. Horizontal polarization of each probe is used in order to fit with the chosen channel models. The basic principle is to create a specific propagation environment at the DUT. The channel emulator has its outputs (8 multiple channels connected to the 8 probes surrounding the DUT) create multipath environment including delay dispersion, fast fading, path delays, and Doppler shift. The multipath signals are then transmitted to the DUT via probes.

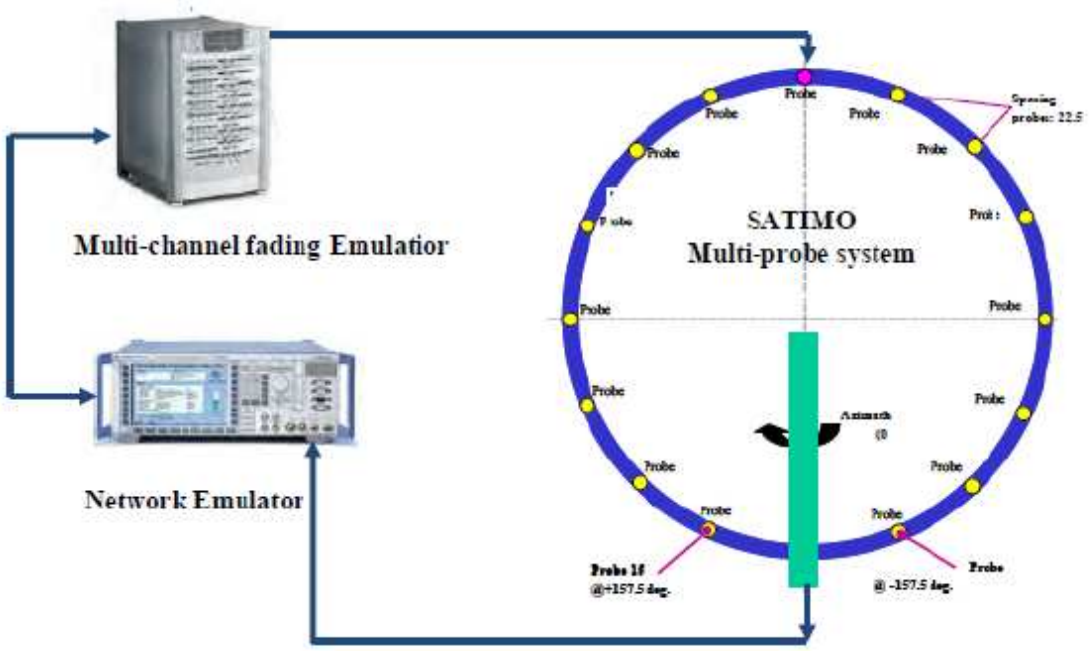

Figure 3-10 SATIMO Test Setup Components. Source [40]

Measurement capabilities of the SATIMO solution include evaluation of receiver diversity-based handsets, evaluation of MIMO performances of Wi-Fi, LTE and WiMAX-based handsets, and emulation of widely standardized 3GPP channel. It employs propagation models in a controlled environment, namely, single cluster, multiple clusters, and uniform. Emulation of variable angles of arrival, angular spread, cross polar ratio (XPR), Doppler, and delay spread are supported. The figures-of-merit are the device throughput in controlled fading environments, channel capacity and bit Error rate and antenna-related parameter characterization such as correlation and diversity gain.

3.3.3.1 Electrobit

Figure 3-11 depicts Electrobit OTA system, three OTA antennas were used in the chamber and they were positioned in a segment of Azimuth space with 20° spacing. The radio channel emulator used was EB Propsim C8. The MIMO OTA test setup is composed of a base station emulator, a multidimensional fading emulator, anechoic chamber, a number of OTA antennas and a DUT.

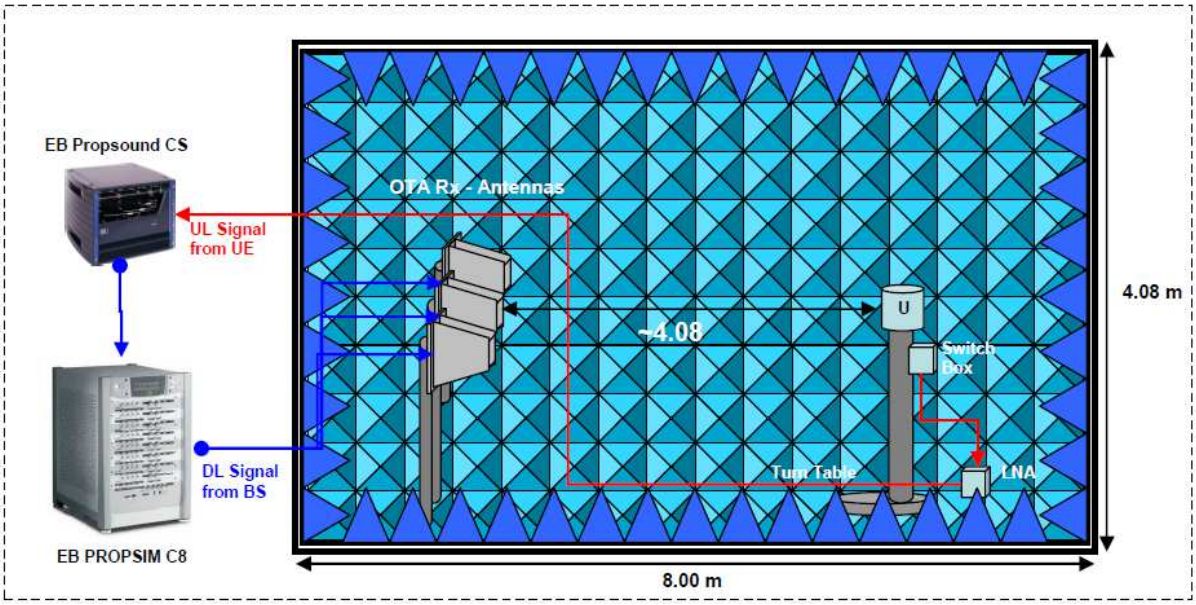

Figure 3-11 Electrobit test setup components. Source [41].

It is a MIMO-OTA test solution where flexible configuration for SISO, MISO/SIMO, and MIMO up to 4 * 4 or 8 * 4 is available. It supports 3GPP Release 10 and Release 11 enhancements including carrier aggregation up to 160 MHz, multiple RF bands, coordinated multi-point, and relaying. It provides the channel modeling applications for MIMO, beam forming, multiuser MIMO, smart antenna, and virtual drive testing. It provides integrated uplink and down-link signal separation, meaning there is no need for external duplexes. Both unidirectional and bidirectional fading modes are available and the system is compatible within the Electrobit Propsim product family. As the DUT antenna array is Electrobit uniform circular array (UCA) at 2.45 GHz. OTA antennas [41], where Aerial's LPD380-220 antennas, as depicted in Figure 3-12.

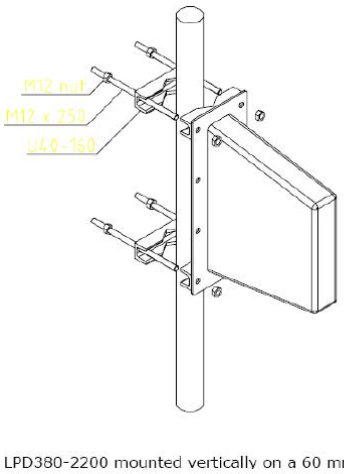

(a) OTA antenna

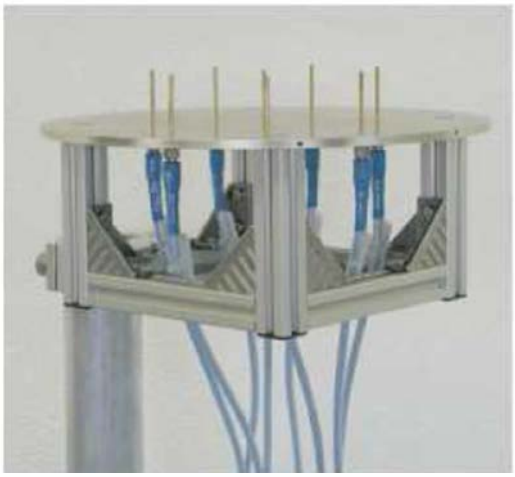

(b) DUT antennas

Figure 3-12 Characteristics of DUT (a) and OTA antennas (b).

3.3.3.1 Spirent

This MIMO-OTA solution determines the downlink MIMO-OTA performance using an anechoic chamber. The software facilitates comprehensive performance characterization including antenna, RF front-end, and base-band signal processing implementations. Through the characterization of antenna gain or efficiency, branch imbalance, and antenna correlation, for dual-polarized antenna conditions, it enables to precisely characterize the difference between a good and a poor design [42].

3.3.3.1 Rhode and Schwarz

The two-channel method was implemented by Rohde and Schwarz. It was focused in verification of the OTA performance on MIMO devices. The major component is on downlink (DL) 2 * 2 MIMO testing for spatial multiplexing and transmits diversity [43]. Measurements of receiver sensitivity and throughput were evaluated with statistical metrics. The TS8991 MIMO-OTA test system supporting the two channel method consists of an OTA chamber having three angular positioners to control angles, two test antennas (downlink), and one circularly polarized communication antenna (uplink) integrated in the azimuth positioner. Furthermore, the access panel permits five RF connections to the test antennas placed in the chamber. Two quad-ridged horn antennas are utilized as test antennas, each of which is capable of creating orthogonal components of linearly polarized field.

3.3.3.2 ETS-LINDGREN

ETS-LINDGREN developed a MIMO-OTA test system (model AMS-8700) for a multipath environment. The simulated environment is suitable for evaluation of downlink MIMO performance for emerging wireless technologies such as LTE, WiMAX, and 802.11n, Wi-Fi as well as receiving diversity performance of existing wireless technologies. The system consists of a dual-polarized antenna array in an absorber lined fully anechoic chamber, connected to technology-specific communication test equipment through a spatial channel emulator. The antenna array transmits downlink signals from a range of angles of arrival (AoA) as seen in Figure 3-13.

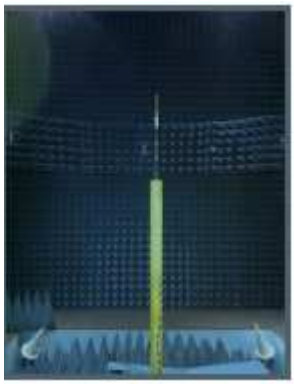

Figure 3-13 ETS-LINDGREN OTA system. Source [44].

The spatial channel emulator uses specially modified spatial channel models to feed each antenna in the array with a statistical sampling of the source signal(s) with appropriate Doppler and delay spreads, to emulate the scattering effect of fixed and moving objects. A positioning system allows the wireless DUT to be rotated through the generated field structure, to determine its relative performance in different orientations.

3.3.3.1 EMITE Ing

They have provided a solution for MIMO measurements with a second-generation multimode-stirred chamber. A MIMO measurement service with the 8 × 8 MIMO Analyzer Series E100 is available where up to 8 radiating element prototypes can be tested. Diversity gain, MIMO capacity, efficiency, and other parameters are provided for a variety of fading scenarios with and without the presence of the user. The developers claim that testing with this service could be the only fast and non-expensive alternative for novel LTE or WiMAX prototypes [45] as shown in Figure 3-14.

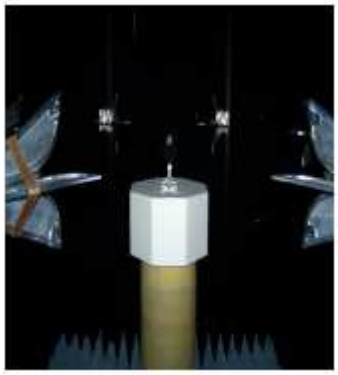

Figure 3-14 EMITE OTA. Source [45].

3.3.3.1 Agilent Technologies

The company is mainly involved in research and development of MIMO-OTA with focus on channel models and test methods for measuring the performance of MIMO devices in realistic environments. Results were presented for three OTA methods: the reverberation chamber method, anechoic chamber OTA, and two-stage OTA The results revealed that although the anechoic chamber method has the flexibility of emulating a variety of multipath conditions and does not require access to the user equipment antenna ports, it can become highly complex and costly to implement especially when dual-polarized measurements are required. This method also has the longest calibration and measurement times as well as the largest chamber requirements compared to other systems. It has been suggested to use a smaller number of probe antennas for reduced complexity and cost, but this makes system accuracy sensitive to calibration and measurement errors [46].

3.3.3.1 Aalborg University (AAU)

Figure 3-15 shows a test setup of the multi-probe setup mounted at AAU for testing DUT which is placed in an anechoic chamber surrounded by 16 probes on a 4 meters diameter. The probes are designed by AAU. The ring is covered by absorbers to avoid interactions with the emulated field. The probes are connected to channel emulator (2 EB F8 Unites) Through Power Amplifiers (PA). A base station (BS) emulator, and CMW500 and a Vector Network Analyzer (VNA) are connected via switching unit to the faders [47].

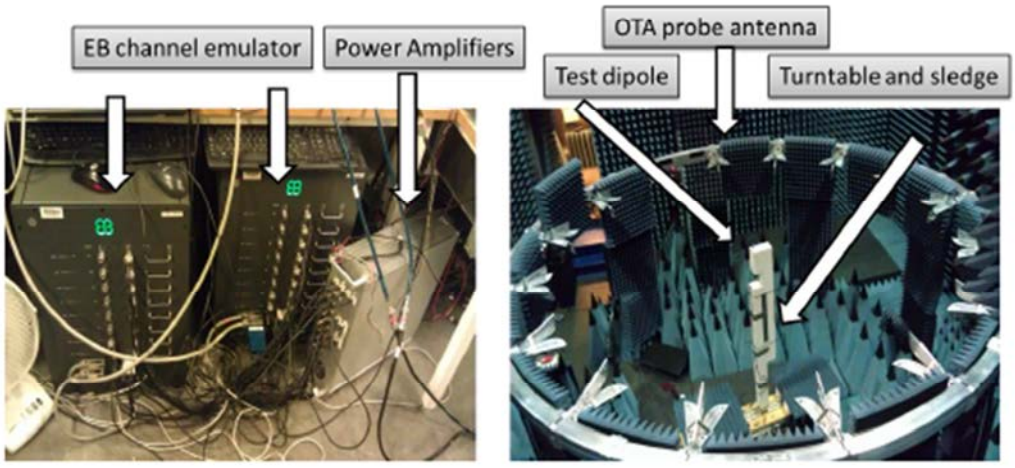

Figure 3-15 Test setup at AAU. Source [47]

Summarizing, the advantages of this method are:

- Measurements can be performed in an end-to-end way. On the contrary to the two-stage method, measurements with anechoic chamber method allow to actually measure the DUT as one complete system, including the antenna effect.
- Flexibility to emulate all the important parameters that characterize a channel model (Doppler shift, AoA, AoD, delay and polarization).

3.4 Recent advances on OTA techniques

3.4.1 Vehicular OTA

Nowadays, the history of technology advancement continues. The field of this development is interested in Intelligent Transport Systems (ITS). The technology called Vehicle-to-Vehicle (V2V) communication is a fast-growing technology that is capable of improving traffic safety and efficiency.

To insure road safety, vehicle industry has until now used some intelligent sensors, like radars, cameras to detect others cars. The received information is transmitted between cars in the dedicated frequency 5.9 GHz. This, technology provides some environmental benefits, which consists in reducing the consumption of fuel. The ability to accomplish the aim of these applications extremely depends on the quality of the V2V communication link, which rely upon the properties of the propagation channel [99]. Therefore, OTA methodologies, replaying the properties of the propagation channel becomes highly important.

In [101], authors test vehicular system by implementing the "virtual road, as seen in Figure 3-16. Vehicles nodes have been embedded into ad hoc meshed network structure, in order to safe, and secure the traffic management. A specific method and complex channel models have been used in V2V systems. Due to the Uncorrelated Scattered (US) channels characteristics. Scenarios to be emulated differ considerably from usual ones. The automotive industry system testing a car with its antennas is described in [100]. Measurements uncertainty of an OTA at 5.9 GHz has been given.

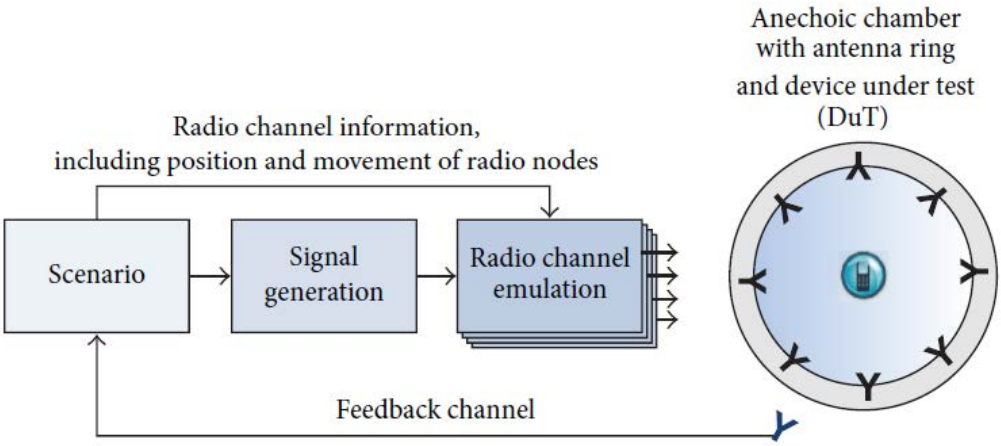

Figure 3-16 A typical implementation of an OTA *in* VEE test setup for the single-user downlink scenario for Mobile communication UE. Source [101].

3.4.2 3D OTA

As we mentioned in chapter 2, the propagation channel models are also dependent on the elevation, thus is three-dimensional. In this context, OTA test methodologies have been deployed to test wireless performance in 3D realistic channels models. Very few works have addressed this issue. Authors in [97] present a channel reconstruction technique for 3D MIMO OTA test setups, it was mentioned that 32 OTA antennas arranged in different elevation angles in a 3D setup were used to emulate 3D channel model, but no experimental realization of system is given. In [98] a 3D OTA test methodology using simulation approach is briefly described.

The OTA test setup where the DUT is placed in 3D plans, i.e. considering a volume test zone. Additionally, we present various realization of 3D OTA system which has been recently developed in the community in Table 3-2.

Table 3-2 OTA test facilities in [101].

Test facility	Chamber type	Hardware support	channel emulation	Frequency range
Forte	Anechoic chamber (5m*3.1m*4.5)	12*32 (physical channels)	Time domain processing similar to tap delay line (32 taps 350 MHz to 3 GHz Forte Anechoic chamber (5m_ 12_32 (physical (per physical channel) and frequency domain processing (unlimited fading paths per channel)	350 MHz to 3 GHz (4_4 channels
Vista	Anechoic (16 m*12 m *9m, max DUT size = 6 m)	Under research	Dynamically evolving geometry-based stochastic channel model	70 MHz to 6 GHz

On the other hand, the main disadvantage of this methodology is the growing complexity and cost when the number of probe antennas grows, compared to the other solutions in Table 3-3.

Table 3-3 Comparison of proposed test setups in anechoic chamber

Solution Developer	Chamber type and dimension	Hardware support	Channel emulation	Frequency range	Other features
Electrobit	Anechoic	2*2 to 8*4 up to 32 channels with 48 fading path per fading channel available	Standard (LTE, ITU, 3G) optional including LTE-A evaluation models, dynamic spatially evolving channel modeling	30-2700 MHz, RF interface channel signal BW 40 MHz	Support carrier aggregation up to 1600MHz Multiple RF bands, coordinate multipoint and relaying
Spirent	Anechoic	4 to 32 probe Layouts	Standard (3GPP, SCM/SCME) Winner, and ITU) and classical user defined models	Up to 6 GHz signal BW 26 MHz SR5500 Wireless channel Emulator	Transmit antenna having single as dual Polarisations
SATIMO	Anechoic	4 to 32 MIMO dual polarized probes	Propagation model in a controlled environment (single cluster, multiple cluster, and uniform)	400 MHz to 6 GHz	Positioner feature allowing to choose desired azimuth for testing the DUT in more orientations
Rhode and Schwarz	Anechoic (5m *5 m* 5m)	2*2 MIMO Downlink	10 MHz BW (LTE static channel)	Test results reported for Quad-ridget horn mode in 0.7 GHz band (TS8991 MIMO OTA)	antennas, dedicated ϕ and θ antennas connectors
ETS-Lindgren	Anechoic (4.9 m*4.9m*3.7m)	Not specified	Specially modified spatial channel models, appropriate Doppler and Delay spread to emulate the scattering effect of fixed and moving objects	700 MHz to 10 GHz(Model AMS-8700)	MIMO dual polarized environments simulation antennas

3.5 Multi-probe OTA channel emulation techniques

The multi-probe anechoic chamber method has appeared as a fundamental solution to reproduce different channels models accurately. The principle element in this methodology is the number of probes; each probe is fed by a channel emulator to generate the temporal characteristics of the desired channel model. Two channel emulation techniques are proposed in the literature. The methods are prefaded signal Synthesis (PFS) and plane wave synthesis (PWS). Both methods can create statistically equal radiated propagation environment within the test volume. The plane wave synthesis focused on individual rays while the PFS focuses on the concept of "cluster". A cluster being constituted by a certain number of rays. In a common terminology the cluster is understood as a propagation path diffused in space, either or both in delay and angle domains. Typically a cluster is composed of a fixed number a rays and has a specific shaped Power Angular Spectrum (PAS), for example, Laplacian function, defined by Angles of Arrives (AOA) and Angular Spread (AS).

The plane wave synthesis for MIMO OTA comes from traditional plane wave synthesis is in the field acoustics and electromagnetic. It is based on synthesis of the electromagnetic field environment using the spherical wave theory[47]. In [47] the influence of the number of probes on the geometrical size of the test zone and quietness of the test zone has been presented of the maximum relative error between the synthesized and intended field on the circumference of the test zone is evaluated, is called equivalent reflectivity level. Authors in [48] present a different approach of PWS, which consists into setting the incoming power angular spectrum (PAS) of the channel which is modeled as a collection of plane waves. This PWS technique can generate a specific AOA on the test zone by selecting properly the complex weights associated to each probe. The time variant channel can be also emulated in controlling the phase of the probes, to emulate a given Doppler effect.

The synthesis technique utilized in [49] is the PWS based on spherical wave theory. According to this theory, any arbitrary electromagnetic fields can be described by means of spherical wave expansion (SWE). This spherical wave expansion is the theoretical justification of the limited number of probes because of its well-known cutoff properties of the basis function. In [49], the rules for the number of probes as a function of the test zone size in wavelengths are presented for both 2D and 3D cases. Then accurate rules for the minimum number of required probes have been established taking into account the uncertainty level of the 2D field synthesis.

With respect to PWS, two types of setup exist, one where the distances between OTA probes satisfy the Nyquist sampling criterion and other one where such criterion is not satisfied. The latter is typically the reciprocal of near-field antenna measurement setups or the real-time equivalent of the near-field setup working with virtual synthesis. The proposed multi-probe based OTA test setups in the literatures are of the latter type. Principally, irrespective of the two types, for synthesis, one should find those excitation voltages of the OTA probes that cause the superposition of the radiated fields to match the prescribed fields tangential to the surface of the test volume [50] .

For the first type of setups, the synthesis is done just by taking the components of the target field at the OTA probe positions tangential to the test surface by utilizing the Huygens' Principle. This is typically the approach studied in acoustic wave field synthesis and in [51].

For the second type of setups, almost invariably inversion, of the known fields generated by the OTA probe on the test zone surface, is used to derive the proper excitations for the OTA probe. The PWS reported in [52], is based on the synthesis of electromagnetic field environment using the spherical wave theory, whereas [53] deals with PWS based on a plane-wave description. In [57], the PWS is considered for pure 2D case with hypothetical line sources while regular OTA ring array is considered in [56].

3.5.1.1 Required theoretical number of OTA probes

In this section, we recall the rule for the minimum number of OTA antennas as a function of the radius of Zone under Test (ZUT) in wavelengths through the spherical wave theory. The spherical wave expansion has been long known and used in this context of radiation problems [45]. The spherical wave function forms an orthogonal set that provides a complete solution to Maxwell's equations in free space. The electric field in a source-free region of space can be written as a weighted sum of the spherical wave functions as:

$$\bar{E}(R,\theta,\phi) = \frac{k}{\sqrt{\eta}} \sum_{c=1}^{4} \sum_{s=1}^{2} \sum_{n=1}^{N} \sum_{m=-n}^{n} Q_{smn}^{(c)} \bar{F}_{smn}^{(c)}(R,\theta,\phi) \tag{3.1}$$

Where $\bar{E}(R,\theta,\phi)$ is the electric field in standard spherical coordinates (R,θ,ϕ) k is the wave number; $\eta = \sqrt{\frac{\mu}{\epsilon}}$ is the free-space field impedance; s, m and n are the spherical mode indices $Q_{smn}^{(c)}$ are the spherical vector wave coefficients; and $\bar{F}_{smn}^{(c)}(R,\theta,\phi)$ represent the power normalized spherical vector wave functions in spherical coordinates. It is known that the $\bar{F}_{smn}^{(c)}(R,\theta,\phi)$functions are separated into radial, elevation and azimuth functions, where the radial functions are specified by the upper index c, the elevation functions are the Associated Legendre function and the azimuth functions are the exponential functions. Index n represents the degree of the radial function, index m is the index for the azimuth functions and values of s = 1 and 2, represent the transverse electric and the transverse magnetic field. The functions $\bar{F}_{smn}^{(c)}(R,\theta,\phi)$ are defined as:

$$\bar{F}_{1mn}^{(c)} = p_{mn}\left\{ z_n^{(c)}(kr) \frac{im\bar{P}_n^{|m|}\cos\theta}{\sin\theta} \overline{a_\theta} + z_n^{(c)}(kr) \frac{d\bar{P}_n^{|m|}\cos\theta}{cos\theta} \overline{a_\phi} \right\} \tag{3.2}$$

And

$$\bar{F}_{1mn}^{(c)} = \frac{n(n+1)}{kr} \bar{P}_n^{|m|}(\cos\theta)\, \bar{a}_r + \frac{1}{kr} \frac{(kr)}{d(kr)}\, z_n^{(c)}(kr) \frac{d\bar{P}_n^{|m|}\cos\theta}{cos\theta} \bar{\theta} \tag{3.3}$$

With

$$p_{mn} = \frac{1}{\sqrt{2\pi}} \frac{1}{\sqrt{n(n+1)}} \left(\frac{m}{|m|}\right)^m e^{im\phi} \quad (3.4)$$

Where $\bar{P}_n^m$ is the normalized Associate Legendre function. $z_n^{(c)}(kr)$ is one the functions
z_n^1 Spherical Bessel function z_n^2 spherical Neumann function z_n^3 Spherical Hankel function of the first kind z_n^4 spherical Hankel function of the second kind where $c = 1$ and $c = 2$ correspond to radial standing waves, finite or infinite at the origin, respectively, whereas $c = 3$ and $c = 4$ correspond to radial outgoing and incoming waves, respectively. Due to the well-known cut-off property of the spherical wave functions, the expansion in (3.3).

$$N = [kr + n_1] \quad (3.5)$$

Where r is the radius of the minimum sphere that fully encloses the device, n_1 is a small integer number, and the square brackets indicate the nearest integer number greater than or equal to the number inside the brackets. Typically, n_1 varies from 0 to 10 depending on the desired accuracy of the field characterization. For electrically relatively small antennas, for instance, antennas $r \leq 2\lambda$, a clearly smaller value, e.g.., n_1= 2 can be applied is the wavelength of carrier frequency. The spherical wave mode, indicated by j index is calculated from j = 2 (n (n + 1) + m - 1) and the total number of modes in spherical wave characterization is:

$$J = 2N(N + 2) \quad (3.6)$$

Now, in theory, for synthesizing all J modes, the minimum number of probes, N_{antmin}, is equal to the number of modes J. Hence the general rule for required number of probes in 3D case, where the probes are distributed over a sphere and both the elevation and azimuthal distribution of the incoming waves are considered, becomes:

$$N^{3D}{}_{antmin} = 2(kr + n_1])^2 + 4([kr + n_1]) \quad (3.7)$$

The noticeable issue in 3.7 is that the (3D) number of the OTA antennas is proportional to the square of the (ZUT) radius r and the value for n_1.

In the azimuth plane, we can derive the minimum number of probes in 2D case as:

$$N^{2D}{}_{antmin} = 2([kr + n_1] + 1) \tag{3.7}$$

We summarize some values of required number of OTA antennas according to DUT radius in Table 3-4.

Table 3-4 ZUT radius as function of number of OTA probes in 2D case.

Number of probes $N^{2D}{}_{antmin}$	ZUT radius r [λ]
4	0.22
8	0.45
16	0.75
32	1.19

3.5.2 Pre-faded signal synthesis (PFS)

This technique was proposed in [95] the focus is on reproducing the channel spatial characteristics in the test volume. The objective is to find the optimum power weights of the OTA probes that minimize the correlation error between the theoretical spatial correlation resulting from the target continuous PAS and the synthesized spatial correlation resulting from discrete PAS. This technique has been implemented in several commercial channel emulators [52][96]. The so-called pre-fading approach differs from the PWS approach because fading results not only from the superposition of the waves at the level of the zone under test but this intended effect is produced partially at the level of the excitation probes of the OTA device.

Of the two described techniques for emulating the field environment inside the test zone, an advantage of the PWS is that the PWS approach supports the emulation of any circumstances of an arbitrary channel whereas PFS doesn't support modeling of LOS path with arbitrary AoA and thus not with dynamic LOS path direction neither. Additionally, PWS supports controlled linear, circular, or elliptic polarization of the multipath. A drawback of the PWS is that it requires a phase calibration which is not needed in PFS.

In PWS technique using Huygens' Principle, the Huygens' sources are placed on the surface of the test volume and thus the required chamber will be small in size, which reduces the cost of the MIMO OTA test setup significantly.

On the other hand, the mutual coupling between the sources will be increased for such a large number of sources placed on the test surfaces, resulting in increased measurement uncertainty and need of complex antenna calibration. Additionally, this method increases the system cost due to a required large number of coherent output channels of the fading emulator. For these reasons, the PFS technique will be adopted in this work to emulate a different channel model. The concept of this method is detailed in the next chapter. Table 3-5 compares different characteristics for OTA test methodologies in this chapter.

Table 3-5 Comparison between different MIMO OTA methodologies.

Attribute	Reverberation chamber	Anechoic chamber	Two stage method
Major components	Reverberation chamber	Channel emulator probe, antennas, anechoic chamber	Channel emulator, probe antenna, anechoic Chamber
Number of antennas	2-4	8- 32 varies	
Channel 2D/3D	3D	2D/3D	2D/3D
Number of spatial cluster	1	2D/3D varies)	2D/3D
Power Angular Spectrum per cluster	Uniform	Controllable	Controllable
As	Random	Controllable	Controllable
PDP	Exponential decay	Controllable	Controllable
DS	Slight Controllable	Controllable	
Doppler sift limited	Controllable	Controllable	
Support channel models	Uniform	SCME, cluster, uniform,	Single cluster, uniform
Cross Polarization Ratio (XPR)	Constant	Controllable	Controllable
Ability to control interference direction	None	Yes	Yes
DUT size constraints	None	0.5-4λ	None
Calibration equipment/ Method	2port VNA	Joint OTA link calibration using 2 port VNA	Chamber calibration by 2 port VNA second stage calibration
Requires non-intrusive test mode for antenna pattern measurement	N/A	No	Yes
Throughput measurement method	OTA	OTA connector	Conducted via temporary antenna

3.6 Conclusion

It is now generally admitted that geometric channel models with well-defined characteristics such as complex amplitudes, directions of arrival directions of departure delays, and polarizations of the multipath components constitute a good means to describe the radio-propagation channel. What is expected is to exploit those channel models in the context of real devices testing. In this chapter we provided an overview of the different approaches and techniques to test devices performances exposed to different radio propagation channel models. The first approach which has been presented is the two stage method which cannot really be qualified as fully "over the air" and two other approaches "fully over the air" which exploits different kind of confined environments either reverberant or anechoic.

The two-stage method has the problem with the cable connection to the antenna ports it requires, which means that the test is never performed in the realistic usage conditions of the device under test. The difficulty with reverberation chamber-based methods is that they are not well suited for synthesizing all channel conditions in line with usual geometric radio channel model. From these technical points of view the anechoic chamber based methods appear to be the most promising method for device performance evaluation. For this reasons we adopted the **multi-probe anechoic chamber** based method. This choice is made for several reasons: the ability to emulate a variety of fading scenarios, while controlling its geometric characteristics (i.e. AoA distribution).

This chapter shows that the major challenge for OTA testing with the multi-probe method is to emulate a realistic environment which accurately reflects the real wireless propagation environment. Mainly two channel emulation techniques have been proposed in the multi-probe based OTA setups. One technique is the plane wave synthesis (PWS) technique reported in [52][53]. The basic idea of the PWS technique is that static plane waves with arbitrary impinging angle of arrivals (AoAs) can be created. The other technique is named the prefaded signal synthesis (PFS) technique and has been adopted in several commercial emulators' tools [56]. The essence of this technique is to reproduce the channel desired spatial characteristics at the receiver side.

After having determined the OTA methodology that meets our needs, we will be interested in the next chapters to address the question of how to dimension the proposed multi-probe OTA test setup, based on simulations approaches in order to propose an optimal experimental realization in the anechoic chamber.

Chapter 4

4 Multi-probes OTA Setup Dimensioning

4.1 Introduction

Different Over-The-Air (OTA) test methodologies have been presented in Chapter 3. Among the OTA methodologies aiming to emulate the radio channel in realistic manner: reverberation chamber, two stage methods, and the multi-probe anechoic chamber based system have been considered. Due to the capability of the multi-probe anechoic chamber method to reproduce multipath environment in repeatable and controllable manner, and the capacity to control the polarization and spatial characteristics of the channel, we considered this approach in our work.

In this approach an array of antennas are disposed in a zone around the Device Under Test (DUT) and connected to a fading emulator that distributes the signal over the proves to reproduce different channels models in the Zone Under Test (ZUT). The probes can be fed in order to reproduce a planar wave impinging from a certain direction, according to the so-called Planar Wave Synthesis (PWS) previously discussed. Alternatively the Pre-Faded Signal (PFS) techniques apply a distorted signal in order to reproduce the stochastic channel characteristics.

In this chapter, we address the issue of dimensioning the two dimensional (2D) and three-dimensional (3D) multi-probes OTA test setup. The purpose is to provide guidelines for the design of the OTA ring and the choice and emplacement of OTA antennas, according to the channel and the size of the aimed ZUT the size of the anechoic chamber, antennas placement, have to be addressed.

For this purpose we first introduce the criteria and the metrics used to dimension the OTA multi-probe setup. Then using the spatial correlation as a figure of merit we investigate the dimensioning of 2D and 3D OTA setups. The Matlab tool developed allows characterizing the spatial correlation in the ZUT by jointly considering to the number of antennas and their emplacement, as well as the ring radius. In the 2D setup also the effect of near field condition are analyzed considering half-wavelength probes as antennas. The analysis is carried out as a function of the frequency and the channel. In particular here we considered a Clarke's scenarios, i.e. isotropic channel, and a single cluster channel. PFS technique is applied in both the 2D and 3D setups in order to reduce the spatial correlation error.

4.2 Criteria and metrics for OTA setup dimensioning

In the literature different works investigated the key aspects related to the multi-probe system setup dimension [60]. One of the issues in OTA multi-probe system design is the location of OTA antennas around the ZUT. Several OTA setup realization in the literature, have employed horn antennas and Vivaldi antennas [103].

The antennas are often disposed on a ring, whose physical dimension determines the emulation accuracy in the OTA system. In [60] criteria for physical dimensions are developed based on field strength stability and phase stability across the test zone. In this section, we start by reviewing some criteria related to dimension multi-probes OTA test setups and provide metrics to determine it.

4.2.1 Far Field criteria

One of the common criteria when measuring the antenna is to respect the far field condition. Let's consider a generic antenna as shown in Figure 4-1. It is very well known that the *reactive near-field* region is the region immediately surrounding the antenna, defined as $0 < r < R1$, where r is the radial distance between the antenna and the point of observation. In this region, the field is reactive and therefore non-radiating. The boundary of this region for a short dipole antenna is defined as $0 < r < \lambda/2\pi$, where λ is the wavelength. The region in the immediate neighborhood of the far-field region is the *radiating near-field region*, i.e., $R_2 > r \geq R_1$. This region is also the intermediate region between the far-field and the reactive near-field regions. In this region, fields decay more rapidly than 1/r and the relative angular distribution of the fields varies with r. Moreover, the phase error decreases with an increase in r (as $r \rightarrow \infty$ the phase error becomes zero). For an antenna with D as the largest dimension, generally larger than one wavelength, the commonly used criterion to define the boundary between the radiating near field and *far field region is* defined in terms of the Fraunhofer distance [104], as follows:

$$r \geq \frac{2D^2}{\lambda} \tag{4.1}$$

In the far field region, the radiation pattern does not change shape with distance (although the fields still die off as 1/r, the power density dies off as $1/r^2$). Also, this region is dominated by radiated fields, with the E- and H-fields orthogonal to each other and the direction of propagation as with plane waves.
These criteria explicitly concern antennas for which the maximum overall dimension, D, is large with respect to the wavelength.

In [105], it was shown that when considering dipoles we can find at $r < \lambda/2\pi$ as much reactive power as active power. Authors demonstrated that this value should rather be set at 1.62 λ for infinitesimal and short dipoles, 2 λ for half-wavelength dipoles, and 3 λ for one-wavelength dipoles. Also they had shown that the transversality condition is more restrictive than the sphericity condition. Thus, the far-field zone lower boundary is located at 10 λ.

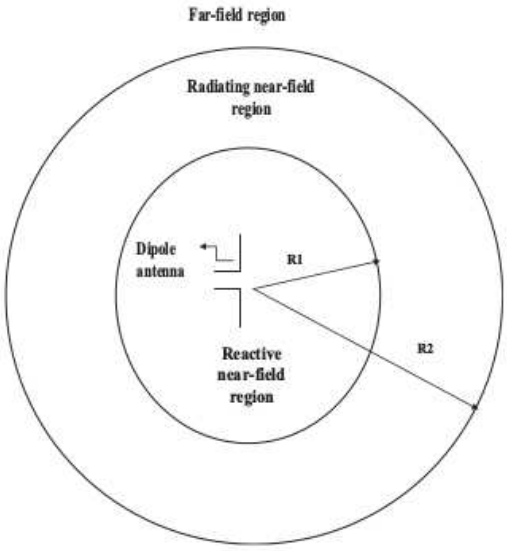

Figure 4-1 Field regions of thin dipole antenna.

CTIA provided a reference document for test of mobile station Over the Air [80]. In this report CTIA specifies minimum *r* with three conventional far field criteria, as below:

- $r > \frac{2D^2}{\lambda}$ (the Fraunhofer distance)
- $r > 3\lambda$
- $r > 3D$

Actually the third criterion is based on the amplitude uncertainty. The more restrictive of these criteria should be employed. However it is worth to notice that this test plan is provided to perform standards measurements of total radiated power (TRP) and total isotropic sensitivity (TIS) for GSM, CDMA, GRPS and LTE systems device. In particular in [80], the device dimension is considered equals to 0.3 m. Let us consider 30 cm and 15 cm as an example of typical device dimension.
Aiming to perform OTA measurements on a wideband in Figure 4-2, we show the far field criteria in the 2-6 GHz band. It can be clearly seen that, accordingly to the frequency and the device dimension one criteria is more stringent than others.

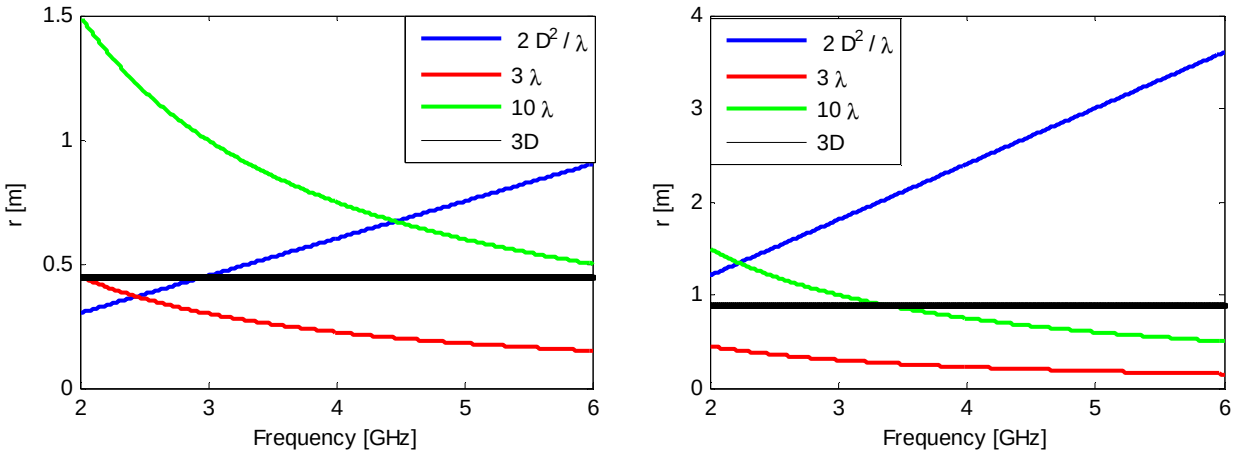

(a) (b)

Figure 4-2 Far field criteria with fixed DUT size: 15 cm (a) and 30 cm (b)

Obviously in emulating the channel one would ideally look for far field condition. However this criterion is not the only one request. Actually, the multi path fading should be reproduced and a dedicated metric should be used.

4.2.2 Spatial correlation

In the previous chapter, we demonstrated the importance of channel modeling for the evaluation of MIMO system and a proposal which enables the consideration of the coexistence of NLOS and LOS paths. Multi-path-richness refers to an environment which is surrounded by many scatterings or tall buildings resulting in waves coming from many different spatial directions. When talking about the propagation channel, spatial correlation is an important metric that indicates how the channel is correlated along time or equivalently distance. In particular for multi-antennas systems it determines the performance and is strictly related to the antenna separation. Here we consider the channel spatial correlation as metric to evaluate the quality of OTA. The underlying assumption is that the channel is Wide Sense Stationary with Uncorrelated Scattering (WSSUS) as explained in chapter 2.

In practice the spatial correlation is determined the Power Angular Spectrum (PAS). When considering two antennas at positions *i* and *j* the spatial correlation coefficient can be expressed as [55]:

$$\rho_{i,j} = \frac{\int_0^{2\pi}\int_0^{\pi} \boldsymbol{E}_{A_i}(\theta,\phi)\cdot \boldsymbol{E}^*_{A_j}(\theta,\phi)\, PAS(\theta,\phi) d\theta\, d\phi}{\sqrt{\int_0^{2\pi}\int_0^{\pi}\left|\boldsymbol{E}_{A_i}(\theta,\phi)\right|^2 PAS(\theta,\phi)\, d\theta d\phi}\ \sqrt{\int_{-\pi}^{\pi}\int_0^{2\pi}\left|\boldsymbol{E}_{A_j}(\theta,\phi)\right|^2 PAS(\theta,\phi) d\theta\, d\phi}} \tag{4.2}$$

Where $\boldsymbol{E}_{A_i}(\phi)$ and $\boldsymbol{E}_{A_j}(\phi)$ are the complex incoming field on DUT antennas *i* and *j* placed on the DUT. $PAS(\theta,\phi)$ is the distribution of Angle of Arrivals (AoAs) in elevation and azimuth. Thus the spatial correlation, and consequently the performance of a wireless system, depends generally on the density distribution of angles of departures and arrivals. In the case of scatterers uniformly distributed [0, 2 π[in the azimuth plane the PAS reduces to:

$$PAS(\phi) = \frac{1}{2\pi}, \phi \in [0,2\pi[\tag{4.3}$$

In this case the module of the complex correlation for a distance *d* is given by the zero order Bessel function [79][106].

$$|\rho(d)| = |J_0(kd)| \tag{4.4}$$

Where $k = \frac{2\pi}{\lambda}$. When the scatterers are uniformly distributed in all 3D space, the amplitude of the correlation coefficient can be described by the sinus cardinal function as [79].

$$|\rho(d)| = \left|\frac{\sin(kd)}{kd}\right| \tag{4.5}$$

In Figure 4-3 we represent the variation of the correlation function as function of distance or equivalently the antenna separation, showing that first null comes at 0.4 λ in 2D and 0.5 λ in 3D.

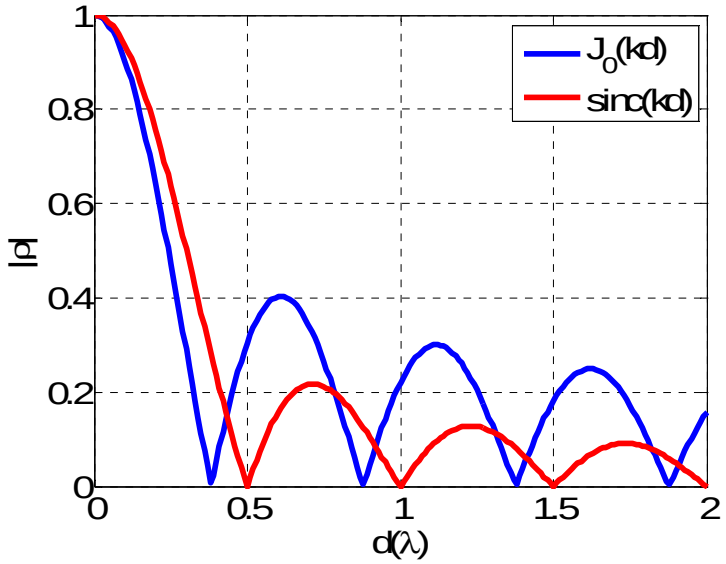

Figure 4-3 Theoretical spatial correlation in 2D and 3D isotropic channel model

To assess the performance of wireless communication systems, various geometrical channel models of realistic radio channel representing real world environments have been proposed in the literature [81][82]. Different angle of arrival distribution have been proposed in different GSCMs studied. For example, the 3GPP model with SCME that is useful for OTA channel emulation in different environments is described. Multipath components are often grouped in clusters whose distribution depends on the environments and model. A commonly used intra-cluster distribution is the Laplacian one, which can be expressed as:

$$PAS(\phi) = \frac{1}{\sigma_\phi \sqrt{2}} e^{\frac{-|\phi - \bar{\phi}|\sqrt{2}}{\sigma_\phi}} \tag{4.6}$$

Where $\bar{\phi}$ is the mean angle of arrival and σ_ϕ is the angular spread. For instance in the single cluster SCME model the AoA distribution is Laplacian and the SCME Urban Micro-cell model with all AoAs assumed to be zero, for OTA purposes the angular spread can be specified with σ_ϕ= 35º or with σ_ϕ= 25º to enable a range of spatial correlation for different types of devices.
For 3D channel a common assumption is to consider independent distribution of azimuth and elevation angles [83]. Under this assumption the 3D Power Angular Spectrum (PAS) can be written as:

$$PAS(\theta, \phi) = PAS(\theta) \cdot PAS(\phi) \tag{4.7}$$

Where $PAS(\phi)$and $PAS(\theta)$ are the power spectrum in azimuth and elevation respectively. Therefore, we considered two antennas under test A_i and A_j separate one from the other by a distance d. It should be noted that we correlated channels and not electromagnetic fields. The implication is that we should always specify what the hypothesis of the projection of the field across DUT. For example if the fields are all vertically polarized, the resultant is also vertical and the orientation of DUT is also a vertical antenna. If all fields are coming from different direction in space with a horizontal polarization, it is no longer possible to stay in the Omni-directionality hypothesis because the orientation of the DUT induced necessarily a polarization of spatial correlation. We considered the first case where antennas are omnidirectional, in vertical polarization.

4.3 Two- dimensions OTA setup

Let us consider two antennas A_i and A_j separate one from the other by a distance *d*. As longs as the scatterers are distributed over the azimuth plane, the spatial correlation can be expressed as [79]:

$$\rho_{theo_{(i,j)}} = \frac{\int_{-\pi}^{\pi} \left|\boldsymbol{E}_{A_i}(\phi)\right| \left|\boldsymbol{E}_{A_j}(\phi)\right| \, PAS(\phi) exp\left(-j2\pi \frac{d}{\lambda}(cos(\phi - \phi_i)\right) d\phi}{\sqrt{\int_{-\pi}^{\pi} \left|\boldsymbol{E}_{A_i}(\phi)\right|^2 PAS(\phi)\, d\phi} \sqrt{\int_{-\pi}^{\pi} \left|\boldsymbol{E}_{A_j}(\phi)\right|^2 PAS(\phi)\, d\phi}} \tag{4.8}$$

Where λ is the wavelength, d is the DUT antennas separation and ϕ_i represents the angular orientation in the azimuth plane of the *i*-the DUT antenna.

Let us consider a 2D OTA ring as depicted in Figure 4-4, where s probe antennas are placed over a finite ring radius *R* and ϕ_s is the angular position of each s-th antennas. DUT antennas are separated by distance *d*. $R_{i,s}$ and $R_{j,s}$ are the distance between OTA antenna and (i,j) DUT antennas. In this work we consider that the *j*-th antenna is opposite to the *i*-th one. Hence ϕ_j=ϕ_i- π.

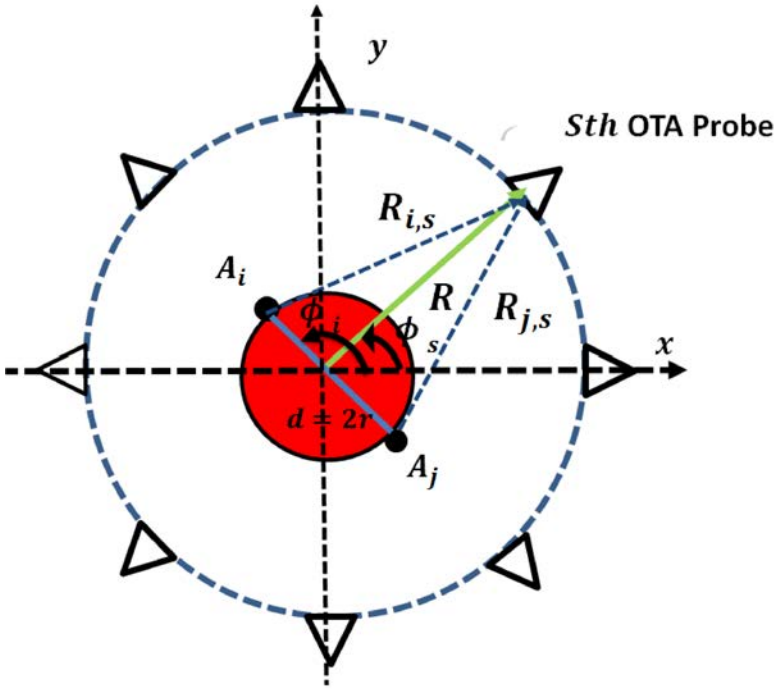

Figure 4-4 Multi-probe OTA setup

$$\rho_{OTA_{(i,j)}} = \frac{\sum_{s=1}^{N_{ant}} \boldsymbol{E}_{A_i}(R_{i,s},\phi_s) \cdot \boldsymbol{E}^*_{A_j}(R_{j,s},\phi_s)\ P_s}{\sqrt{\sum_{s=1}^{N_{ant}} \left|\boldsymbol{E}_{A_i}(R_{i,s},\phi_s)\right|^2 P_s}\ \sqrt{\sum_{s=1}^{N_{ant}} \left|\boldsymbol{E}_{A_j}(R_{j,s},\phi_s)\right|^2 P_s}} \tag{4.9}$$

Where $\boldsymbol{E}_{A_i}(R_{i,s},\phi_s)$ and $\boldsymbol{E}_{A_j}(R_{j,s},\phi_s)$ are the incident field on A_i and A_j antennas respectively, and P_s is the power weight of the s-th OTA probe.

Based on the spatial correlation, the accuracy of the OTA emulation can be analyzed in terms of error in correlation as expressed here below:

$$\varepsilon(d) = \sqrt{\left\langle \left| |\rho_{theo_{(i,j)}}(d)| - |\rho_{OTA_{(i,j)}}(d)| \right|^2 \right\rangle} \tag{4.10}$$

This metric is then used in simulations in order to dimension the OTA setup in terms of radius of the OTA ring and number of antennas, according to the wavelength and DUT dimensions. However it has to be noticed that the spatial correlation expressed in (4.8) is based on the hypothesis of far field and planar wave condition. In practice this could not be verified in realistic OTA deployment because of some physical constraints.
Let us consider a generic dipole of length *l*, as depicted in Figure 4-5.

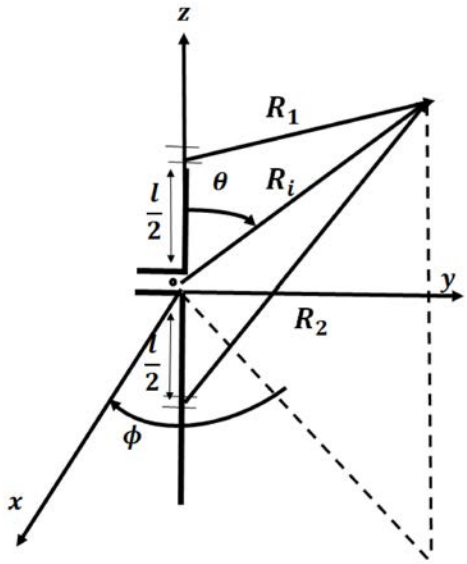

Figure 4-5 Dipole antenna of length *l*

The incident field on the generic antenna A_i, on the vertical polarization (here the z-axis) can be expressed in cylindrical coordinates as [64]:

$$\boldsymbol{E}_{A_i} = \widehat{\boldsymbol{a}_\rho} E_\rho + \widehat{\boldsymbol{a}_z} E_z \tag{4.11}$$

where

$$E_\rho = \quad E_y = -j\eta \frac{I}{4\pi y}\left[\left(z - \frac{l}{2}\right)\frac{e^{-jkR_1}}{R_1} + \left(z + \frac{l}{2}\right)\frac{e^{-jkR_2}}{R_2} - 2z\cos\left(\frac{kl}{2}\right)\frac{e^{-jkR_{i,s}}}{R_{i,s}}\right] \tag{4.12}$$

and

$$E_z = -j\eta \frac{I}{4\pi}\left[\frac{e^{-jkR_1}}{R_1} + \frac{e^{-jkR_2}}{R_2} - 2\cos\left(\frac{kl}{2}\right)\frac{e^{-jkR_{i,s}}}{R_{i,s}}\right] \tag{4.13}$$

where η is the free space impedance, k is the wavelength number, and

$$R_1 = \sqrt{\rho^2 + \left(z - \frac{l}{2}\right)^2} \tag{4.14}$$

$$R_2 = \sqrt{\rho^2 + \left(z + \frac{l}{2}\right)^2} \tag{4.15}$$

It should be noticed that the second term of (4.12) and (4.13) disappear when the overall length is an integer number of odd half-wavelength.
In the following, we will consider half-wavelength as OTA antenna probes, in order to assess about the effect of the radius of the ring in the accuracy of the spatial correlation in 2D OTA setups.

4.3.1 Simulation framework

In order to assess the correlation accuracy of 2D OTA multi-probe setups, we considered two antennas at DUT, i.e. A_i and A_j, separated by a distance *d*.

The DUT is arbitrarily oriented in the azimuth plane, hence ϕ_i is considered uniformly distributed in [0, 2π [.
Here we consider two channels:

- **isotropic channel**, corresponding to the Clarke's scenario where the scatterers are uniformly distributed according to (4.3)
- **single cluster channel**, where the scatterers are distributed according to Laplacian distribution (4.6), whose angular spread is chosen to be equal to 35°[82].

DUT was chosen to be arbitrarily oriented, hence in simulations $\phi_i$was uniformly distributed in [0, 2π [. Spatial correlation is computed from 100000 realizations, corresponding to different DUT orientations. As a first step the $P_s$weights in (4.9) were computed by direct sampling of the PAS of the desired channel model.

4.3.2 Results

4.3.2.1 2D isotropic scenario

In Figure 4-6 we show the absolute value of the spatial correlation as a function of DUT size, in the isotropic 2D channel. Here all incoming paths at DUT are supposed to have the same energy contribution. Hence the expected correlation follows the classical first kind zero order Bessel function $J_0(kd)$ This behavior is verified for a huge number of scatterers, i.e. OTA antenna probes, and correlation approaches the zero value at the integer multiple of 0.4λ, as expected.

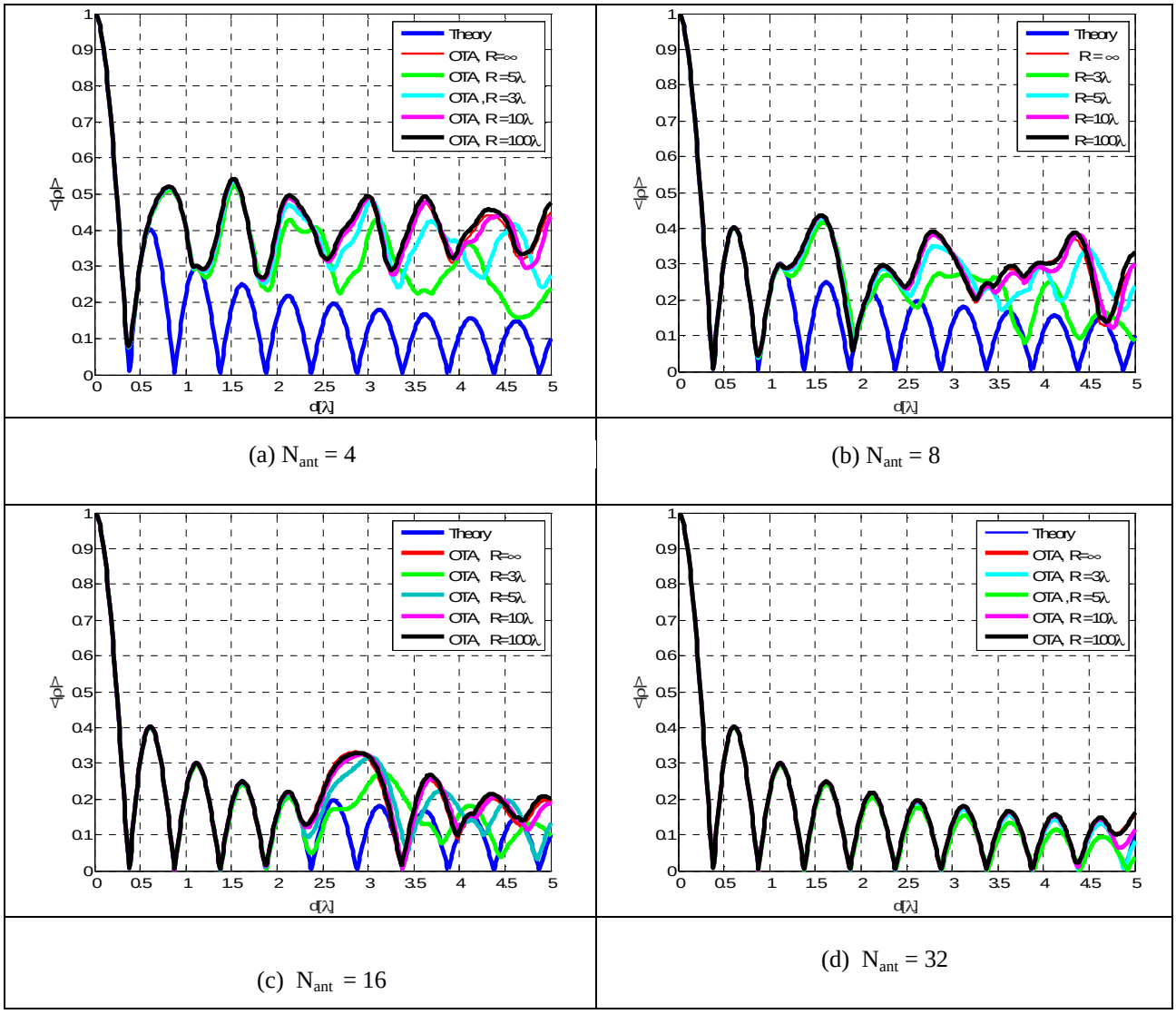

Figure 4-6 Spatial correlation in 2D isotropic channel as a function of the number of probes and radius of OTA ring

The accuracy of the OTA emulated spatial correlation is affected by the number of antenna probes: a high number of antennas allows a fine sampling of the PAS and increases the quality of the OTA channel emulation.

By reducing the radius R the OTA ring, the emulated correlation obviously differs from the far field condition. This effect is particularly evident for R smaller than 5λ and small number of antennas. In Figure 4-7 we show the error introduced in correlation for 2D isotropic scenarios. It can be noticed that the antenna radiation properties has an important effect on the correlation. For instance, when considering a low number of probes, e.g. N_{ant} the combined fields on the test zone, could bring a smaller correlation error, thanks to the weighting given by the antenna itself.

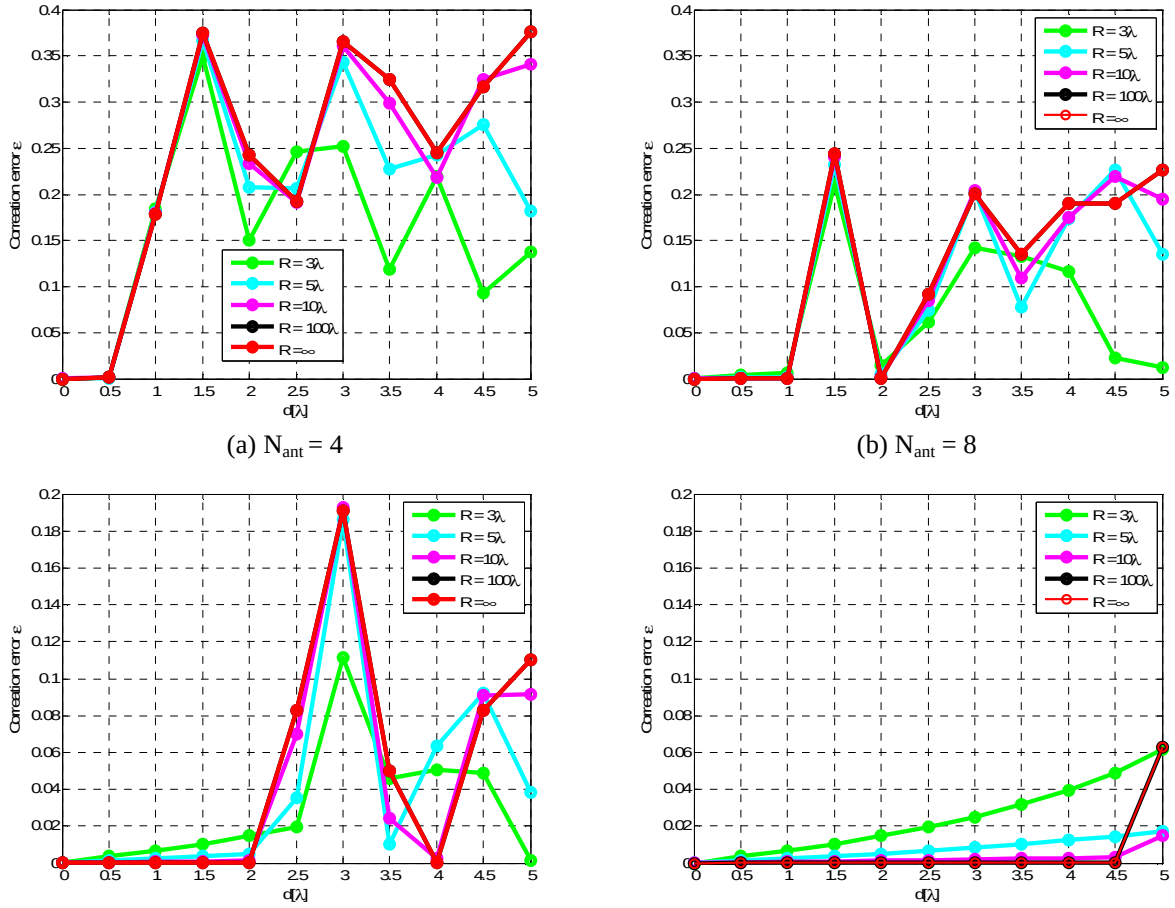

(a) N_{ant} = 4 (b) N_{ant} = 8

(c) N_{ant} = 16 (d) N_{ant} = 32

Figure 4-7 Correlation error in 2D isotropic scenario as a function of the number of antennas and radius of OTA ring

4.3.2.2 2D single cluster scenario

Here we considered a single cluster scenario, with mean angle of arrival $\bar{\phi}$ = 0° and angular spread $\sigma_\phi = 35°$. As in the previous simulations, DUT is considered randomly oriented. As shown in Figure 4-8 , a small number of equally separated probes allow to correctly reproduce for very small DUT size. This is due to the fact that a uniform distribution of antenna probes does not allow a fine emulation of a cluster channel, while a distribution on an angular sector would allow better reproducing the PAS with the same number of antennas. A feature observed in both isotropic and single cluster scenarios is that the correlation error decreases along with the number of OTA antennas and DUT size.

An unexpected feature, in both scenarios is that in the setup considered, with half-wavelength dipoles, the correlation error is slightly reduced for ring radius lower than 5λ.
This is clearly visible in Figure 4-8 where the correlation error is depicted as a function of DUT size. This effect is particularly evident for larger DUT size and depends on the considered antenna effect.

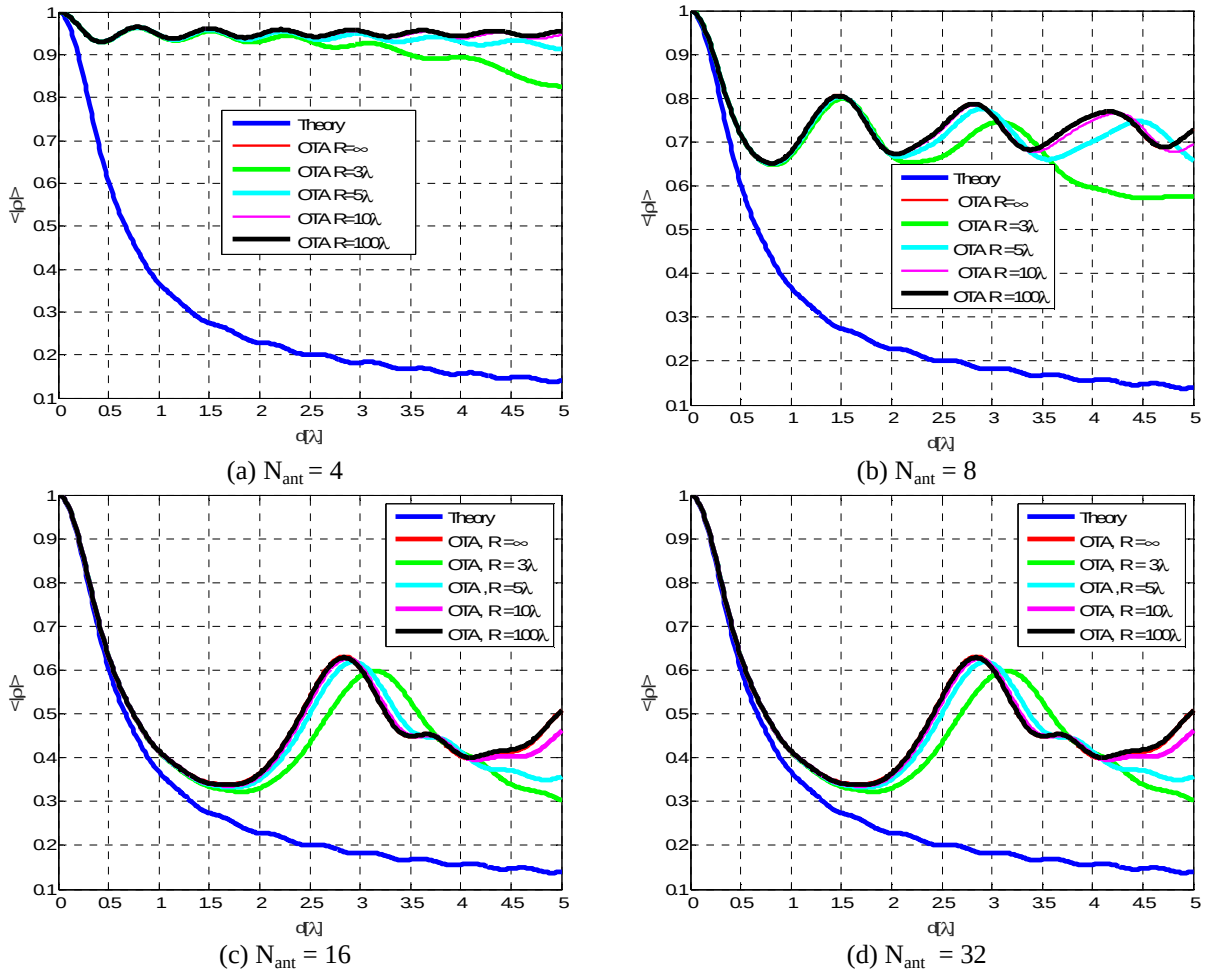

(a) $N_{ant} = 4$ (b) $N_{ant} = 8$

(c) $N_{ant} = 16$ (d) $N_{ant} = 32$

Figure 4-8 Spatial correlation in 2D single cluster channel as a function of the number of probes and radius of OTA ring

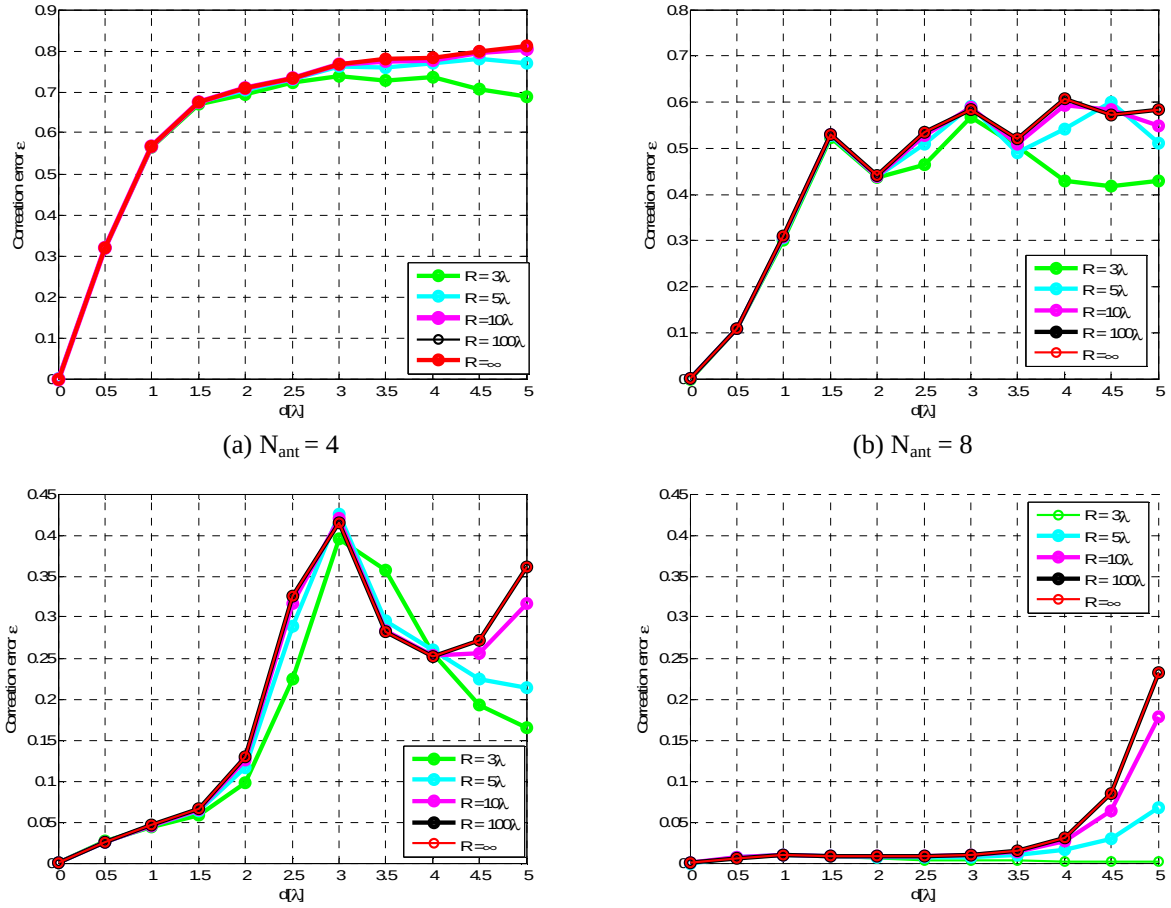

(a) N_{ant} = 4 (b) N_{ant} = 8

(c) N_{ant} = 16 (d) N_{ant} = 32

Figure 4-9 Correlation error in 2D single cluster scenario as a function of the number of antennas and radius of OTA ring

4.3.3 Optimization of OTA antenna feeding

As explained in chapter 3, different techniques can be applied to feed the OTA probe. Here, as extension of the PFS technique, the signal transmitted from the probes is weighted in order to reduce the target correlation error. In previous section we obtained the P_s weight from direct sampling of discrete PAS at the angular OTA antennas locations. This is a sub-optimal operation since the correlation error of (4.10) can be further reduced by opportunely choosing the antenna weights, eventually complex, in order to compensate of the effect of reduced number of antennas, or ring radius.

Here the antenna weights vector $\boldsymbol{w} = [w_1, w_2, \dots, w_{Nant}]$ were iteratively optimized through Conjugate Gradient Method, the objective being to minimize error in (4.10), where the power weight is $P_s = |w_s|^2$. Hence

$$w_{s_{opt}} = \min_{w_s}\left(\varepsilon(w_s)\right) \quad (4.16)$$

where

$$\sum_{s=1}^{N_{ant}} |w_s|^2 = 1$$

The constraint given by the fact the integral of PAS over the azimuth plane should be equal to 1.

In Figure 4-10, we show the spatial correlation obtained with optimal antenna weight compared to the ones obtained by direct sampling of the PAS, in the single cluster scenario in far field. It can be noticed that the higher accuracy achieved as a consequence of the optimization used to calculate the complex weights, yielding to a lower correlation error.

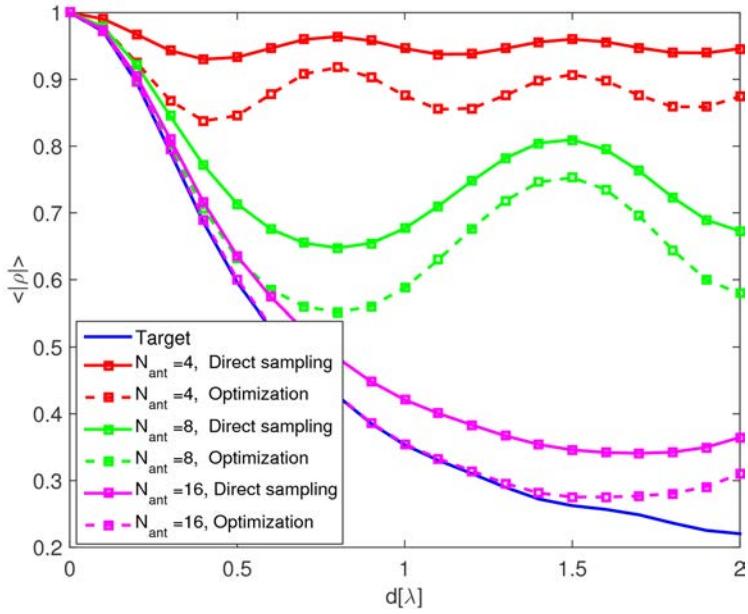

(a)

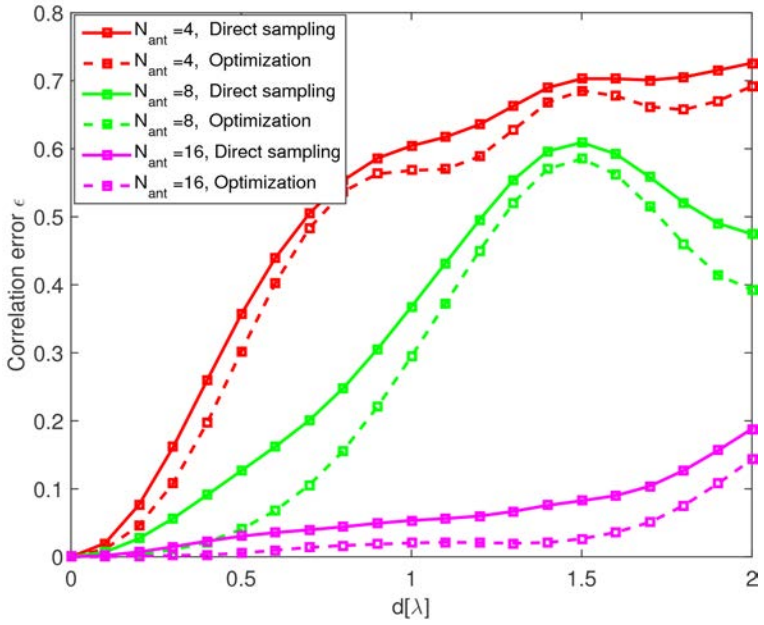

(b)

Figure 4-10 Single cluster channel, effect of antenna weight optimization: spatial correlation (a), correlation error (b)

It should be noted that the proposed weighting method was also employed for the uniform channel model. In this case, simulations results with the proposed weighting method, is similar to the previous results, presented in section 4.3.2.1. This is due to the fact that to emulate uniform model with uniform antenna separation, there is no other way than exciting the probes with the same weight. Hence the number of antennas is the only parameter of interest for the uniform case.

In order to determine the maximum DUT size, we fixed a maximum error threshold equal to 0.05. Figure 4-11 shows the maximum DUT size considering an error equal to 0.05 as a function of number of OTA antennas in two channel models.

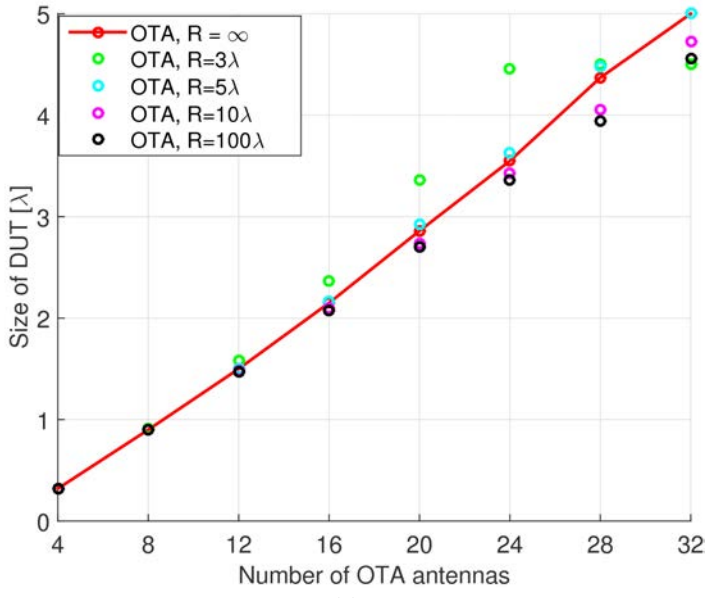

(a)

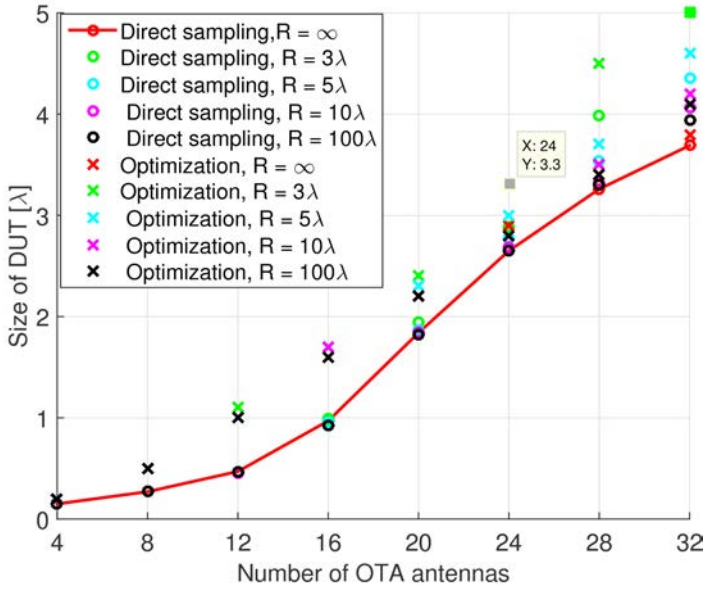

(b)

Figure 4-11 DUT size as function of number of OTA antennas: 2D isotropic (a) and single cluster (b) scenarios

In far field condition, when considering $N_{ant} = 8$, the maximum DUT size is 0.9 λ and 0.2 λ in the uniform and single cluster scenarios. Nevertheless this situation is not realized in practice and finite radius should be considered. For instance when considering R = 3 λ , N_{ant} = 8, the maximum DUT size is 0.1 λ and 0.2 λ in the uniform and single cluster scenarios, when direct PAS sampling is performed.

In the 2D isotropic channel, all angle of arrives are the same amplitude, i.e., the transmission of all OTA antennas is weighted with the same value. Consequently, the emulated spatial are the same for direct sampling and optimization technique, thus, OTA antennas weights and their angular positions could be carefully optimized, for giving a better emulation. Figure 4-11 highlights also the effect of weight optimization in PFS technique in single cluster model. As shown, by increasing size of DUT it becomes necessary to increase the number of OTA antennas.

To illustrate the obtained simulations results by indicative values. Table 4-1 depicts the minimum DUT size obtained from our simulations. Results are given for direct sampling technique and optimization in single cluster scenario for different configuration of probes antennas.

Table 4-1 Maximum of DUT size as function of number of probes with Direct sampling and PFS techniques for 2D uniform channel

	DUT (diameter) size [λ]							
	Direct Sampling				**Optimization**			
	4	**8**	**16**	**32**	**4**	**8**	**16**	**32**
R = ∞ (diameter = ∞)	0.1	0.2	0.9	3.7	0.2	0.5	1.6	3.8
R = 3 λ (diameter = 6 λ)	0.1	0.2	1	5	0.2	0.5	1.7	5
R = 5 λ (diameter = 10 λ)	0.1	0.2	0.9	4.35	0.2	0.5	0.9	4
R =10 λ (diameter =20 λ)	0.1	0.2	0.9	4.1	0.2	0.5	1.7	4.2
R =100 λ(diameter = 200 λ)	0.1	0.2	0.9	3.9	0.2	0.5	1.6	4.1

In this section we jointly analyzed the effect of number of probes, ring radius, and antenna radiation for 2-D OTA multi-probe setup. Simulations were performed considering a device under test arbitrarily oriented, in a uniform and single cluster channel. It was shown that antenna effect at short distance, i.e. ring radius, affect the correlation accuracy. Despite this phenomenon, the field combination on the zone test could be beneficial in terms of spatial correlation accuracy. Actually the OTA antenna transfer function acts as a filter, modifying the excitation of each probe. Hence Prefaded Signal Synthesis techniques should take into account the antenna effect, in order to better optimize the power, eventually complex, weights and achieve better accuracy. This optimization here was shown for OTA rings composed by half-wavelength dipoles, and proven to be effective in order to test larger devices while keeping low the number of antennas.

4.4 Three-dimensions OTA setup

Most of the MIMO OTA multi-probe configuration considers a two-dimension probe distribution over a ring. However the radio channel is intrinsically three-dimensional and some channel extensions, including elevation angles have been introduced in literature [83]. Recently 3D MIMO OTA setups have been investigated [68][69]proposing different probe configurations and analyzing the effect on channel emulation accuracy.

Most of the configurations proposed are based on spherical layouts, while for practical reasons cylindrical configurations could be useful. Nevertheless in cylindrical configurations the separation between the DUT and the probe is not constant according to the setup, and this could affect the correlation accuracy in the OTA configuration. 3D probes OTA antennas configurations sphere radius, as well as cylinder radius and height were set at 10λ.

In this part we analyze the correlation accuracy in spherical and cylindrical setups composed by three rings. Effect of Elevation Spread angular (ES) on emulating channel spatial characteristics is studied in 3D multi-probe configurations. In order to reproduce 3D target PAS of the channel model with higher accuracy, PFS technique is adopted. Simulation results show the potential of this technique to emulate 3D spatial correlation.

4.4.1 Simulation framework

The 3D PAS is a function of both the elevation $(\theta)$and azimuth (ϕ) angles. In order to simplify the model, the angular azimuth and angular distributions are often considered independent [71], hence the PAS can be considered as in (4.7).

Here we consider two channels:

- **isotropic channel**, corresponding to uniform distribution in both azimuth and elevation angles (Figure 4-12 (a))
- **single cluster channel**, where both azimuth and elevation follow a Laplacian (Figure 4-12 (b))

DUT was chosen to be arbitrarily oriented, hence in simulations $\phi_i$was uniformly distributed in [0, 2π [.

Spatial correlation is computed from 100000 realizations, corresponding to different DUT orientations.

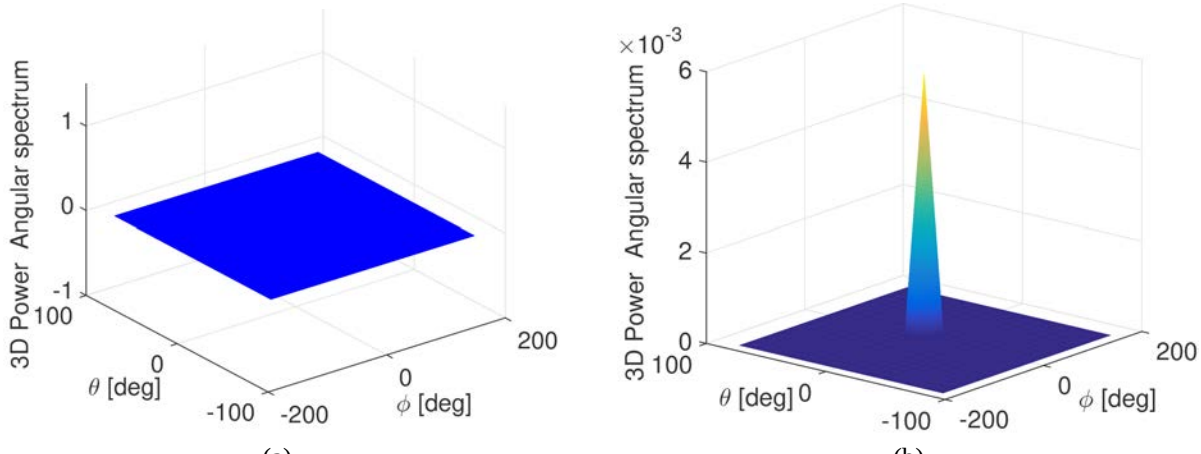

(a) (b)

Figure 4-12 3D model PAS: Uniform (a), Single cluster (b)

When considering a 3D OTA setup with a limited number of antennas N_{ant} the correlation can be written as:

$$\rho_{OTA_{(i,j)}} = \frac{\sum_{s=1}^{N_{ant}} \boldsymbol{E}_{A_i}\left(R_{s,}\theta_s,\phi_s\right).\boldsymbol{E}^*_{A_j}\left(R_{s,}\theta_s,\phi_s\right)\ P_s}{\sqrt{\sum_{s=1}^{N_{ant}}\left|\boldsymbol{E}_{A_i}\left(R_{s,}\theta_s,\phi_s\right)\right|^2 P_s}\ \sqrt{\sum_{s=1}^{N_{ant}}\left|\boldsymbol{E}_{A_i}\left(R_{s,}\theta_s,\phi_s\right)\right|^2 P_s}} \tag{4.17}$$

Where P_s is the power of the *s*-th OTA antenna, obtained by PFS technique. Here with respect to the 2D setup we highlight in the notation that the impinging field on the i-th antenna depends on the actual spherical coordinate $\left(R_{s,}\theta_s,\phi_s\right)$ *s*-th of the probe. This is obviously true also in the 2D case, but in OTA 2D ring this reduces to a correction phase factor which only depends on the angular position of the probe. In 3D according to the antenna position and probes emplacement the distance is not constant.
In the following we present the results for 3D spherical and cylindrical configurations. On the contrary of what has been done in the 2D space, here we consider specific alignment of the DUT antennas along one of the three main axes.

4.4.2 Spherical configuration results

Two spherical probe setups considered are shown in Figure 4-13 (a), Figure 4-13 (b), respectively. The probes are placed on a three different rings and angular coordinates are reported in Table 4-2.

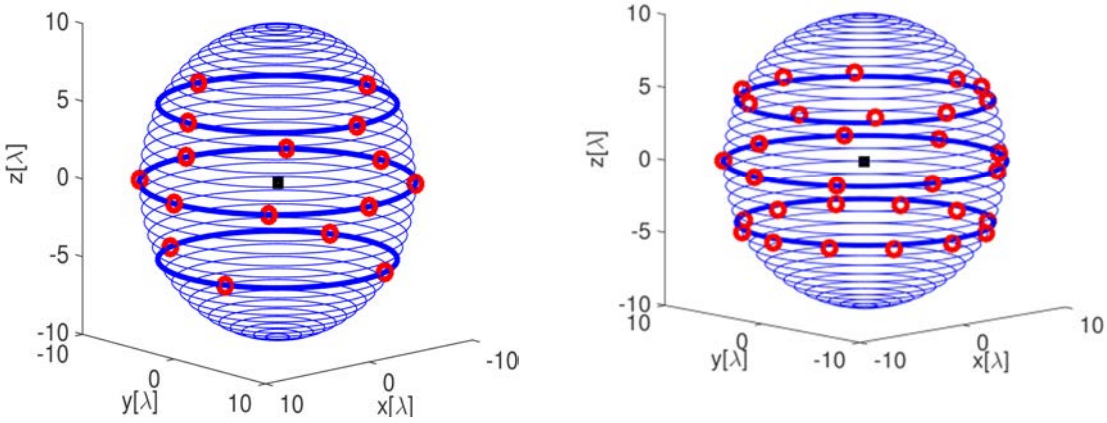

(a) 16 3R spherical configuration (b) 32 3R spherical configuration

Figure 4-13 Spherical configuration of OTA test setup (a) and (b)

Table 4-2 Angular locations of two spherical probes configurations

Probe setup	OTA antennas configuration [deg]
16 3R	$\theta_1 = -30°, \phi = 0\ 90\ 180\ 270$; $\theta_2 = 0°, \phi = 0\ \ 45\ 90\ 135\ 180\ 225\ 270\ 315$; $\theta_3 = 30°, \phi = 22{,}5\ \ 112{,}5\ \ 205.5\ 292.5$;
32 3R	$\theta_1 = -30°, \phi = 0\ \ 45\ 90\ 135\ 180\ 225\ 270\ 315$; $\theta_2 = 0°, \phi = 0\ 22.5\ 45\ 67.5\ 90\ 112.5\ 135\ 157.5\ 180\ \ 202.5\ 225\ 247.5\ 270\ 292.5\ 315337.5$; $\theta_3 = 30°, \phi = 0\ 90\ 180\ 270$;

Figure 4-14 shows the absolute value of the spatial correlation as a function of DUT size, in the 3D uniform PAS model. In this uniform scenario the theoretical spatial correlation follows the analytically expressions $sinc(kd)$ [76] . Here the antenna weights are obtained by direct sampling of the 3D PAS. Generally spherical configurations offer better accuracy, when the DUT is placed along the x or y axis or z axis. The reconstruction accuracy depends on the probe setup, the target channel and the number of probes.

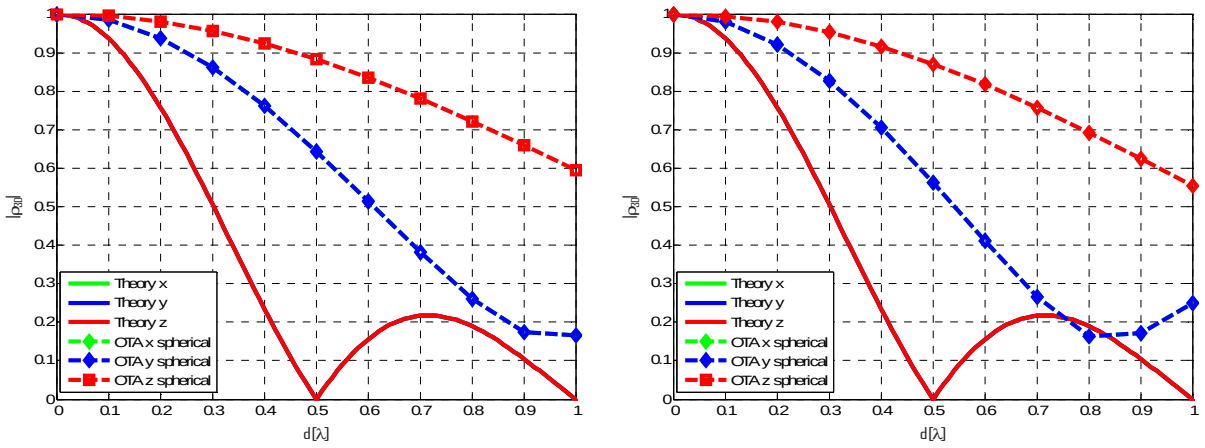

(a) (b)

Figure 4-14 Correlation in 3D isotropic scenario two spherical configurations: 16 3R (a), 32 3R (b).

In the single cluster scenario we considered mean angles of arrival equals to 0°, an azimuth angular spread of 35° and an elevation spread equals to 15.5°[84]. As shown in Figure 4-15 theoretical spatial correlation depends on the DUT antenna orientations in the three axes.

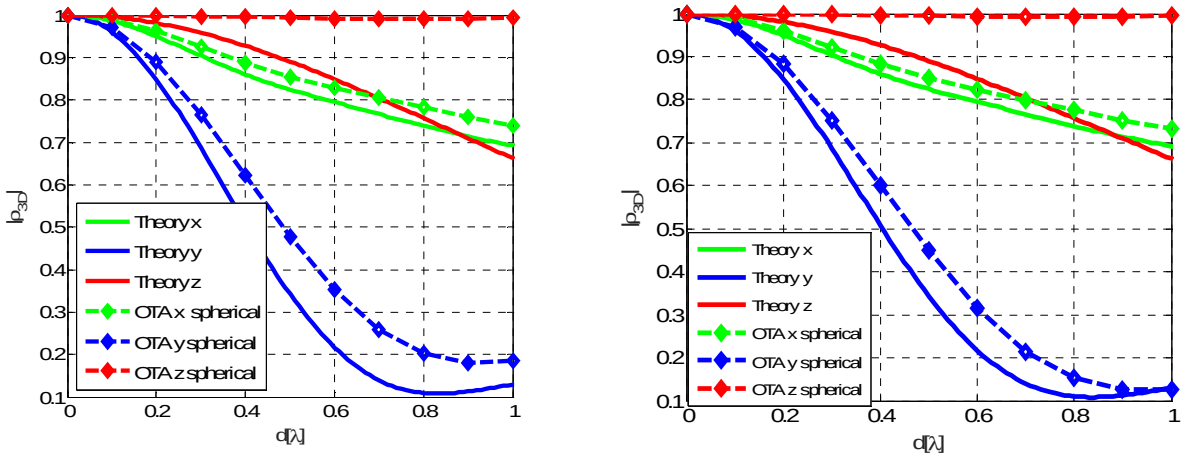

(a) (b)

Figure 4-15 Correlation in 3D isotropic scenario two spherical configurations: 16 3R (a), 32 3R (b).

It is easier to emulate a 3D isotropic channel, considering DUT in x axis. Larger number of probes according Figure 4-15(b), give us accurate channel emulation in two-dimensional plane. In y and z axis, the elevation component appears and it becomes more challenging to test a wavelength DUT size, based on these proposed configurations. A large number of probes is needed according to the elevation spread. This obviously depend on the DUT considered as well as the channel to be emulated.

In order, to test DUT in z orientation, we have proposed to study a new 3D configuration, that could we be useful. The major characteristic of the proposed cylindrical configuration is the height. It must be studied carefully.

4.4.3 Cylindrical configuration results

Figure 4-16 shows two configurations considered in simulations. The first is 16 OTA antennas distributed in three OTA ring as illustrated in Figure 4-16 (a). The second consists in embodiment the 32 OTA antennas in three OTA ring as shown in Figure 4-16 (b). We opted for a uniform cylinder, with $x = 10\lambda$, y = 10λ and z = 10λ, where z is height of the cylinder.

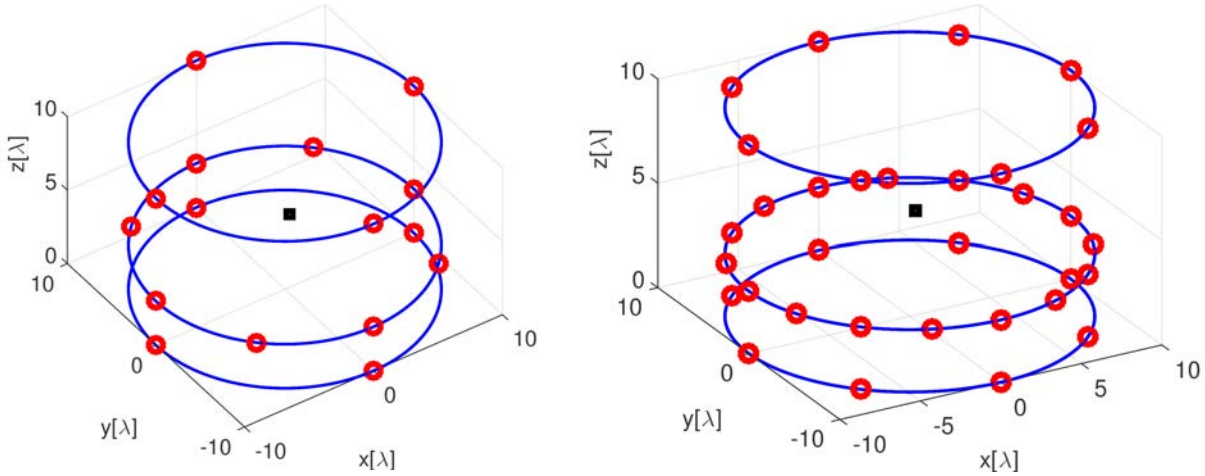

(a) 16 3R cylindrical configuration (b) 32 3R cylindrical configuration

Figure 4-16 Cylindrical configuration of OTA test setup (a) and (b)

Comparison of target and emulated 3D OTA spatial correlation on three orthogonal axes are illustrated in Figure 4-17. Therefore, the spatial correlation values on the x, y coincides due to the uniform PAS model assumption. In the probe setup illustrated in Figure 4-17 (b), 32 probes offer good reconstruction accuracy.

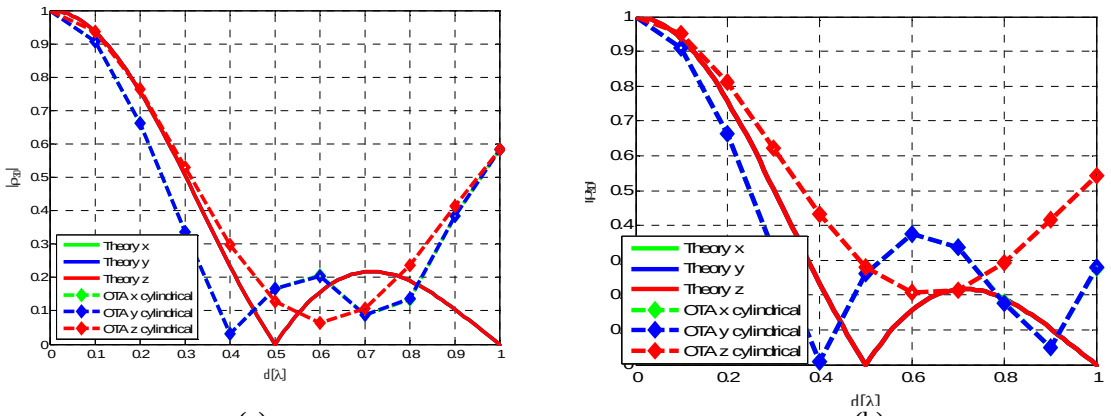

(a) (b)

Figure 4-17 Correlation in 3D isotropic scenario two cylindrical configurations: 16 3R (a), 32 3R (b).

The cylindrical configuration offers better results when the DUT is along the z axis. Thus, the impact of height of cylinder must be studied. The emulated and target spatial correlation for single cluster scenario are illustrated in Figure 4-18. It can be noticed that the elevation angle affects the spatial correlation.

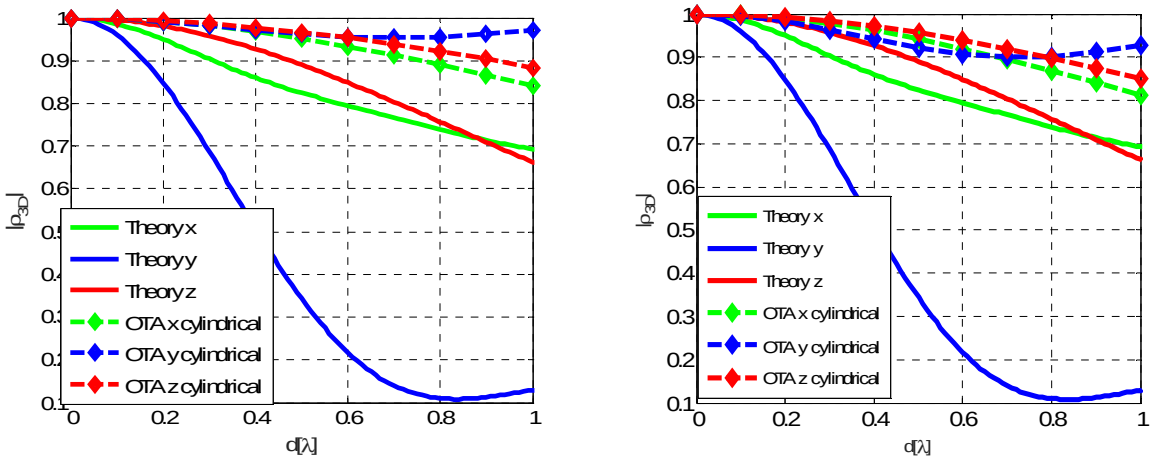

(a) (b)

Figure 4-18 Correlation in 3D isotropic scenario two cylindrical configurations: 16 3R (a), 32 3R (b).)

Height effect of 3D OTA test setup in cylindrical probes configuration (32 3R) is here studied. Figure 4-19 shows the absolute value of spatial correlation as a function of DUT size with different values of cylindrical height, in two 3D channel scenarios, by considering direct sampling of the 3D PAS. As shown in Figure 4-19 (a) and Figure 4-19 (b), increasing cylindrical height OTA test setup to h =100λ spatial correlation from DUT along x and y axis offers better accuracy than h = 10λ, when considering uniform scenarios. When the antennas are aligned along z axis OTA spatial correlation with h=100 λ becomes less accurate in this test setup.

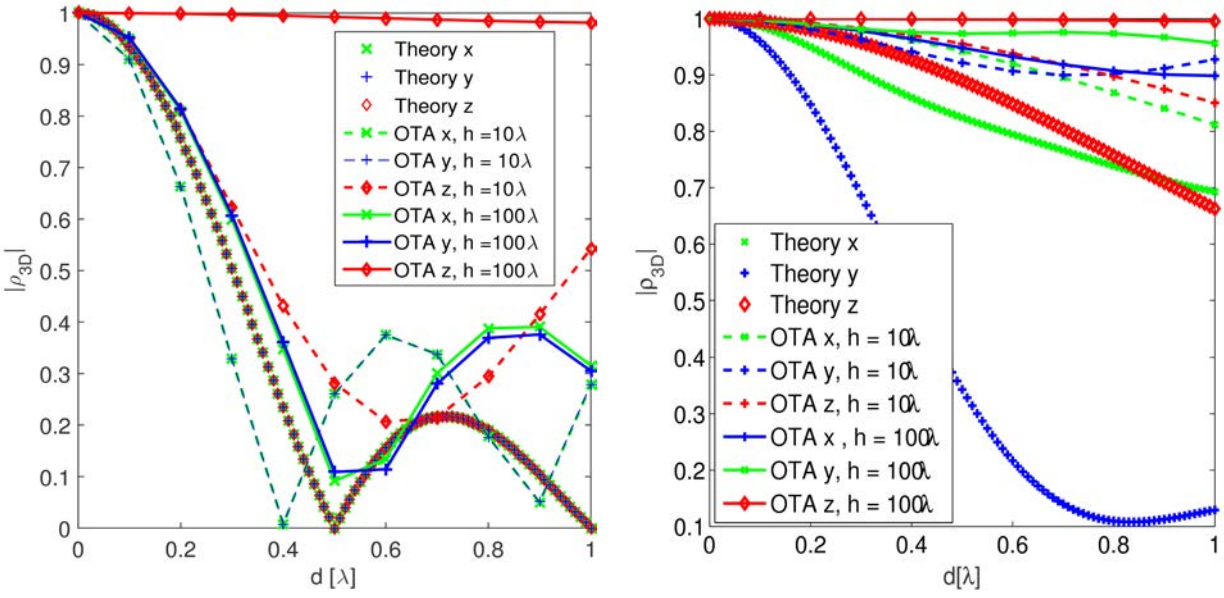

(a) (b)

Figure 4-19 Correlation for cylindrical configuration with height effect in 3D uniform (a) and single cluster (b)

In single cluster scenario Figure 4-19 (b), the height effect strongly depends on the elevation spread. The OTA antennas positions must be determined according the height and ES characteristics.

4.4.4 Effect of elevation spread and weight optimization

The quality of OTA emulation depends on the kind of channel we target. For what concerns 3D OTA setups, the effect of Elevation Spread (ES) has a direct consequence on the dimensioning and antenna position. Here we investigate the ES effect with finite number of probes on spatial correlation in spherical probe configuration 163R. Figure 4-20 shows the simulation results of OTA spatial correlation as a function of DUT size d. We considered a direct sampling of the 3D PAS of single cluster channel model, where we fixed the azimuth spread AS = 35° and different elevation spreads ES = 10°, 15°, 20°. The effect of ES becomes more evident when the DUT antennas are aligned along the z axis, and generally the correlation decreases along with an augmentation of ES. When we consider the DUT antennas on x or y axis the effect is somewhat limited. For instance, when considering an antennas separation d = 0.5 λ as highlighted the in, the value of spatial correlation between vertically adjacent elements antennas of DUT (red line) is approximately 0.5 with ES = 20° and 0.9 with 0.5 with ES = 10°.

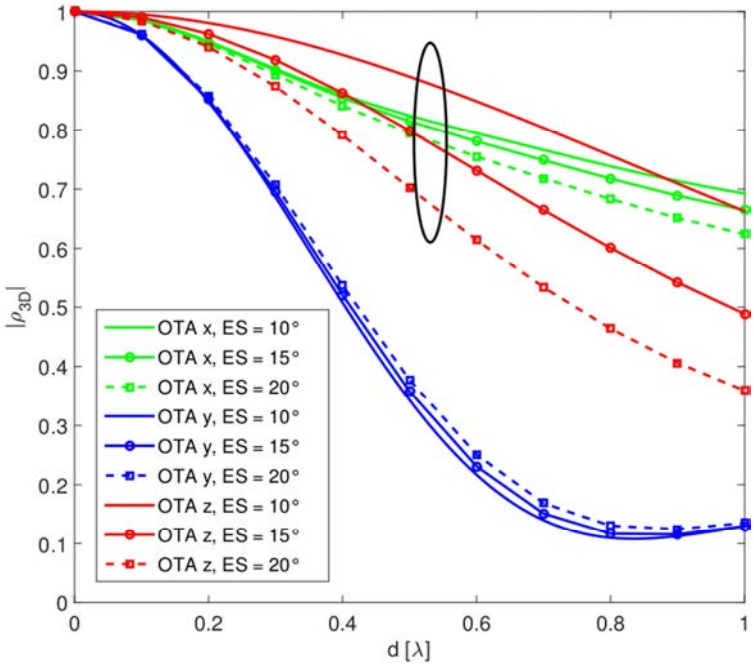

Figure 4-20 ES spread impact on correlation in 16 3R spherical configuration

In PFS technique, the signal transmitted by the probes is weighted in order to reduce the target correlation error. In the previous section we obtained the P_s weights from direct sampling of the discrete 3D PAS at the angular locations of the OTA antennas in elevation and azimuth, here we apply PFS technique to 16 3R configurations and single cluster channel model.

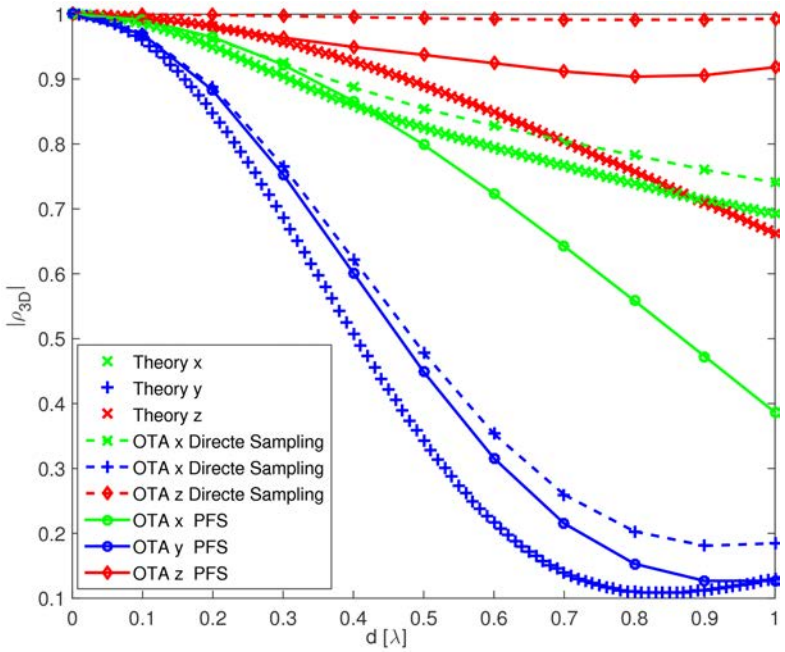

Figure 4-21 Correlation in 16 3R spherical configuration with direct sampling and optimization

In Figure 4-21 we compare the results obtained by direct sampling and PFS with the expected spatial correlation for single cluster scenario. It can be seen that the accuracy achieved by the PFS is higher than the direct sampling technique. However, when we consider the DUT aligned along the z-axis, the PFS technique allows increasing the accuracy only for small values of d. However since the typical distance between antennas is around the 0.5λ, these results can be considered acceptable.

4.5 Conclusions

This chapter focuses on multi-probe OTA anechoic chamber testing, which, starting from the analysis of chapter 3, has been retained as a promising method to evaluate device performances.

We discussed several criteria to dimension the OTA set up. It was shown that classical far field conditions are not sufficient to evaluate the quality of the OTA emulation. While the far field criterion can give an indication on the OTA ring radius, it does not provide any guideline on the number and disposition of OTA probes around the zone under test.
A dimension study of OTA multi-probe was based on the establishment of OTA spatial correlation with finite number of probes. Simulation results showed that the required number of probes is a key issue, as it directly determines the system accuracy. Investigation on OTA far field condition was addressed on a case study employing half-wavelength OTA dipoles.
It was shown that indeed the antenna effect has an impact on the emulated correlation, according to the ring radius. However this effect seems less important than the number of antennas.

Based on the Pre-Faded Signal (PFS) technique presented in chapter 3, an optimized weighting of probes was proposed. This study was first conducted on the two dimensions (2D) setup for two channel models: uniform and single cluster.

The study has been continued to cover a 3D OTA dimension. We compared different 3D probe configurations to emulate the spatial correlation in MIMO OTA considering 3D channel models. A comparison between different setups as a function of the angular spreads has been presented. It was shown that, when DUT antennas are along the z-axis, the cylindrical configuration could be also used to emulate elevation spread. PFS technique results applied to the 3D setup show the feasibility to emulate 3D channel models in cylindrical and spherical configurations.

The analysis carried out by simulation, show that there is not a unique setup, regardless the frequency, device size and channel model. Hence the OTA setup should be flexible enough to adjusted according for the test needs. For this reason it was decided to realize a hemispheric OTA setup that can be mechanically modified to have a different antenna emplacement in both azimuth and elevation. This setup, as well as its characterization is presented in the next chapter.

Chapter 5

5 Multi-probes OTA Experimentation

5.1 Introduction

Several OTA measurement methodologies have been proposed in chapter 3, as promising solutions to evaluate devices performances in realistic situations. Among different options we considered in this work the multi-probes anechoic chamber method, to emulate OTA multipath environments in which the performances of the devices have to be evaluated.
The majority of existing methodologies in the literature targets only one specific standard of communication. It means testing device for one center frequency. Moreover, their performances in terms of resolution are limited by the number of probes, and globally emulate two dimensional channel models. Thus, our investigation is focused on proposing a new multi-probe OTA test setup, adapted to the any devices testing, able to overcome the encountered difficulties, in order to emulate three dimensional channel models.

In chapter 4, it has been shown that the essence is to find a complete dimension of a multi-probes OTA test bed, such that channel spatial characteristics can be recreated. We have established some criteria related to physical dimension of the proposed OTA test setup that is not limited to the classical far field condition. In particular spatial correlation was selected as figure of merit to dimension OTA test setup, deriving the number and position of OTA antennas as a function of DUT size and frequency.

Most of realistic channels are tri-dimensional. The 3D OTA design setup has been discussed. (3D) spatial correlation in 3D OTA setup is adopted as criterion to perform a DUT radiation in different orientations in 3 axes. Two different configurations have been compared. The first one is instinctively spherical probes configurations, and the second is cylindrical configurations. Their main drawbacks are the chamber cost and the lack of flexibility to emulate specific channel realizations. Both methods, based on cylinder and spherical configurations are used in combination with OTA test setup.

In this chapter, we present an experimental 3D hemispheric multi-probe OTA test-bed that can be used in a wide span of applications from 2 to 6 GHz. The proposed OTA multi-probes setups provide an efficient way to characterize the performance of today's advanced wireless communication systems. We describe extensive measurements that were performed to validate channel emulation in the proposed 3D multi-probe OTA setup, considering two frequencies of interest setup.

5.2 OTA test bed realization

The OTA set-up is composed by four metallic arcs covered by electromagnetic absorbers, to place the OTA probe antennas at different azimuth and elevation angles.
The vertical masts of 1.5 height hold the 4 arches whose diameter is equal to 1 m, in order to fit in the anechoic chamber, whose dimensions are $6 \times 2.5 \times 3$ m^3.

Actually, when considering the mechanical support, the distance from the OTA antenna aperture, described below, actually reduces the ring radius to less than 1m (i.e. R = 660 mm).

The mechanical setup allows testing different configurations. Here we considered two different configurations:

- a **uniform configuration** with 3 different rings of 4 antennas at different elevations and equally spaced in the azimuth plane
- a **sectorial configuration** with 3 different rings of 4 antennas at different elevations, placed in half space of the azimuth plane

5.2.1 Antennas

The source antenna in the OTA test-bed must enable the control of direction of incidence and polarization of the incoming waves to the test zone. Thus, a directive, dual polarized and wideband antenna system has been specifically designed for the OTA test-bed.
The OTA source antenna is designed based on two crossed Linear Tapered Slot Antennas (LTSAs) used for this purpose. The feeding of these antennas is commonly realized with a coupling micro strip etched on the opposite face of the PCB. The PCB shape is cut with an elliptical profile in order to limit cross polarization effect. The LTSAs are notched so that they can be inserted one in the other. The ground continuity between the two combined LTSAs is insured by soldering the two PCBs.
The final prototype is shown in Figure 5-1 (a) and (b). Each port allows considering either the vertical or the horizontal polarization.
The return loss of the antenna is below -10 dB for both port 1 and 2 over the 2-6 GHz band and isolation between the two ports is higher than 20 dB. In Figure 5-1 we show the measured gain patterns in the main and cross polarization for both ports at 2 GHz, 4 GHz and 6 GHz. The maximum gain varies between 5 and 8.5 dBi in the band of interest, and the cross-polar discrimination is larger than 20 dB.

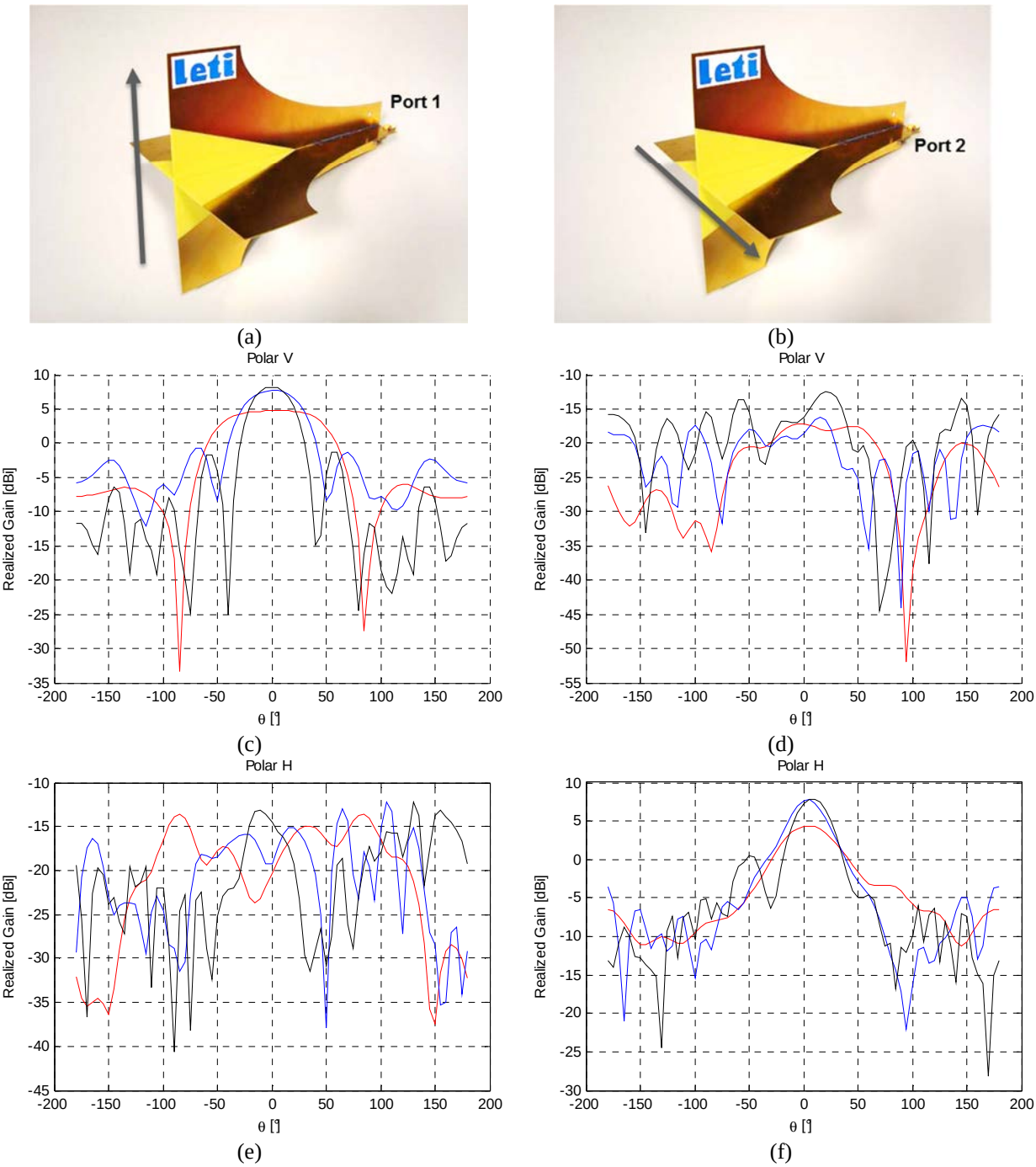

Figure 5-1 OTA antenna gain pattern port 1 (a) (c) (e) & port 2 (b) (d) (f): 2 GHz (red), 4 GHz (blue), 6 GHz (black)

5.3 Test Bed Characterization

Before characterizing the Zone under Test (ZUT), the mutual coupling between OTA antennas has been measured by means of a Vector Network Analyzer (VNA). In Figure 5-2 we show the mutual coupling in the uniform configuration for co-polar and cross-polar combination of all twelve antennas in the OTA test-bed, which is generally lower than -30 dB.

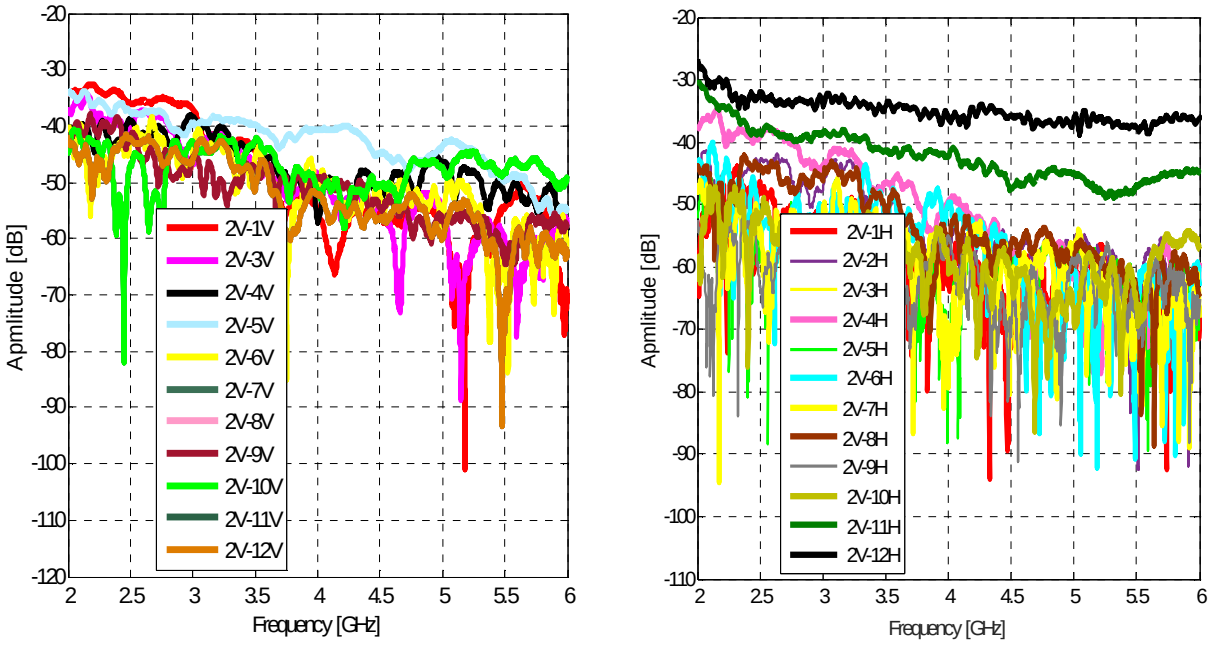

(a) (b)

Figure 5-2 Mutual coupling for uniform configuration: vertical-to-vertical polarization (a) and vertical-to-horizontal polarization (b)

Besides the antenna mutual coupling, the OTA antennas act also as scatterers that can perturb the measurements introducing, together with the setup residual scattering.

In order to characterize the radiated field in the ZUT a frequency domain setup was realized based on Vector Network Analyzer. A 4-port R&s ZVA24 performs a frequency sweep from 2 to 6 GHz by step of 10 MHz. The intermediate frequency bandwidth was chosen equal to 1 kHz and Output Power equal to 0 dBm. A wide-band monopole antenna was placed on a 3-axis positioner, scanning a ZUT of 150x150x150 mm^3 placed in the middle of the hemisphere of the OTA setup. The positioner has a precision of 0.02mm and scans the ZUT by step of 10 mm.

Port 1 of the VNA is connected to the monopole scanning the ZUT, while port 2, 3 and 4 are connected to the OTA antennas on the same arc. An external PC controls both the positioner and VNA acquisitions through a Matlab code. The setup is presented in Figure 5-3.

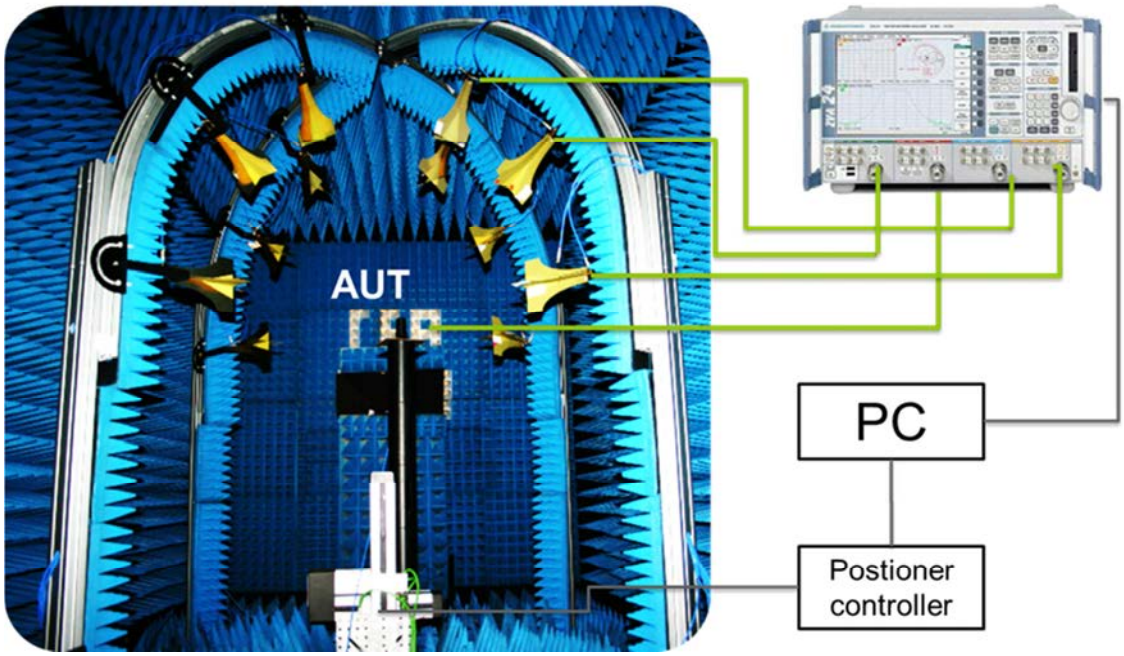

Figure 5-3 Setup for OTA test-bed characterization

In practice the measured parameters S_{21} S_{31} and S_{41} correspond to transfer functions between the OTA antenna and the antenna under test.
Ideally, in far field condition, for a given polarization, this corresponds to:

$$H_{i,s}(f) = -j\frac{\lambda}{4\pi R_{i,s}} e^{-j\frac{2\pi}{\lambda}R_{i,s}} \cdot H_{AUT}\left(f, \theta_{i,s}, \phi_{i,s}\right) \cdot H_S\left(f, \theta_{s,i}, \phi_{s,i}\right) \quad (5.1)$$

Where $H_{AUT}\left(f, \theta_{i,s}, \phi_{i,s}\right)$ is the i-th Antenna Under Test (AUT) transfer function in the direction $(\theta_{i,s}, \phi_{i,s})$ towards the s-th antenna, and $H_S\left(f, \theta_{s,i}, \phi_{s,i}\right)$ is OTA antenna transfer function in the direction $(\theta_{s,i}, \phi_{s,i})$ towards the i-th antenna.
Here because of the non-ideality of the setup, the residual scatterers, and the reduced distance, the transfer function in measurements can differ from (5.1). The aim of the following measurements is to analyze the difference in terms of transfer function, or equivalently field distribution, in the considered ZUT.
Two frequencies were selected for analysis: 2 GHz testing Wi-Fi devices and 5.9 GHz for IEEE 802.11 devices.

5.3.1 Uniform setup configuration

Firstly, we realized uniform configuration of experimental test bed, where OTA antennas are placed uniformly in three elevation ring. The objective of this implementation is mainly to emulate an isotropic channel model. An illustration of this configuration is presented in Figure 5-4 together with a schematic view. Samples over test zone are marked with black grid. Antenna angular positions are reported in Table 5-1.

Table 5-1 Angular locations of OTA antennas in uniform setup

OTA elevation ring	Azimuth Angular locations
$\theta_{1,2,3,4} = 90°$	$\phi_1 = 45°, \phi_2 = 135°, \phi_3 = 225°, \phi_4 = 315°,$
$\theta_{5,6,7,8} = 30°$	$\phi_5 = 45°, \phi_6 = 135°, \phi_7 = 225°, \phi_8 = 315°,$
$\theta_{9,10,11,12} = 60°$	$\phi_9 = 45°, \phi_{10} = 135°, \phi_{11} = 225°, \phi_{12} = 315°,$

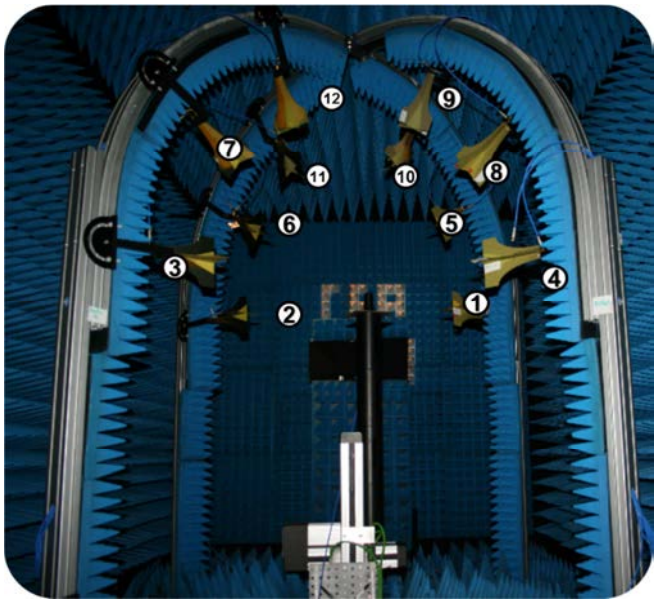

(a)

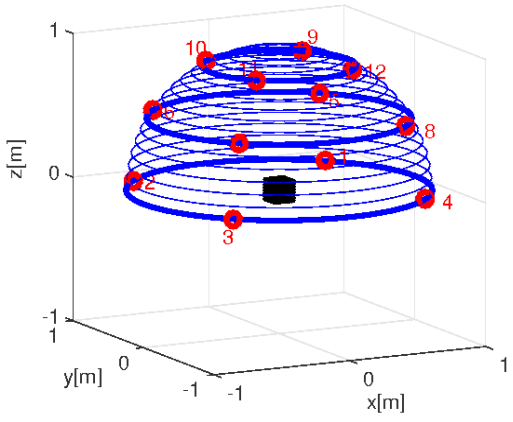

(b)

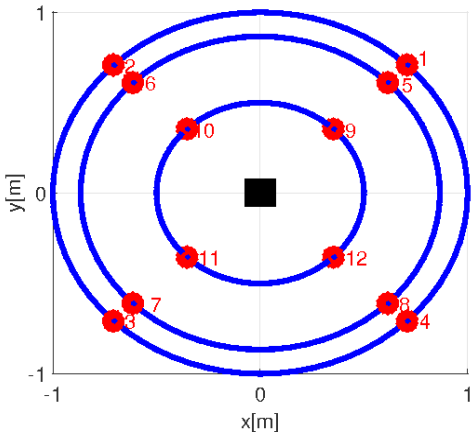

(c)

Figure 5-4 OTA uniform setup configuration: (a) picture, (b) 3Dview, (c) top view

Here we present, for sake of simplicity the transfer function in the azimuth plane corresponding to the first ring of antennas, i.e. elevation $\theta_{1,2,3,4} = 90°$and ϕ_1= 45°, ϕ_2 = 135°, ϕ_3 = 215°, ϕ_4 = 315°. When performing measurements all the antennas were loaded on 50 Ω.

In this first steep, we describe the map of the distribution of the emulated field for different positions of the antennas in the simulations and measurements. The emulation of the field to test zone is given based on the synthesis electromagnetic field. To verify this, we start by developing the expression of the intended electromagnetic field, which we want, emulated in our uniform OTA configuration. Figure 5-5 and Figure 5-6 present the amplitudes of transfer functions in the ZUT of the ideal free space condition and the measured one. One can clearly notice that despite the presence of absorber, the residual scattering in the setup (and eventually on the positioner), create some fading effect up to 3 dB.

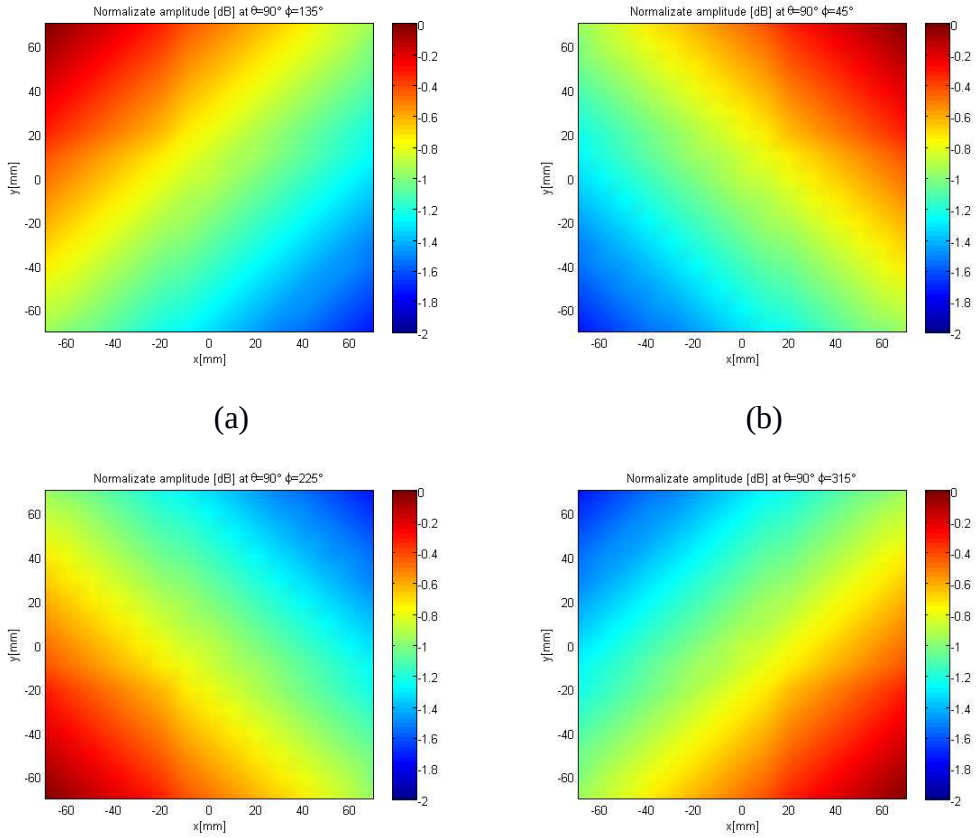

Figure 5-5 Normalized simulated transfer function amplitude [dB] at 2 GHz: antenna 2 (a), antenna 1 (b), antenna 3 (c), antenna 4 (d)

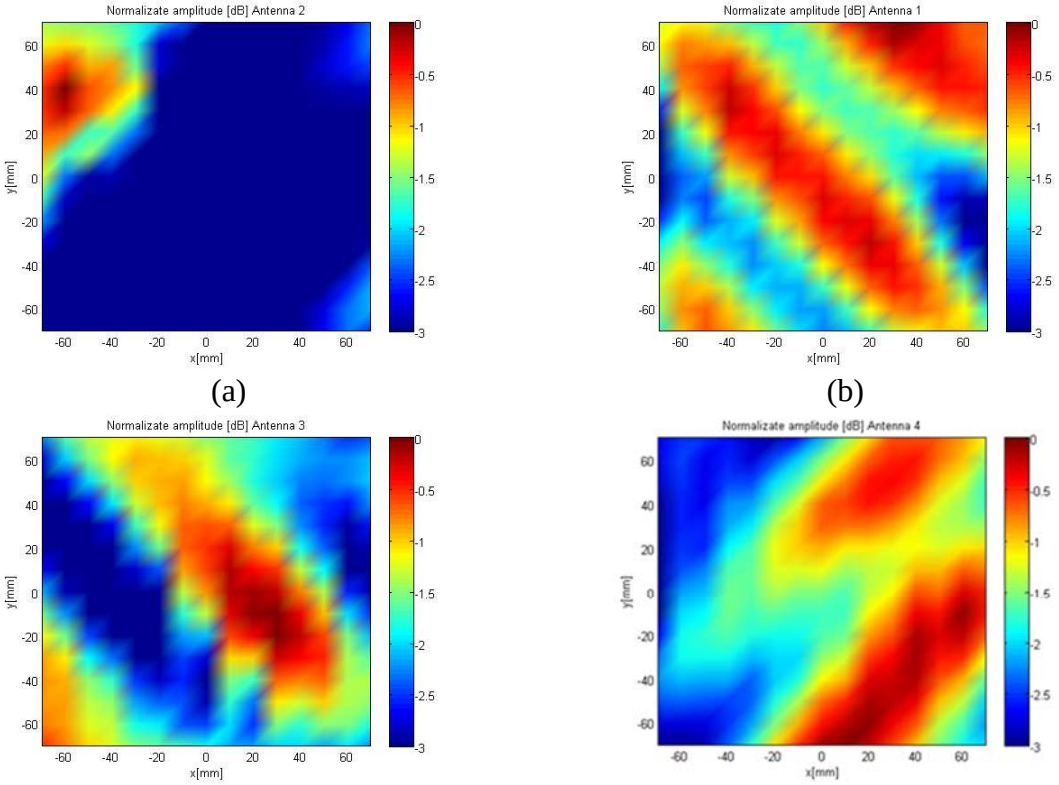

(a) (b)

(c) (d)

Figure 5-6 Normalized measured transfer function amplitude [dB] at 2 GHz: antenna 2 (a), antenna 1 (b), antenna 3 (c), antenna 4 (d)

On the other hand the measured phase of the transfer function Figure 5-8 is very close to the expected one (Figure 5-7), despite some sphericity due to the small distance between the source antenna and the AUT.

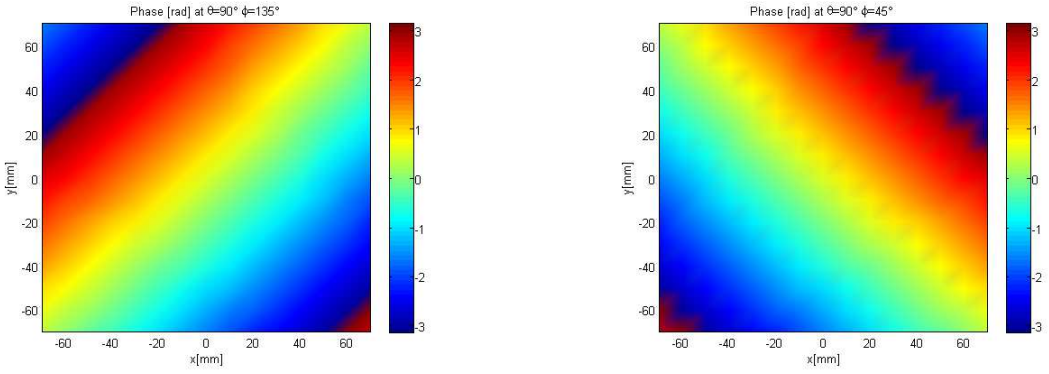

(a) (b)

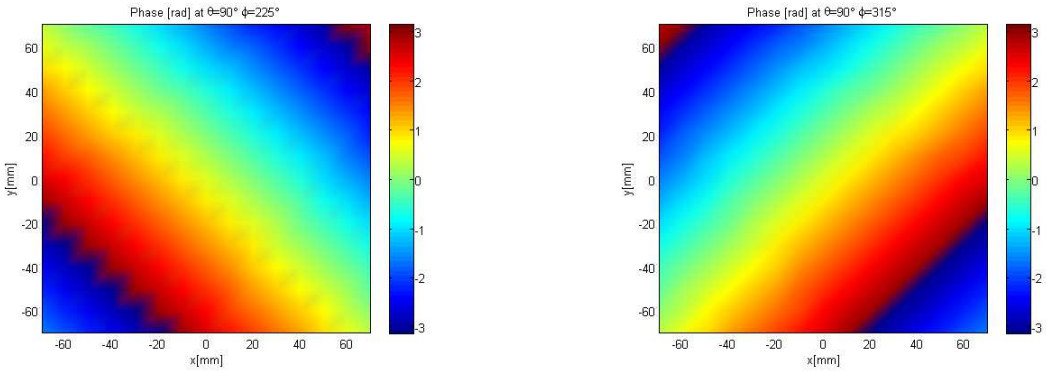

(c) (d)

Figure 5-7 Simulated transfer function phase [rad] at 2 GHz: antenna 2 (a), antenna 1 (b), antenna 3 (c), antenna 4 (d)

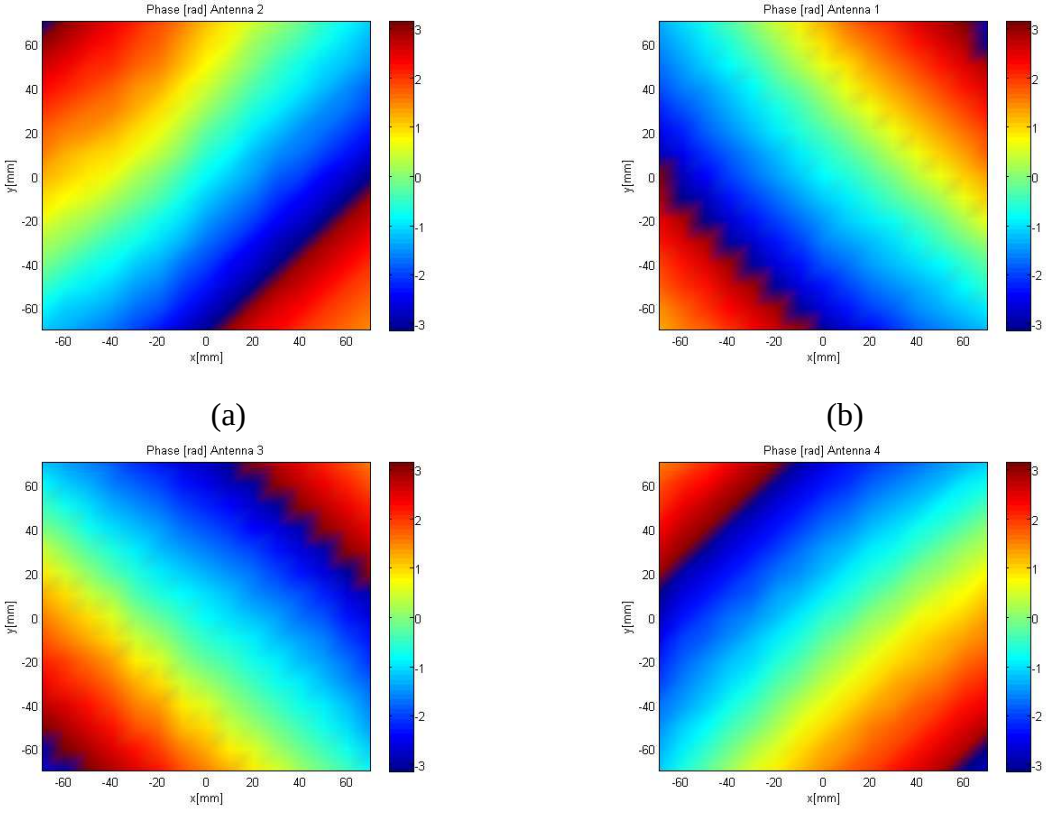

(a) (b)

(c) (d)

Figure 5-8 Measured transfer function phase [rad] at 2 GHz: antenna 2 (a), antenna 1 (b), antenna 3 (c), antenna 4 (d)

When comparing the amplitudes at 5.9 GHz (Figure 5-9, Figure 5-10) there is still some scattering, but the fading effect are quite reduced with respect to the low frequency.

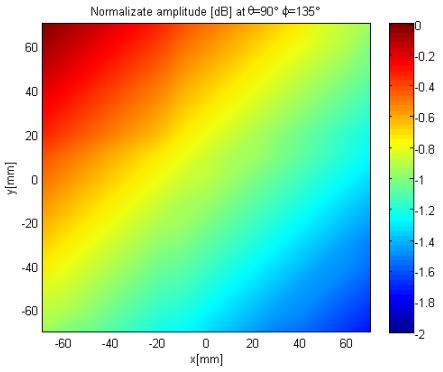

(a)

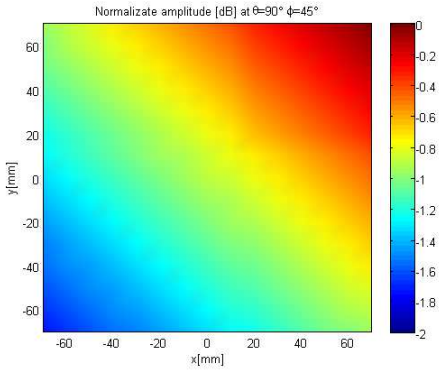

(b)

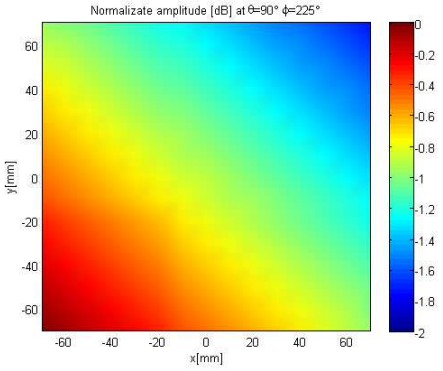

(c)

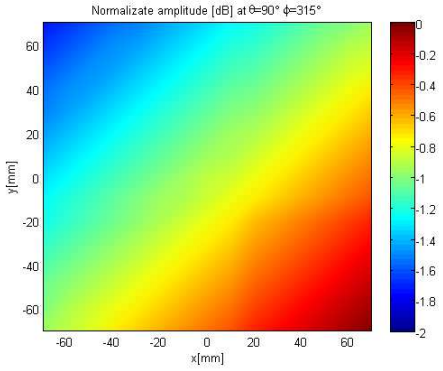

(d)

Figure 5-9 Normalized simulated transfer function amplitude [dB] at 5.9 GHz: antenna 2 (a), antenna 1 (b), antenna 3 (c), antenna 4 (d)

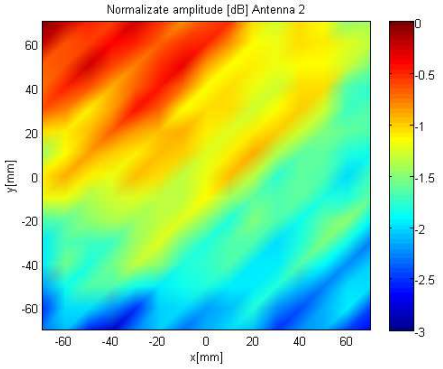

(a)

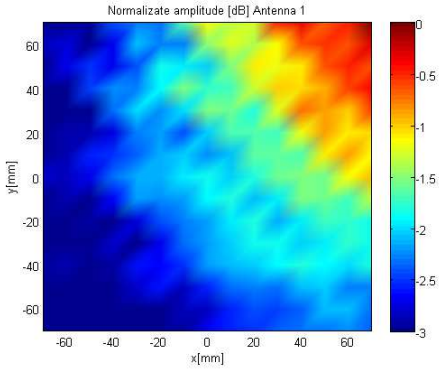

(b)

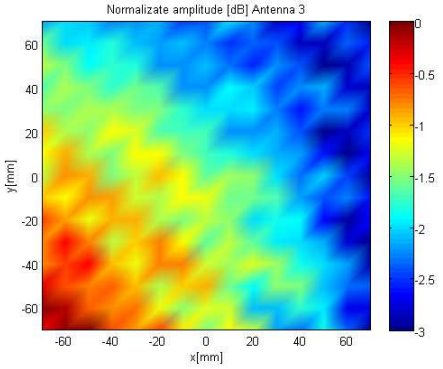

(c)

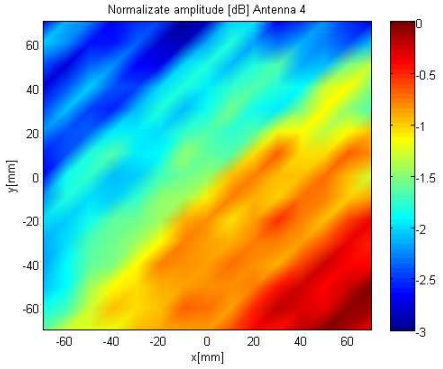

(d)

Figure 5-10 Normalized measured transfer function amplitude [dB] at 5.9 GHz: antenna 2(a), antenna 1(b), and antenna 3 (c) antenna 4(d)

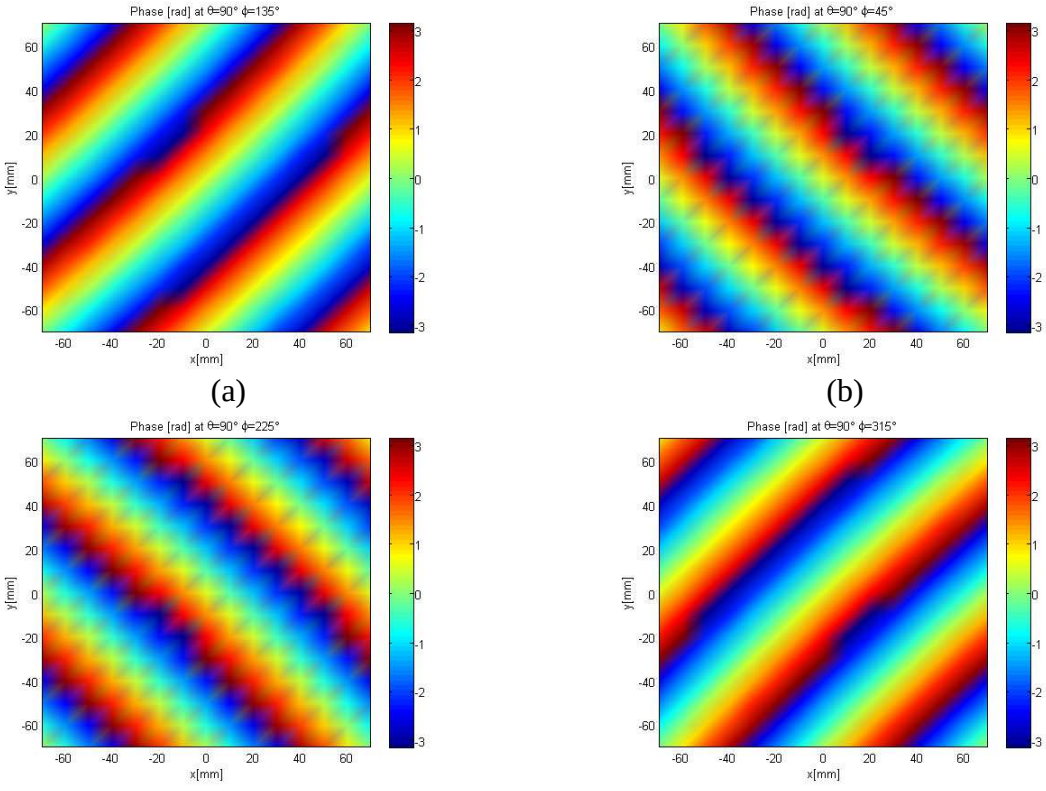

(a) (b)

(c) (d)

Figure 5-11 Simulated transfer function phase [rad] at 5.9 GHz: antenna 2 (a), antenna 1 (b), antenna 3 (c) antenna 4 (d)

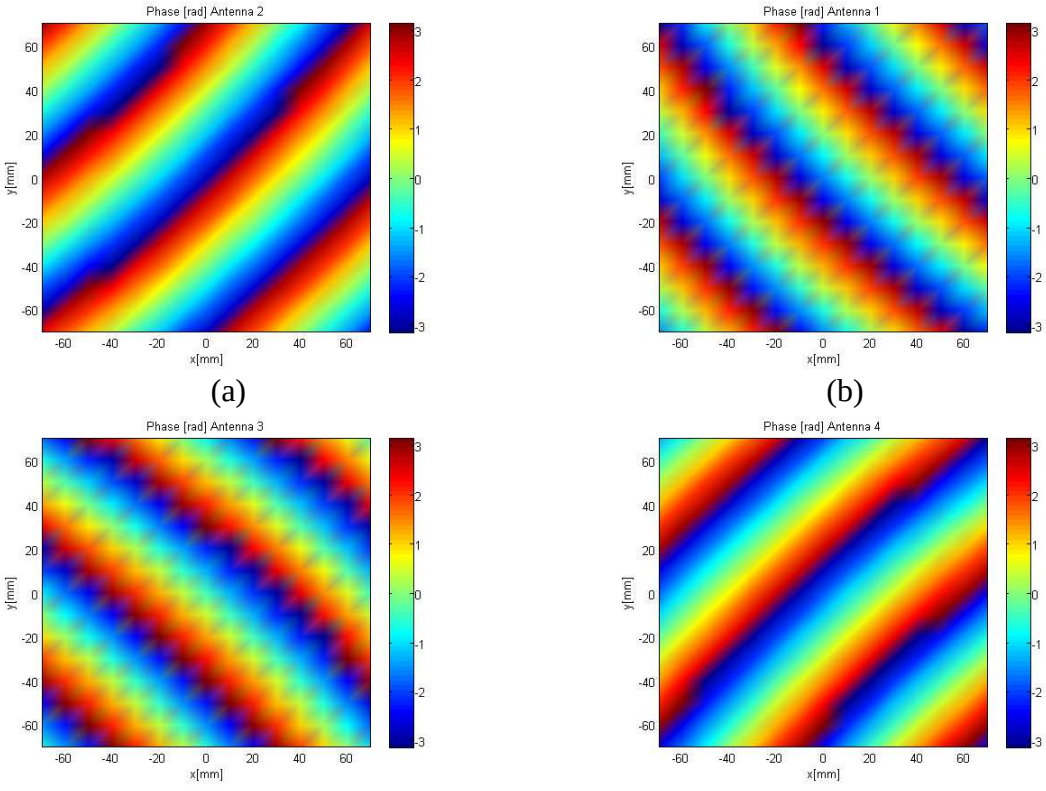

(a) (b)

(c) (d)

Figure 5-12 Measured transfer function phase [rad] at 5.9 GHz in the: antenna 2 (a), antenna 1 (b), antenna 3 (c), antenna 4 (d)

Figure 5-11 and Figure 5-12 show a good agreement between the measured and the simulated complex field in term of phase. It is important to notice that at 5.9 GHz, the planar wave condition is poorly verified in both simulation and measurements.

5.3.2 Sectorial setup configuration

Here we use the flexibility of the proposed tri-dimensional structure to realize a second sectorial configuration. This configuration is chosen to potentially emulate directional channel or single cluster one. An illustration of this configuration is presented in Figure 5-13 together with a schematic view. Samples over test zone are marked with black grid. Antenna angular positions are reported in Table 5-2.

Table 5-2 Angular locations of OTA antennas in sectorial setup

OTA elevation ring	Azimuth Angular locations
$\theta_{1,2,3,4} = 90°$	$\phi_1 = 0\,°, \phi_2 = 60\,°, \phi_3 = 120°, \phi_4 = 180\,°,$
$\theta_{5,6,7,8} = 30°$	$\phi_5 = 0\,°, \phi_6 = 60\,°, \phi_7 = 120°, \phi_8 = 180\,°,$
$\theta_{9,10,11,12} = 60°$	$\phi_9 = 0\,°, \phi_{10} = 60\,°, \phi_{11} = 120\,°, \phi_{12} = 180\,°,$

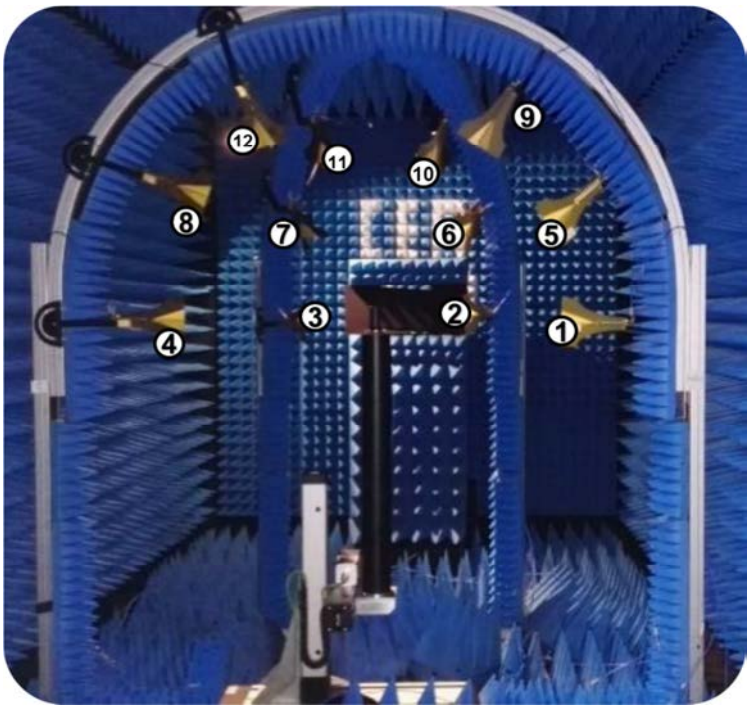

(a)

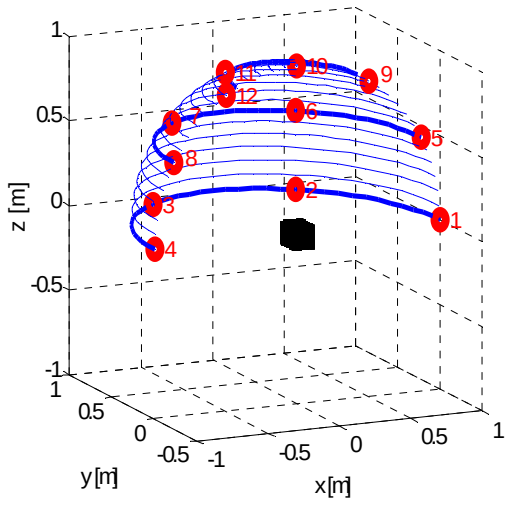

(b)

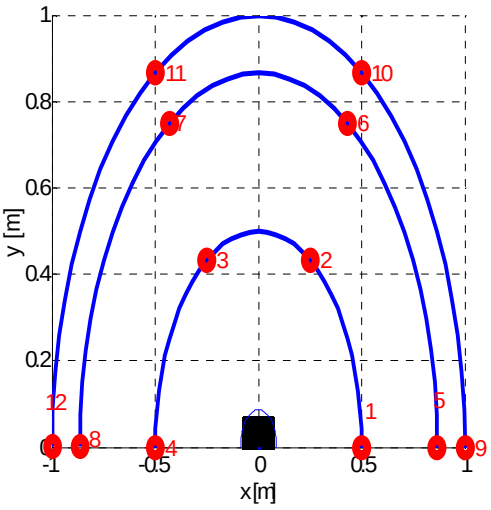

(c)

Figure 5-13 OTA sectorial setup configuration: (a) picture, (b) 3Dview, (c) top view

As for the uniform configuration here, for sake of briefness, we only show the results in the azimuth plane at 2GHz and 5.9GHz.

The comparison of the simulated (Figure 5-14) and measured (Figure 5-15) amplitude of the transfer function, show the presence of some residual scattering in the setup, which can locally yield to a higher attenuation up to 3 dB.

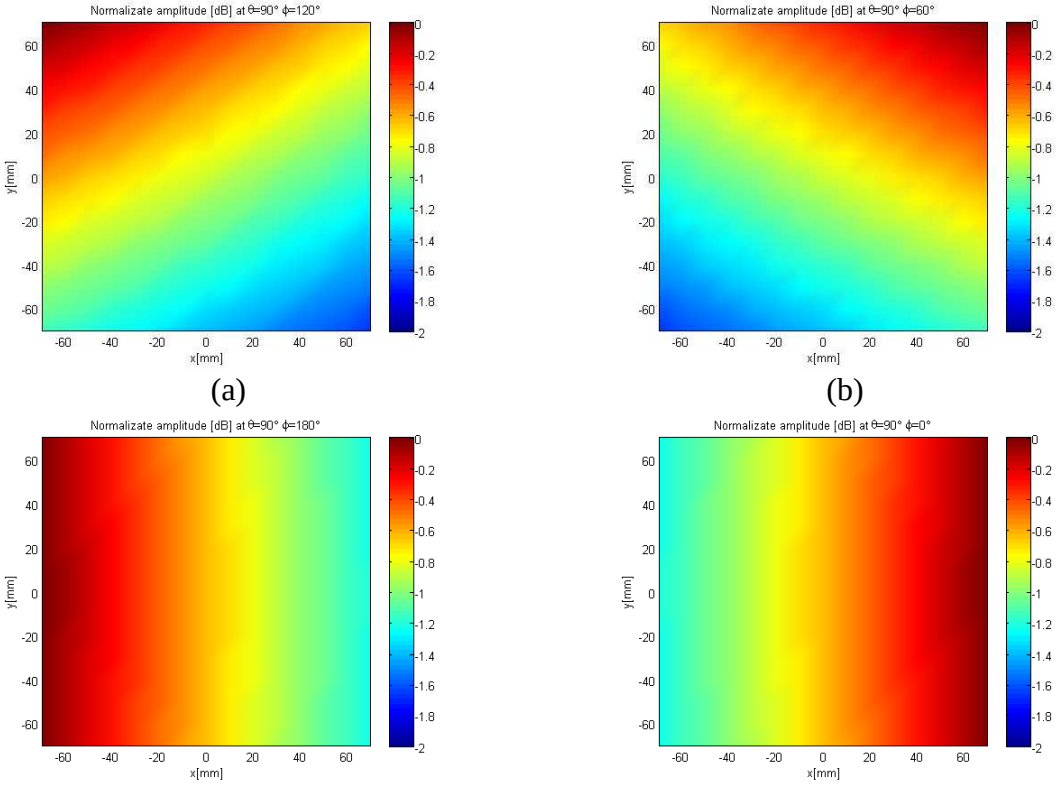

(a) (b)

(c) (d)

Figure 5-14 Normalized simulated transfer function amplitude [dB] at 2 GHz: antenna 1 (d), antenna 2 (b),antenna 3 (a), antenna 4(c)

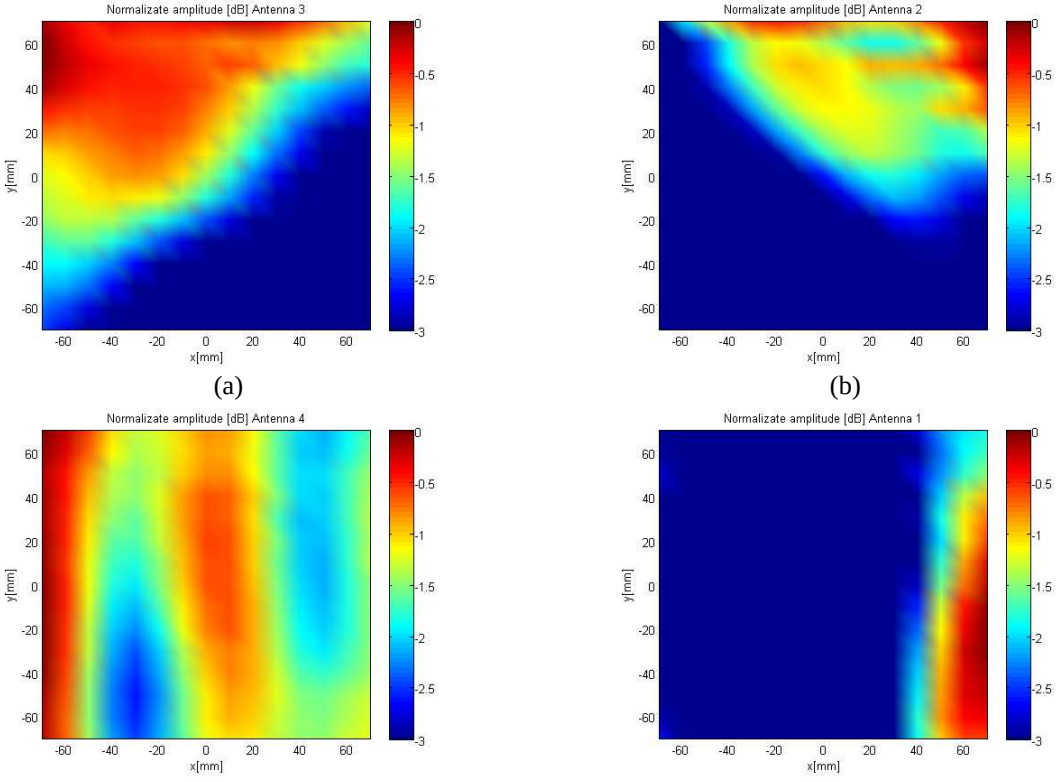

(a) (b)

(c) (d)

Figure 5-15 Normalized measured transfer function amplitude [dB] at 2 GHz: antenna 1 (d), antenna 2 (b), antenna 3(a), antenna 4(c)

Figure 5-16 and Figure 5-17 compare the simulated and measured transfer function's phase. We can notice that the phase fronts arrive with wavelengths corresponds well to the emulated frequency (2 GHz), but the impinging phase fronts from OTA antennas at $\phi = 60\,°$ and $\phi = 120\,°$ are more spherical than the one at $\phi = 180°$ and $\phi = 0\,°$.
As for the uniform configuration the agreement in phase between the simulation and measurement is verified for the phase, which suffers less than amplitude of residual scattering in the setup.

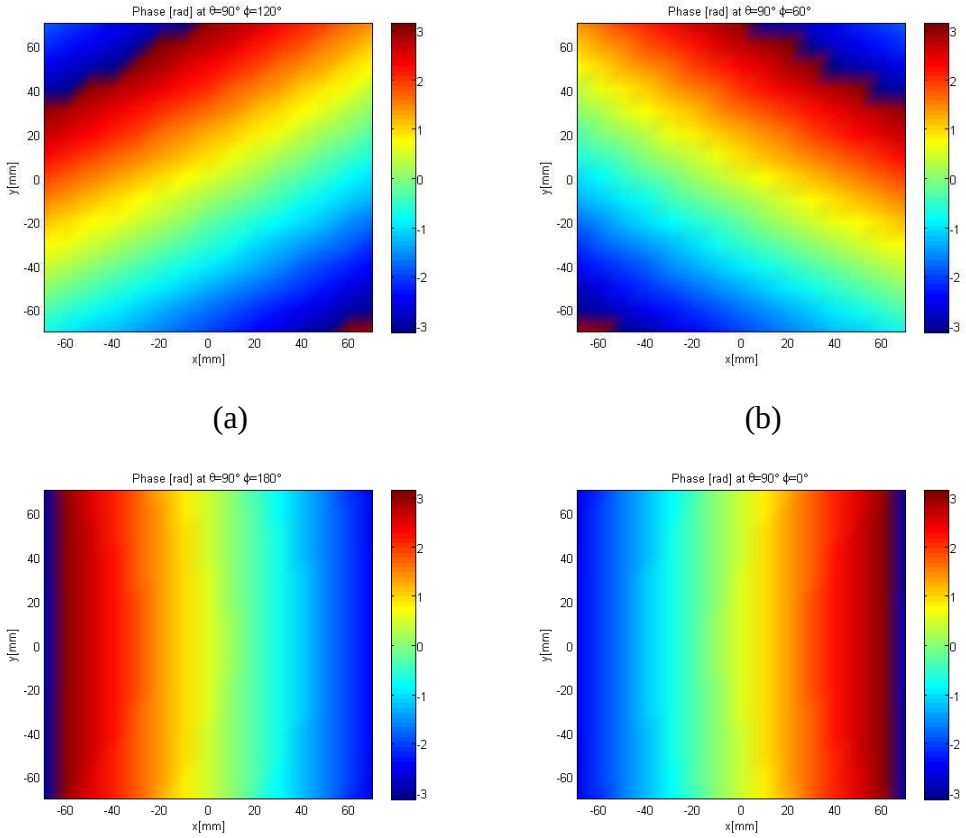

(a) (b)

(c) (d)

Figure 5-16 Simulated transfer function phase [rad] at 2 GHz: antenna 1 (d), antenna 2 (b), antenna 3 (a) antenna antenna 4 (c)

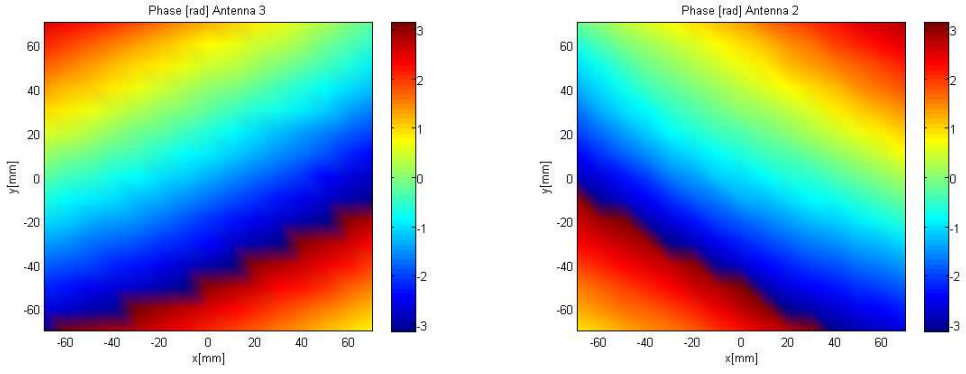

(a) (b)

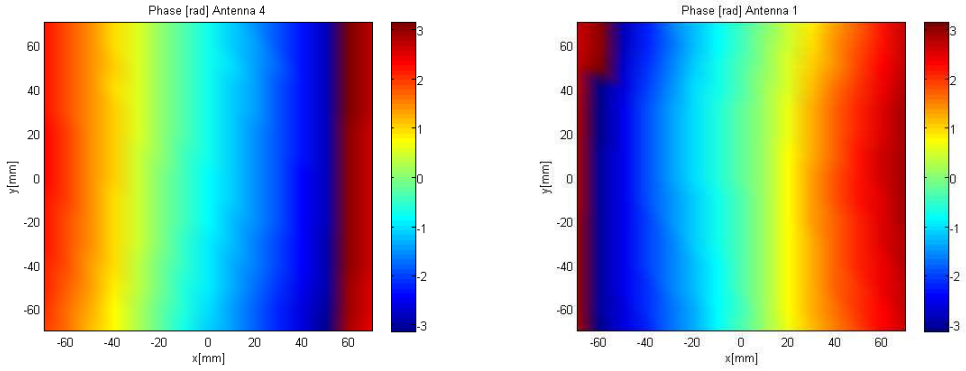

(c) (d)

Figure 5-17 Measured transfer function phase [rad] at 2 GHz: antenna 1 (d), antenna 2 (b), antenna 3 (a) antenna 4(c)

The same analysis has been carried out at 5.9 GHz for the amplitude as illustrated in Figure 5-18 and Figure 5-19 in term of synthesis amplitude field in simulations and measurements. Phase transfer function component is illustrated in Figure 5-20 and Figure 5-21.
As expected the planar wave assumption seems less verified at 5.9 GHz than 2 GHz.

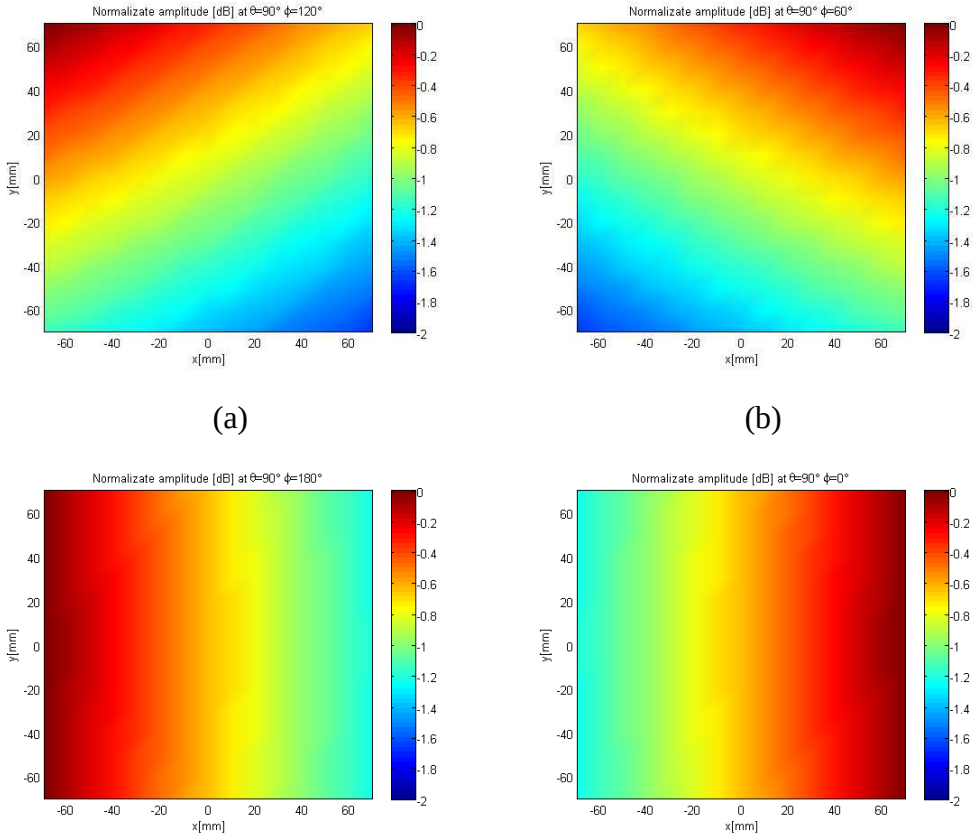

(a) (b)

(c) (d)

Figure 5-18 Normalized simulated transfer function amplitude [dB] at 5.9 GHz: antenna 1 (d), antenna 2 (b), antenna 3 (a), antenna 4 (c)

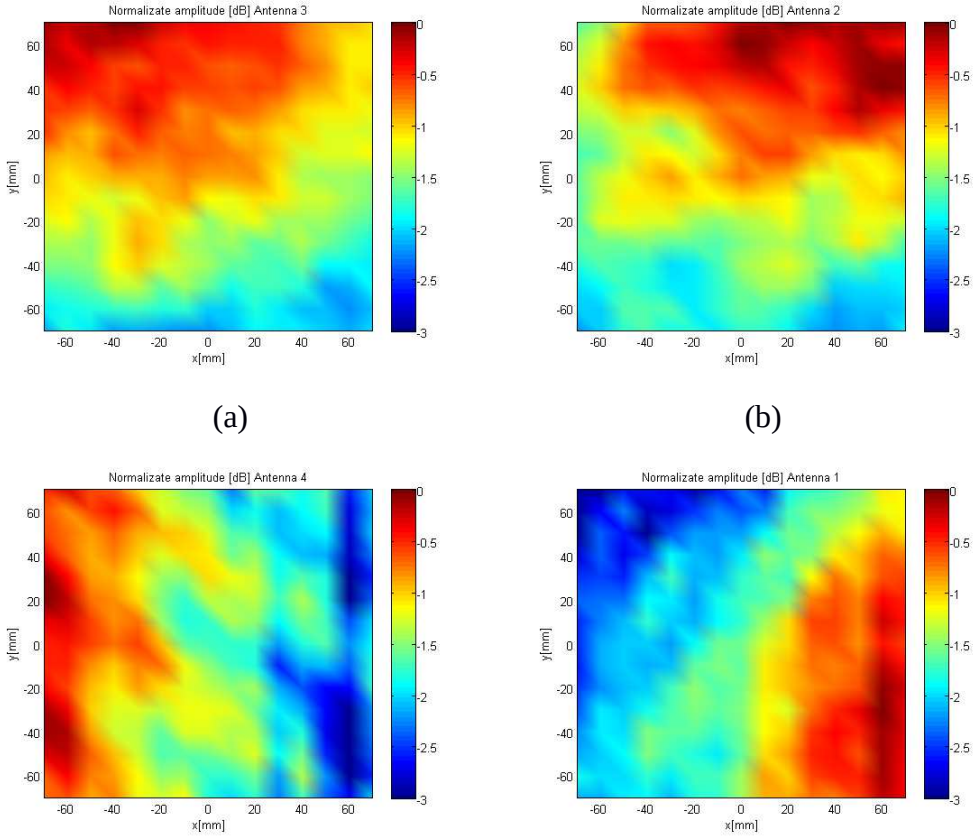

(a) (b)

(c) (d)

Figure 5-19 Normalized measured transfer function amplitude [dB] at 5.9 GHz: antenna 1 (d), antenna 2 (b), antenna 3 (a), antenna 4(c)

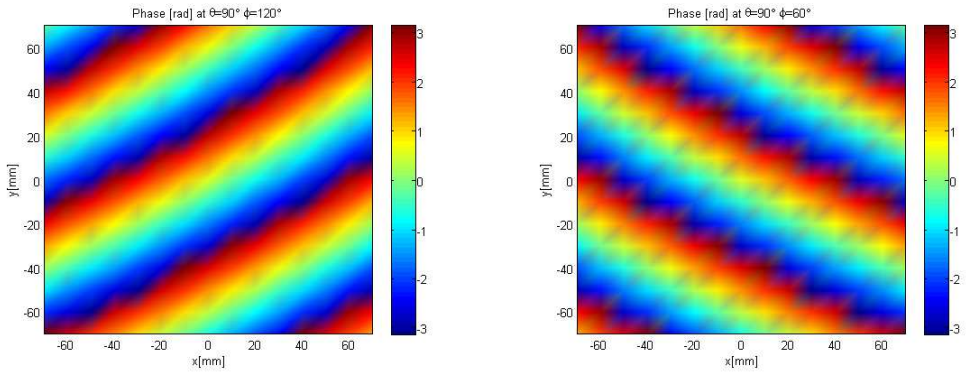

(a) (b)

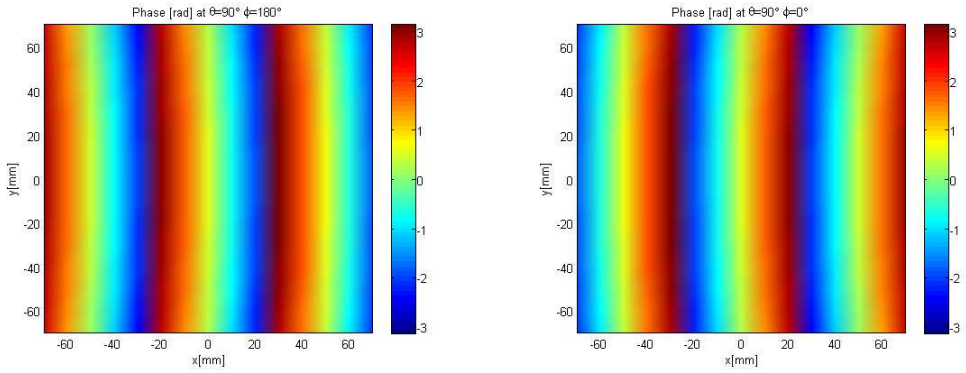

(c) (d)

Figure 5-20 Simulated transfer function phase [rad] at 5.9 GHz: antenna 1 (d), antenna 2 (b), antenna 3 (a), antenna 4 (c)

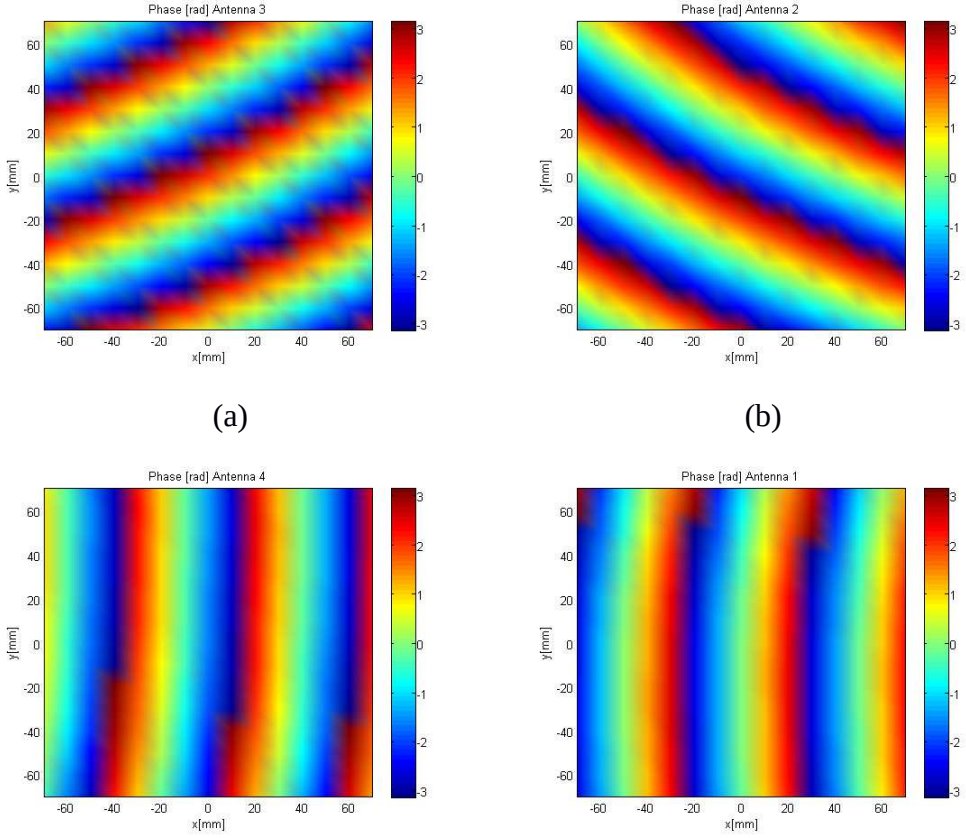

(a) (b)

(c) (d)

Figure 5-21 Measured transfer function phase [rad] at 5.9 GHz: antenna 1 (d), antenna 2 (b), antenna 3 (a), antenna 4 (c)

In conclusion, two possible configurations of the OTA test-bed have been realized and characterized in terms of field distribution in the Zone Under Test.
It has been shown, that despite the presence of absorber, some residual scatterers and eventually some error in alignment can yield to a discrepancy between the target field and realized one. In practice the residual scattering can create some undesired fading, which is clearly visible on the amplitude distribution.

Moreover the physical constraint of the setup, i.e. reduced dimensions of the anechoic chamber, can limit the space between the Zone Under Test and the source OTA antenna, which could nullify the planar wave condition especially at high frequency. The impact of these imperfections is then studied in the following section.

5.4 OTA emulated channel correlation

In the previous chapters we presented different techniques to emulate realistic channel conditions using the multi-probes anechoic chamber: the Plane Wave Synthesis (PWS and Prefaded Signal synthesis. (PFS) The PWS technique synthesizes the intended electromagnetic field inside the test zone by weighting the multiple probes with proper excitations, such that the total field from the probes resembles the intended field at a location in the test zone.

Based on spherical wave theory we have been demonstrated theoretical justification of the required number of OTA antennas, to emulate target field on the test zone as wavelength. It has been demonstrated, that for larger ZUT, we need four OTA antennas in 2D configuration of probes. That, we give us an idea on size of quiet zone. Yet, our focus is on how to reproduce the desired channel conditions within the test zone where device is placed.

The purpose of the PFS channel emulation technique is to emulate spatial channel characteristics such as power angular spectrum within the test zone. Here we consider different channel models to be emulated:

- an isotropic channel (in 2D and 3D) ;
- a single cluster channel (in 2D and 3D).

While the first one is aimed in the uniform configuration, the second one is emulated through the sectorial configuration.
The probe weights, as described in chapter 4, have been obtained in order to reproduce the desired power angular spectrum and corresponding correlation.
Here for each position *i* in ZUT, and polarization, we compute the total channel as a weighted sum over all the OTA antennas

$$H_i(f) = \sum_{s=1}^{N_{ant}} w_s \cdot H_{i,s}(f) \tag{5.2}$$

Where w_s are the optimized weights to reproduce the PAS (see chapter 4), and $H_{i,s}(f)$ is the transfer function corresponding to (5.1).
As explained in the previous section, we scan a 3D ZUT. Here in the following subsection we analyze the autocorrelation of the total channel of (5.2), by performing a 2D cross correlation over the plane of interest.

5.4.1 2D Isotropic channel, OTA uniform configuration

To verify the capacity of our uniform configuration to reproduce an accurate field distribution, we uniformly weighted the OTA antennas from 1 to 4.

In Figure 5-22(a), we show the total transfer function at 2 GHz in the ZUT in the ideal case where the number of OTA antennas are infinite. One should notice that the correlation present the symmetric omnidirectional pattern with some fading that is due to the multipath combination. However the quality of the map, in terms of visual representation depends on the sampling of the ZUT. Figure 5-22(b) presents the same result, but with a sampling equal to the one used in measurement.
Finally Figure 5-22(c) and Figure 5-22(d) show the simulated and measured total field with a reduced number of OTA antennas. One can first notice that the reduced number of antenna generates some discrepancy with respect to the ideal one. This is mainly due to the poor sampling of the PAS, and depends on the specific OTA antenna location in the setup. On the other hand the realization introduces additional difference because of the fading related to the residual scattering in the environment as discussed before.

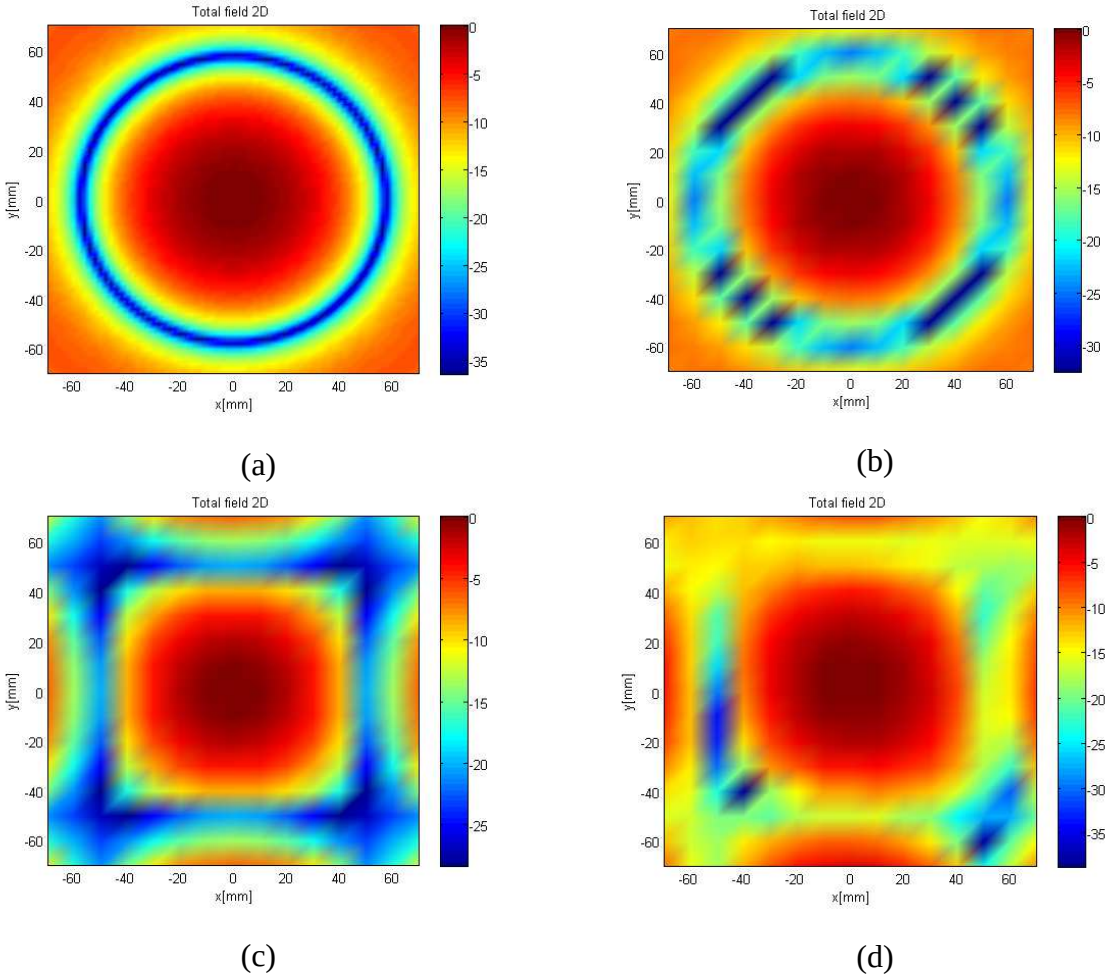

Figure 5-22 2D isotropic channel. Normalized total transfer function amplitude at 2 GHz: simulation isotropic antenna Nant=∞ (a); simulation isotropic antenna N_{ant}=∞ , sampling 10 mm (b); simulation isotropic antenna N_{ant}=4, sampling 10 mm (c); measured N_{ant}=4, sampling 10 mm(d).

In order to analyze the quality of the OTA emulation, here we consider the total field correlation as in Figure 5-23. Here we clearly see that there is a good agreement on correlation in a small zone before the fist 0. Than the correlation lobes are affected by both the spatial sampling and number of antennas. However when comparing similar condition in simulation and measurements, there is a poor effect of the setup imperfections on the accuracy of correlation, which reduce to a “blurring” of the side lobes (Figure 5-23 (b)).

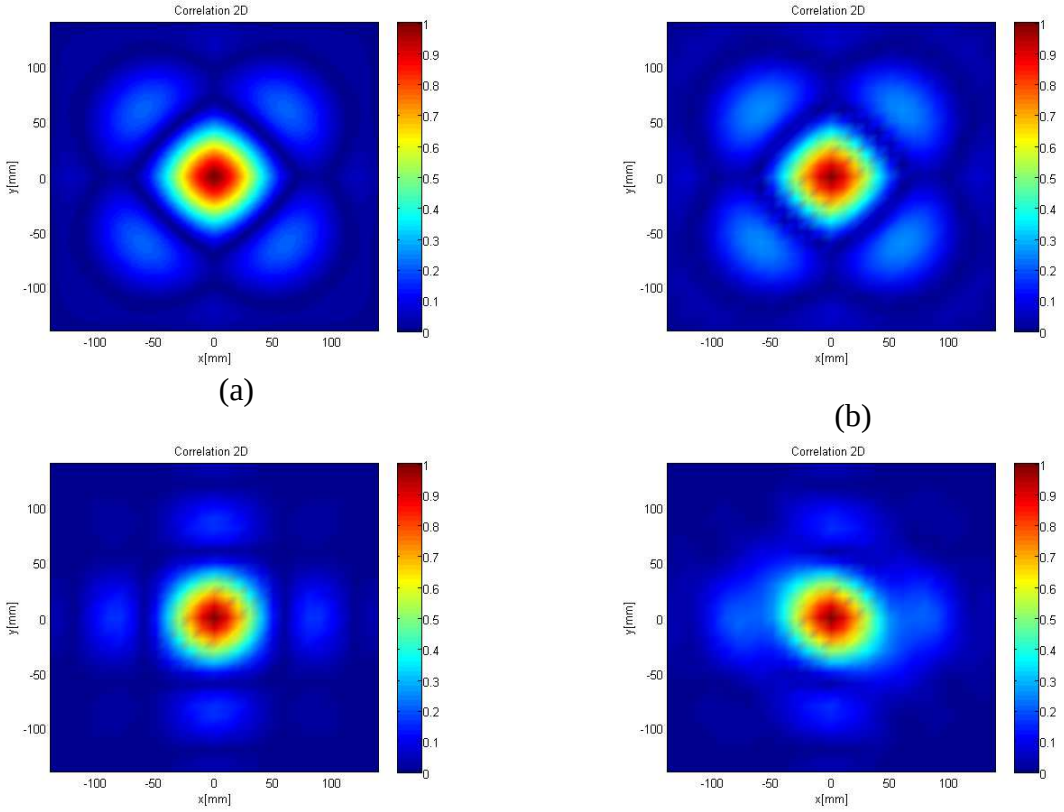

(a) (b)

(c) (d)

Figure 5-23 2D isotropic channel. Correlation at 2 GHz: simulation isotropic antenna Nant=∞ (a); simulation isotropic antenna N_{ant}=∞ , sampling 10 mm (b); simulation isotropic antenna N_{ant}=4, sampling 10 mm (c); measured N_{ant}=4, sampling 10 mm(d)

Similar analysis has been done for the 5.9 GHz. As depicted in Figure 5-24 (d) the scattering in the setup can destroy the symmetry of the total field amplitude (Figure 5-24 a-c).
However in terms of correlation, the result for the sampling 10 mm and limited number of antennas are very similar in simulation and measurements (Figure 5-25 (c) (d)).

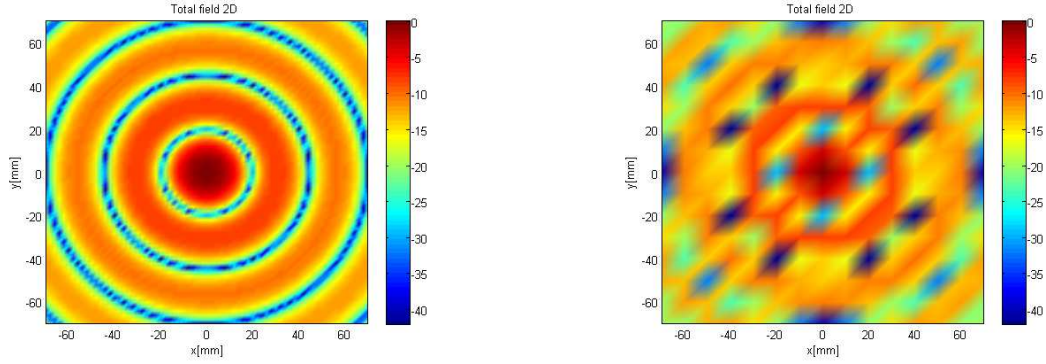

(a) (b)

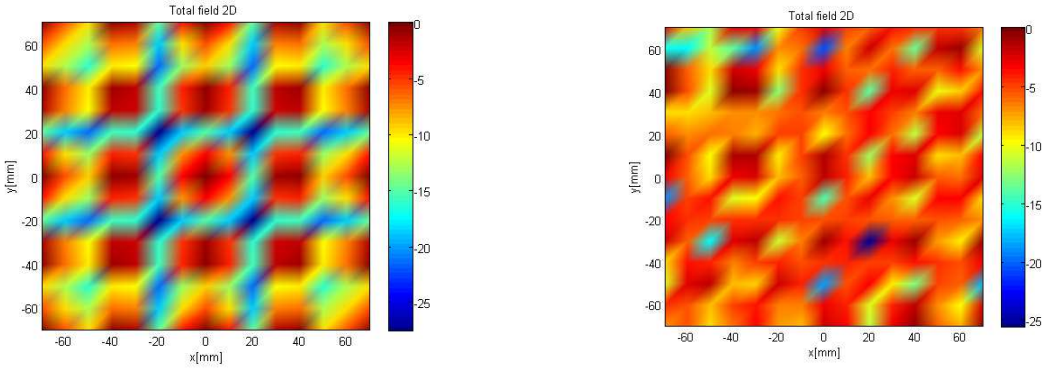

(c) (d)

Figure 5-24 2D isotropic channel. Normalized total transfer function amplitude at 5.9 GHz: simulation isotropic antenna Nant=∞ (a); simulation isotropic antenna Nant=∞ , sampling 10 mm (b); simulation isotropic antenna Nant=4, sampling 10 mm (c); measured Nant=4, sampling 10 mm(d).

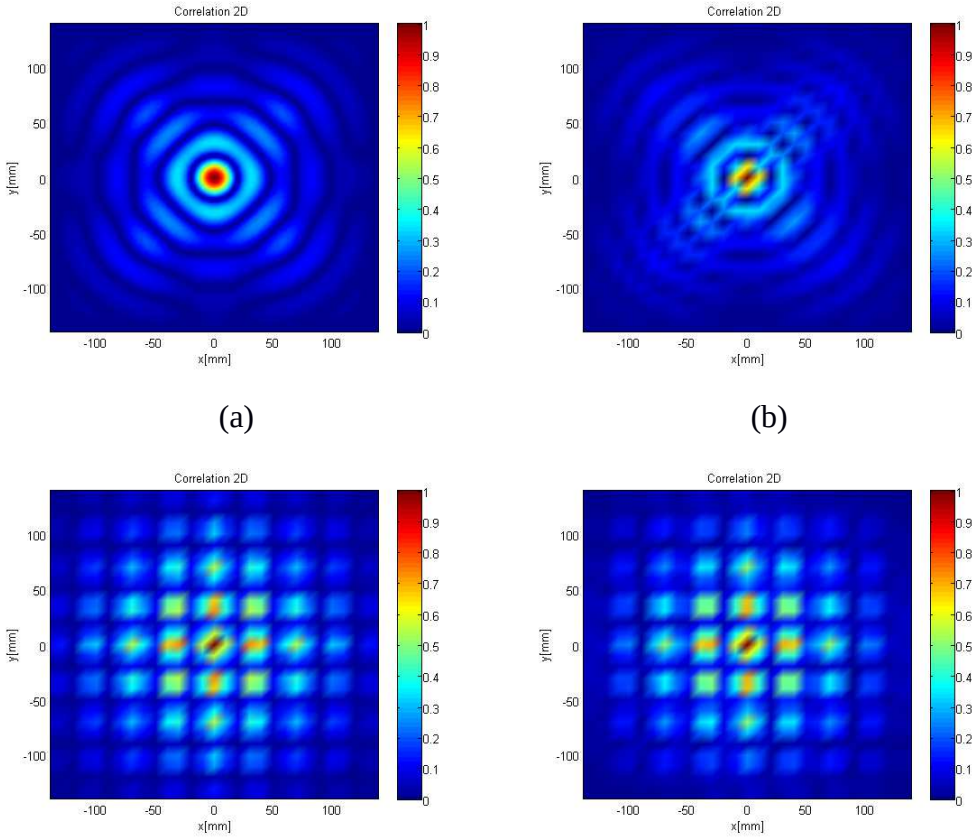

(a) (b)

(c) (d)

Figure 5-25 2D isotropic channel. Correlation at 5.9 GHz: simulation isotropic antenna Nant=∞ (a); simulation isotropic antenna Nant=∞ , sampling 10 mm (b); simulation isotropic antenna Nant=4, sampling 10 mm (c); measured Nant=4, sampling 10 mm(d).

5.4.2 3D Isotropic channel, OTA uniform configuration

A 3D isotropic channel was aimed by feeding with the same weights all the twelve antennas in the uniform setup.

The total field at 2 GHz is presented in Figure 5-26. The reduced number of antennas breaks the aimed symmetry of the field amplitude distribution in the ZUT. Moreover the setup dispersion can reduce even more the distribution Figure 5-26 (c)-(d). Here most likely, beside the residual scattering, some misalignment on the higher ring antennas could have occurred. This is also visible on the correlation of Figure 5-27 and Figure 5-28 where the measured ones are shifted version of the simulated ones.

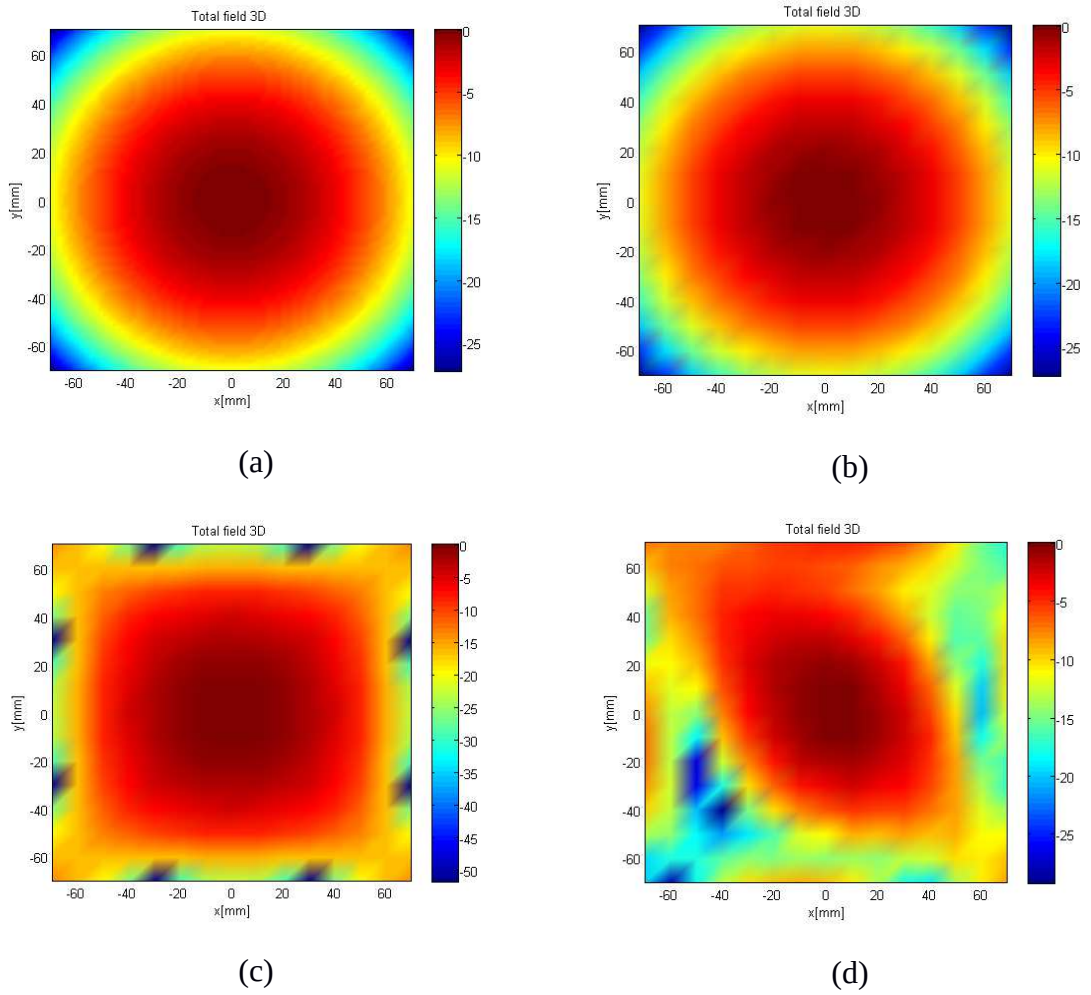

Figure 5-26 3D isotropic channel. Normalized total transfer function amplitude at 2 GHz: simulation isotropic antenna $N_{ant}=\infty$, sampling 2 mm (a); simulation isotropic antenna $N_{ant}=\infty$, sampling 10 mm (b); simulation isotropic antenna $N_{ant}=12$, sampling 10 mm (c); measured $N_{ant}=12$, sampling 10 mm(d).

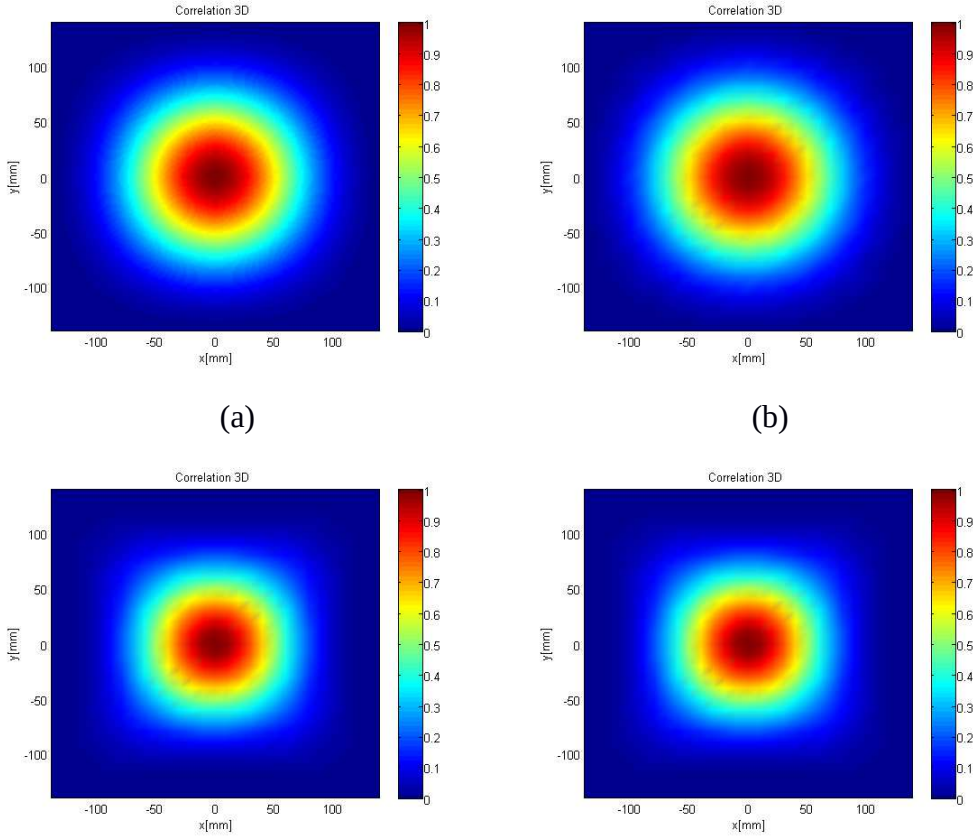

Figure 5-27 3D isotropic channel. Correlation at 2 GHz: simulation isotropic antenna $N_{ant}=\infty$, sampling 2 mm (a); simulation isotropic antenna $N_{ant}=\infty$, sampling 10 mm (b); simulation isotropic antenna $N_{ant}=12$, sampling 10 mm (c); measured $N_{ant}=12$, sampling 10 mm(d).

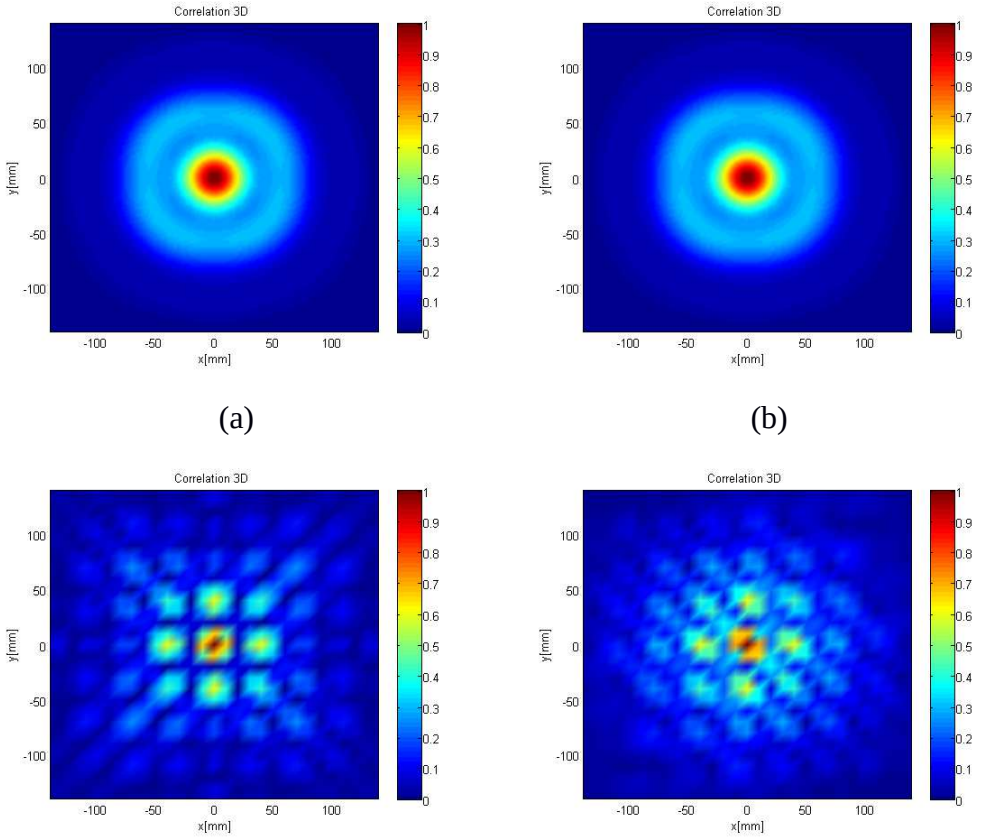

Figure 5-28 3D isotropic channel. Correlation at 5.9 GHz: simulation isotropic antenna $N_{ant}=\infty$, sampling 2 mm (a); simulation isotropic antenna $N_{ant}=\infty$, sampling 10 mm (b); simulation isotropic antenna $N_{ant}=12$, sampling 10 mm (c); measured $N_{ant}=12$, sampling 10 mm(d).

In practice from the autocorrelation point of view the size of validity of the ZUT at 5.9 GHz seems smaller than the one at 2 GHz.

This could be explained not only by the imperfections of the setup, and the non-planarity of the impinging wave, but also by the OTA antenna effect. Actually the LTSA employed, being a constant aperture antenna, has higher directivity at 5.9 GHz, which could somewhat affects the illumination of the ZUT.

From simulation results, we found that the minimum number of OTA antennas to fulfill the acceptance criteria depend on the size of ZUT, positions of OTA probes and on the channel model. Due to the directionality of isotropic channel model, the OTA uniform configuration should be relevant, to cover all (AoA) s of scatterers.

5.4.3 2D Single cluster channel, OTA sectorial configuration

The concept of clusters has been widely adopted to model the multipath phenomenon, as mentioned in chapter 2. Clusters generally arrive with different delay and angle of arrival. Here

the goal is to recreate OTA the cluster characteristics. The uniform configuration is the one that is the most suited to emulate every AoA distribution. However, as show in chapter 3, the number of antennas required could be too high with respect to the cost.

Hence we opted here for a sectorial configuration to emulate a single cluster channel, with AoA equals to 90° and azimuth spread equal to 35°. The PAS presents a Laplace distribution. The goal is to employ the sectorial setup in 5.3.2 to have a reduced number of antennas, and assess the quality of the emulation OTA.

Figure 5-29 shows a comparison between simulations and measurement results of normalized field synthesized at 2 GHz. The sampling grid effect of ZUT is also verified in single cluster model as seen in Figure 5-29 (b). Measurement of synthesized complex field in OTA sectorial configuration, Figure 5-29 (c) matches the simulation in terms of field distribution, as depicted in Figure 5-29 (d).

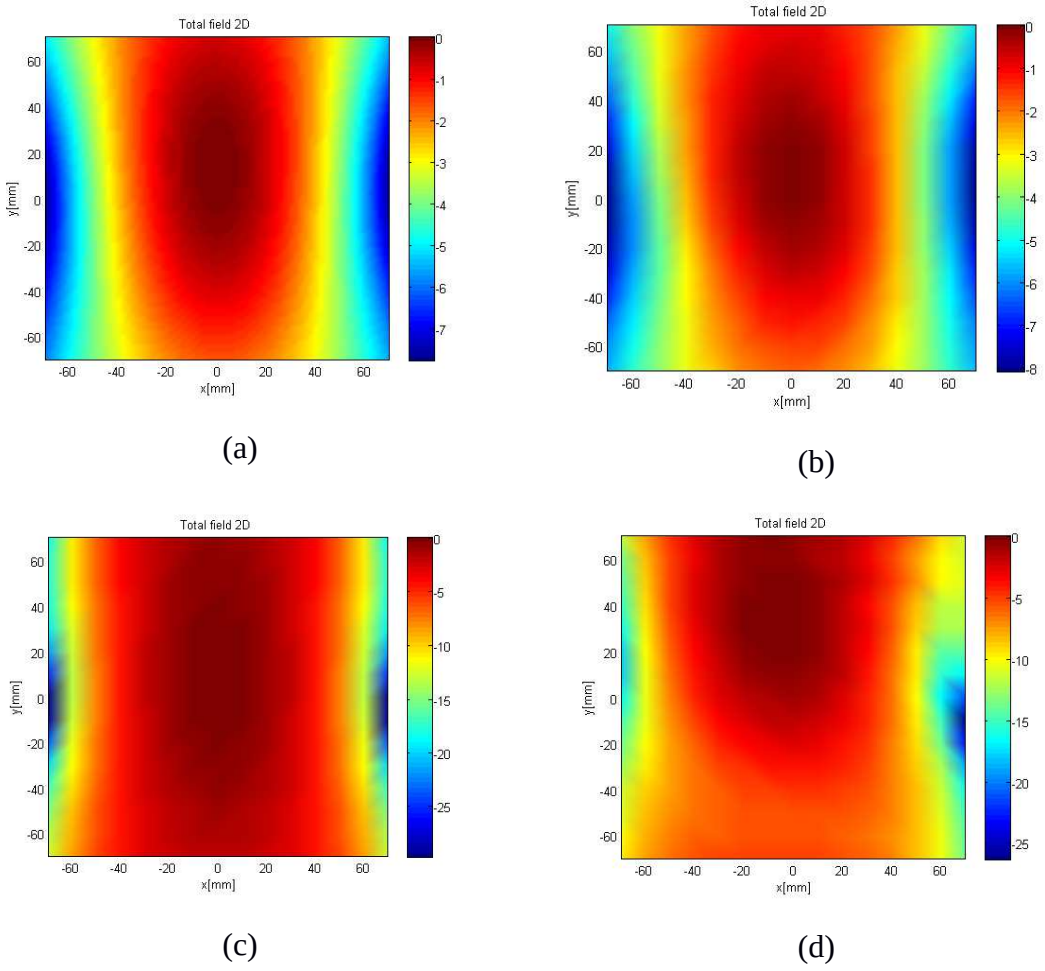

Figure 5-29 2D single cluster channel. Normalized total transfer function amplitude at 2 GHz: simulation isotropic antenna Nant=∞ (a); simulation isotropic antenna Nant=∞ , sampling 10 mm (b); simulation isotropic antenna Nant=4, sampling 10 mm (c); measured Nant=4, sampling 10 mm(d).

After verifying that the field synthesized in the sectorial configuration, matches the one expected from simulation, we compared the autocorrelation obtained from measurements with the one from simulation in Figure 5-30.

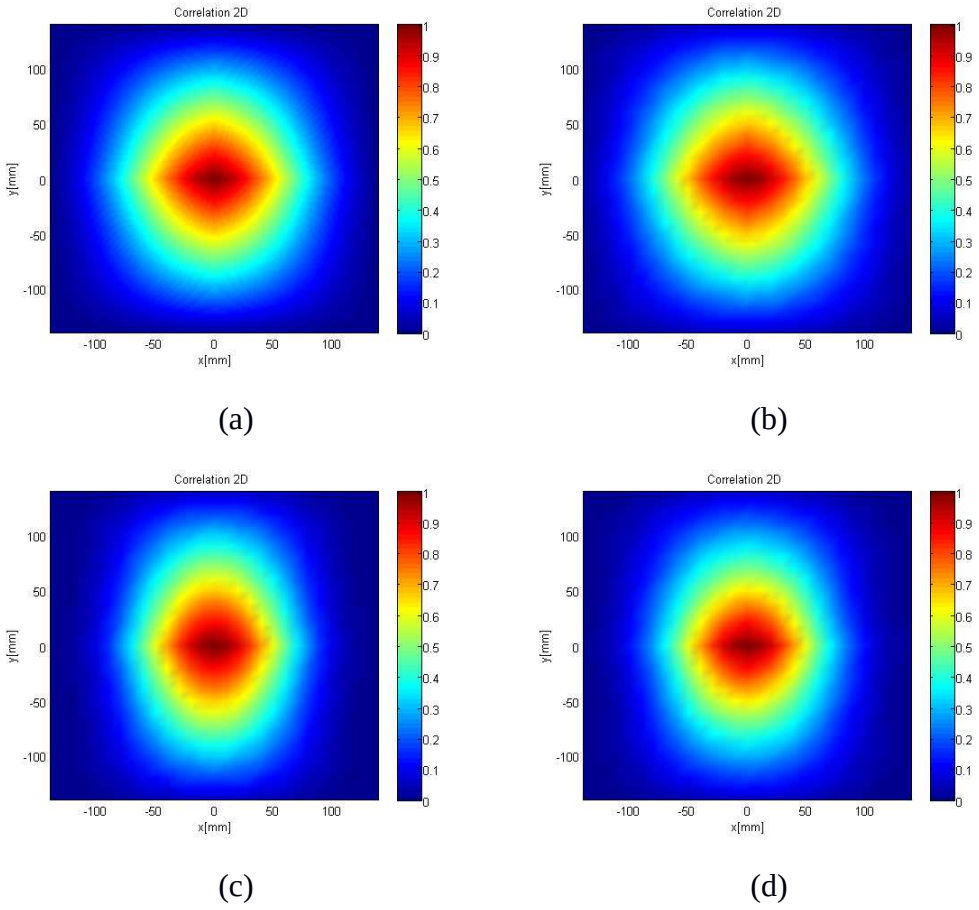

Figure 5-30 2D single cluster channel. Correlation at 2 GHz: simulation isotropic antenna $N_{ant}=\infty$ (a); simulation isotropic antenna $N_{ant}=\infty$, sampling 10 mm (b); simulation isotropic antenna $N_{ant}=4$, sampling 10 mm (c); measured $N_{ant}=4$, sampling 10 mm(d).

A good agreement between simulation and measurement results, see Figure 5-30(c) and Figure 5-30 (d).

The same analysis and comparison between 2D map of synthesized fields at 5.9 GHz is depicted in Figure 5-31. Here the sampling of the ZUT can have a high visual impact on the maps of amplitude distribution. However one can notice that simulation and measurement under the same sampling have a similar pattern. (Figure 5-31 (c)-(d)).

In order to illustrate the potentiality of the sectorial configuration, on OTA channel emulation. The measurements campaigns are carried out at 5.9 GHz. The impinging of the distribution of measurement field, as seen in Figure 5-31(d) correspond at AOA = 90° of single cluster channel model. This can be also verified in simulation of 2D field distribution, as shown in Figure 5-31(c). Figure 5-32 highlights the impact of ZUT sampling on the target spatial correlation at 5.9 GHz, as seen in Figure 5-32 (a) and Figure 5-32 (b). It is clearly shown that the larger sampling, i.e. 10 mm affects the resolution of the 2D correlation map. 2D spatial and measured spatial correlation as illustrated in Figure 5-32 (c) and Figure 5-32 (d). Nevertheless good agreement between simulation and measurement result is observed.

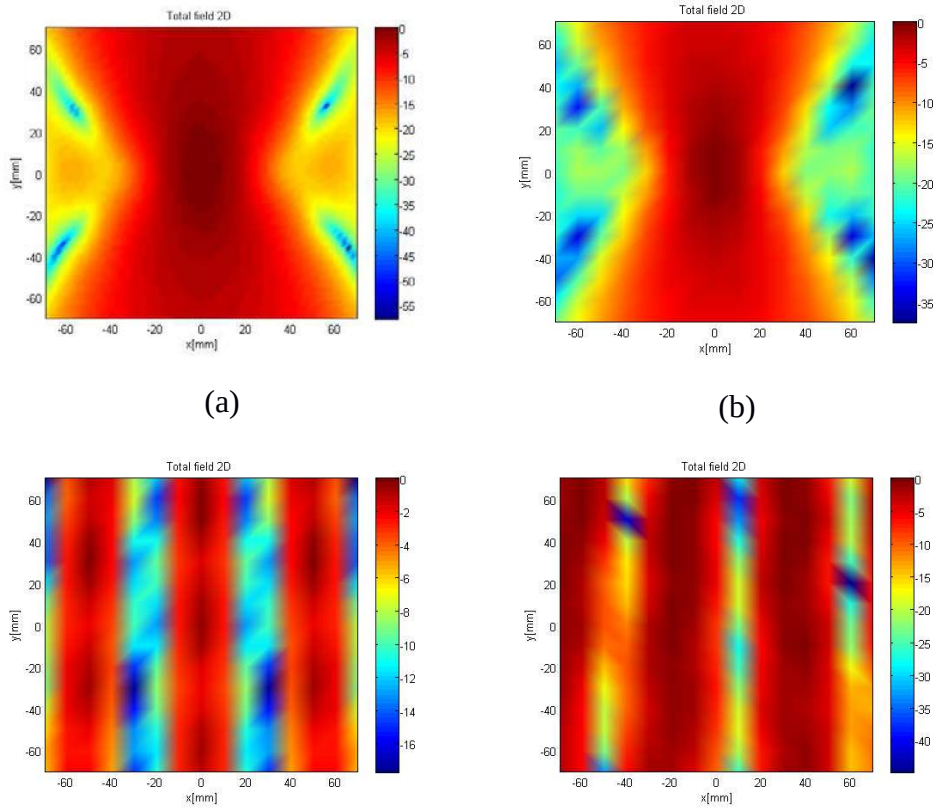

Figure 5-31 2D single cluster channel. Normalized total transfer function amplitude at 5.9 GHz: simulation isotropic antenna $N_{ant}=\infty$ (a); simulation isotropic antenna $N_{ant}=\infty$, sampling 10 mm (b); simulation isotropic antenna $N_{ant}=4$, sampling 10 mm (c); measured $N_{ant}=4$, sampling 10 mm(d).

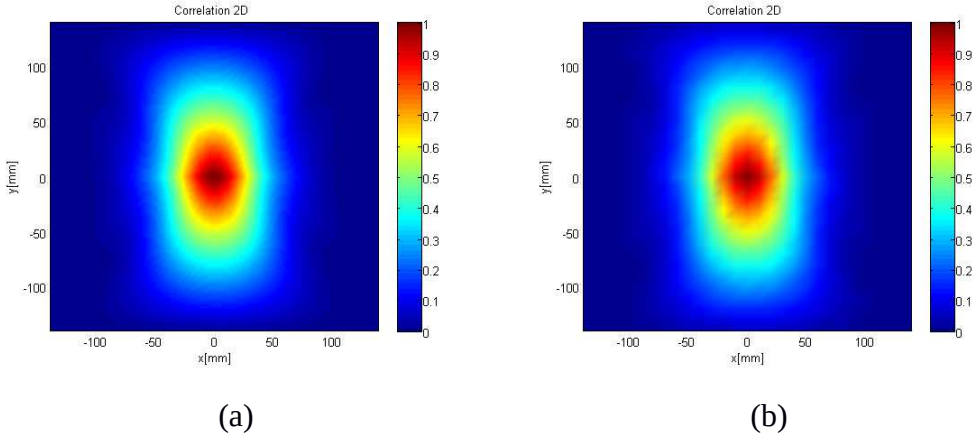

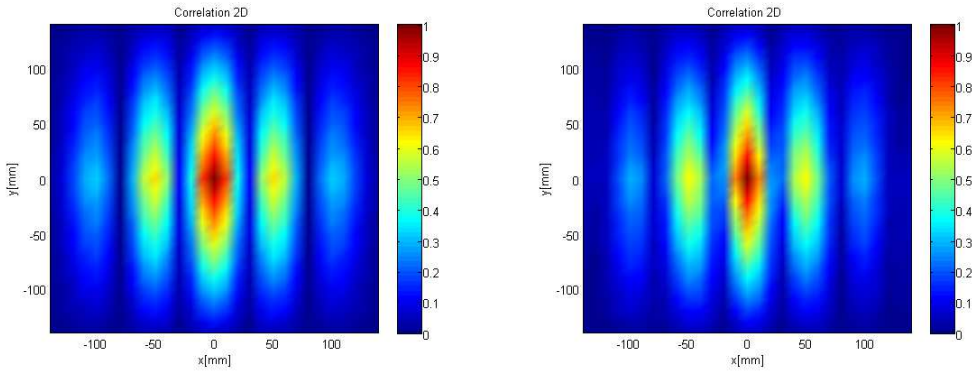

(c) (d)

Figure 5-32 Spatial correlation (a) target spatial correlation (b) emulated with finite number of Isotropic probes (c) with sampling 10 mm and (d) measured spatial autocorrelation f = 2 GHz

5.4.4 3D single cluster channel, OTA sectorial configuration

In the 3D case of sectorial OTA multi-probes setup, we compare the field obtained by summing 12 OTA antennas in azimuth and elevation, Figure 5-33, in simulation and measurements. Here the elevation spread was taken equals to 15°. It can be seen that despite some discrepancy between the simulated and measured field distribution, the correlation in Figure 5-34 is quite in good agreement.

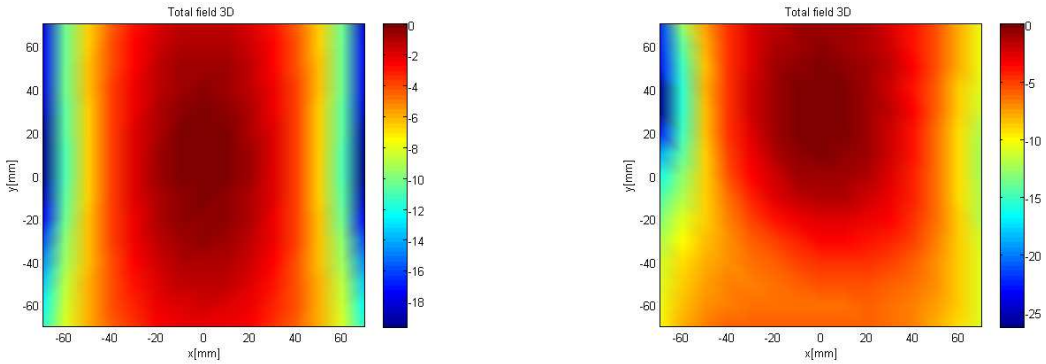

(a) (b)

Figure 5-33 3D single cluster channel. Normalized total transfer function amplitude at 2 GHz: simulation isotropic antenna N_{ant}=12, sampling 10 mm (a); measured N_{ant}=12, sampling 10 mm(b).

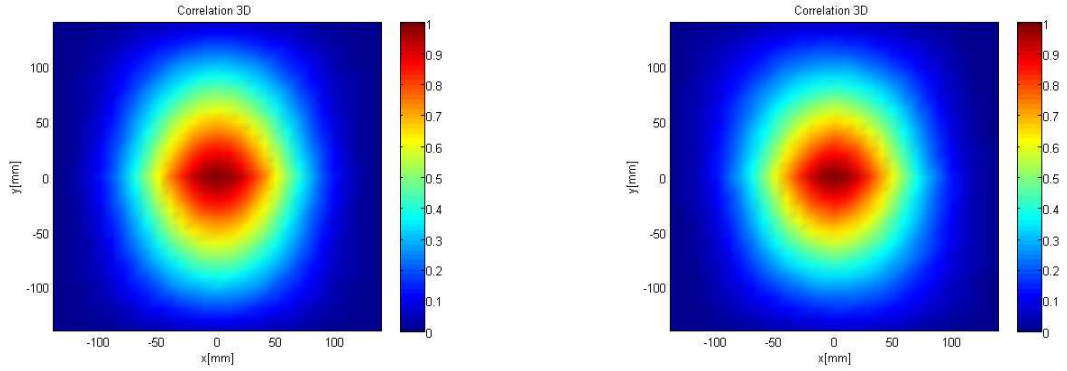

(a) (b)

Figure 5-34 3D single cluster channel. Correlation at 2 GHz: simulation isotropic antenna N_{ant}=12, sampling 10 mm (a); measured N_{ant}=12, sampling 10 mm(b).

5.5 Conclusion

In this chapter we presented an experimental realization of 3D multi-probe setup for OTA test. Linearly Taped Slot Antennas, working between 2 and 6 GHz were employed as probes. These antennas were chosen to recreate a channel over a wide band, while controlling the polarization.

The setup was presented and characterized by means of Vector Network Analyzer and a 3D positioner. The antenna under test employed was a wide band monopole.

Two dispositions of 12 antennas were considered. The first one is a uniform configuration over three elevation ring. The second configuration covers a half plane, i.e. 180° and named sectorial configuration.

Mutual coupling between antennas is generally lower than -30 dB. The field distribution was characterized in both amplitude and phase. While the phase is very close to the expected one, the amplitude shows some fluctuations which are most likely due to the non-ideality of the system and possible scattering on the setup.

Nevertheless when analyzing the channel autocorrelation for a uniform and single cluster model, it was shown that by using an appropriate weighting of antennas it is possible to have a good agreement between the measurement and simulation results.

Chapter 6

6 Conclusion and Perspectives

In this thesis, we addressed various aspects related Over-The-Air (OTA) methods, with the objective to develop a technique to emulate the radio channel in a controlled manner.

As explained in the introduction of the first chapter, this work is motivated by the need of evaluating the performance of wireless devices, without performing costly and time-consuming field trials. This requirement is already a reality for the existent 3G/4G mobile devices, as well as for Wireless Local Area Networks (WLANs), and it is expected to be fundamental for the deployment of the fifth generation (5G) of mobile networks, Vehicular-to-everything (V2X) communication, as well as for Internet of Things (IoT) solution. Hence the work has been focused on a wide spectrum of frequencies below 6 GHz, aiming to have a versatile setup for OTA tests.

In the second chapter we introduced the fundamentals of radio channel. The deterministic and stochastic approaches of modeling were presented. In particular classical mathematic representation of the channels, by means of the functions firstly introduced by Bello, and classical fading models (e.g. Rayleigh or Rician) were introduced. It was discussed how the spatial channel characteristics are of fundamental importance for Multiple Input Multiple Output (MIMO) channels exploiting multi-antennas approaches. For this reason Geometrical Stochastic Channel Models (GSCMs), like the one proposed in the WINNER project, are of interest for system performance evaluation. This kind of models is based on the concept of clusters, which are described by their Power Angular Spectrum (PAS). Hence we retained this modeling approach for OTA testing in the three dimension (3D) space from 2 to 6 GHz.

The third chapter provided an overview of different OTA methodologies presented in literature. It described the work about OTA standardization carried out in 3GPP and CTIA groups, as well as different solutions proposed by instrument providers or academia.
The different methodologies were discussed and we show that the test methodology based on multi-probe deployed in anechoic chamber with a fading emulator is a promising solution for OTA tests. Actually, with respect to the other solutions, this approach has the advantage of being able to emulate a variety of fading scenarios, and to control the spatial characteristics of the reproduced OTA channel, by means of Prefaded Signal synthesis (PFS).

Based on the choice of the multi-probes approach, we developed, in chapter 4, a Matlab simulation tool to dimension the final setup. Different criteria were discussed and it was shown how the far field condition is not enough to define the OTA configuration. Hence we choose to use the spatial correlation accuracy as a figure of merit for OTA dimensioning. We considered a uniform and a single cluster channel in both 2D and 3D space. It was shown how the emplacement and the number of probes is strictly dependent on the device under test (DUT) electrical size. Generally the larger the DUT, the higher is the number of probes needed.

In a simple case study using half wave-length dipoles as probes, it was shown that the number of probes is a parameter which is predominant with respect to the ring radius, to accurately reproduce the channel correlation. The number of probes, which is an important parameter for the cost of the setup, can be reduced by a “smart” disposition of the antennas around the DUT, or by means of PFS technique which optimizes the weight of each probe to reproduce the aimed PAS. In particular for some directional, single cluster, channels it could be convenient to have more antennas on a smaller angular sector, instead of having them uniformly distributed around the DUT. For this reason a flexible and versatile OTA setup was realized.

In chapter 5 we introduced the experimental realization in the anechoic chamber. The setup is based on twelve linearly taped slot directive antennas placed on the 3D space around the DUT. These antennas have two ports in order to independently address the vertical and horizontal polarization. The setup allows to address frequency from 2 to 6 GHz, and mechanically adjust the positions of the probes. Here, for instance, we considered a uniform setup on a hemisphere composed by three rings of antennas to reproduce omnidirectional channels, and a second sectorial setup on half space to reproduce single cluster channels

The characteristic of the field reproduced in anechoic chamber was investigated through measurements employing a vector network analyzer and a 3D positioner scanning the zone under test (ZUT). It was shown that amplitude fluctuations in the ZUT could occur because of the residual scattering of the positioner, the setup itself and eventually the probes. However, despite this fading, the autocorrelation of the channel is close to the one expected from the simulation.

The work carried out in this thesis is foundation stone for future development of OTA tests. The setup is available to reproduce wideband channel over a 3D space, while controlling the polarization. The very first next step is to interface the setup with a fading emulator enabling the OTA emulation of time variant channels. In some cases a number of antennas higher than twelve could be required to emulate OTA channels. This would mean to have a fading emulator with a large number of ports, or to investigate new approaches of probe feeding eventually using switching state.

Moreover the OTA test of large devices, e.g. cars, is expected to be in the next year a need for the automotive market and the advent of autonomous driving. In this sense a methodology to emulate V2X channels needs to be investigated as long with the need of testing the full car or eventually only a representative part of it.

Finally OTA tests are expected to play an important role for 5G technologies that will employ massive arrays or millimeter wave, opening new perspectives in this field of research.

7 References

[1] J. Hansen, D. S. Baum, and A. Paulraj, “Design approach for a time reversal test bed for radio channels,” in 2004 12th European Signal Processing Conference, 2004, pp. 697–700.

[2] S. Salous, “Radio Propagation Measurement and Channel Modeling,” Whiley Publishing, Sep. 2013.

[3] S. P. Yeh, S. Talwar, G. Wu, N. Himayat, and K. Johnsson, “Capacity and coverage enhancement in heterogeneous networks,” IEEE Wirel. Commun., vol. 18, no. 3, pp. 32–38, Jun. 2011.

[4] [S. P. Yeh, S. Talwar, G. Wu, N. Himayat, and K. Johnsson, “Capacity and coverage enhancement in heterogeneous networks,” IEEE Wirel. Commun., vol. 18, no. 3, pp. 32–38, Jun. 2011.

[5] F. M. Berens, P. Jung, and J. Plechinger, “Uplink spectral capacity of an MC/JD-CDMA mobile radio system,” in Vehicular Technology Conference, 1998. VTC 98. 48th IEEE, 1998, vol. 3, pp. 1825–1829 vol.3.

[6] A. Stavridis, M. D. Renzo, P. M. Grant, and H. Haas, “Performance Analysis of Receive Space Modulation in the Shadowing MIMO Broadcast Channel,” IEEE Trans. Commun., vol. PP, no. 99, pp. 1–1, 2017.

[7] L. Tian, J. Zhang, and C. Pan, “Small Scale Fading Characteristics of Wideband Radio Channel in the U-Shape Cutting of High-Speed Railway,” in 2013 IEEE 78th Vehicular Technology Conference (VTC Fall), 2013, pp. 1–6.

[8] B. Bing, “Wireless Local Area Networks: The New Wireless Revolution [Book Review],” IEEE Commun. Mag., vol. 41, no. 8, pp. 8–10, Aug. 2003

[9] P. Bello, “Characterization of Randomly Time-Variant Linear Channels,” IEEE Trans. Commun. Syst., vol. 11, no. 4, pp. 360–393, Dec. 1963.

[10] “J.D. Parsons. The mobile radio propagation channel, volume 81. Wiley Online Library, 2000. 19, 20, 21, 33, 65, 66, 87.”

[11] J. Medbo et al., “Radio propagation modeling for 5G mobile and wireless communications,” IEEE Commun. Mag., vol. 54, no. 6, pp. 144–151, Jun. 2016.

[12] P. Masek et al., “Experimental Evaluation of Dynamic Licensed Shared Access Operation in Live 3GPP LTE System,” in 2016 IEEE Global Communications Conference (GLOBECOM), 2016, pp. 1–6.

[13] J. M. Gorce, K. Jaffres-Runser, and G. de la Roche, “Deterministic Approach for Fast Simulations of Indoor Radio Wave Propagation,” IEEE Trans. Antennas Propag., vol. 55, no. 3, pp. 938–948, Mar. 2007

[14] M. Luo, G. Villemaud, J. M. Gorce, and J. Zhang, “Realistic prediction of BER for adaptive OFDM systems,” in 2013 7th European Conference on Antennas and Propagation (EuCAP), 2013, pp. 1504–1508.

[15] Antennas and propagation for wireless communication systems. Wiley.”2001

[16] “J. Keller. A geometrical theory of diffraction. Courant Institute of MathematicalSciences, New York University, 1958. 13.”

[17] A. Taflove, “Application of the Finite-Difference Time-Domain Method to Sinusoidal Steady-State Electromagnetic-Penetration Problems,” IEEE Trans. Electromagn. Compat., vol. EMC-22, no. 3, pp. 191–202, Aug. 1980.
[18] A. Rial. Applying the finite-difference time-domain to the modelling of large-scale radio channels. PhD thesis, University.
[19] “J. Maxwell. Xxv. on physical lines of force. The London, Edinburgh, and Dublin Philosophical Magazine and Journal of Sciences.” .
[20] K. Yee, “Numerical solution of initial boundary value problems involving maxwell’s equations in isotropic media,” IEEE Trans. Antennas Propag., vol. 14, no. 3, pp. 302–307, May 1966.
[21] “T.S. Rappaport. Wireless communications: principles and practice. PrenticeHall PTR New Jersey, 1996. 2, 4, 13, 17, 63.”
[22] “M.K. Simon and M.S. Alouini. Digital communication over fading channels,volume 86. Wiley-IEEE Press, 2004. 13, 17, 19, 3.
[23] COST Action. Digital Mobile Radio Towards Future Generation Systems:Final Report. Directorate General Telecommunications.”
[24] P. I. Lazaridis, S. Kasampalis, Z. D. Zaharis, J. P. Cosmas, L. Paunovska, and I. A. Glover, “Longley-Rice model precision in case of multiple diffracting obstacles,” in 2015 1st URSI Atlantic Radio Science Conference (URSI AT-RASC), 2015, pp. 1–1.
[25] M. A. Khalighi and M. Uysal, “Survey on Free Space Optical Communication: A Communication Theory Perspective,” IEEE Commun. Surv. Tutor., vol. 16, no. 4, pp. 2231–2258, Fourthquarter 2014
[26] J. Karedal et al., “Measurement-Based Modeling of Vehicle-to-Vehicle MIMO Channels,” in 2009 IEEE International Conference on Communications, 2009, pp. 1–6.
[27] J. W. Wallace and M. A. Jensen, “Time-Varying MIMO Channels: Measurement, Analysis, and Modeling,” IEEE Trans. Antennas Propag., vol. 54, no. 11, pp. 3265–3273, Nov. 2006
[28] D. S. Baum, J. Hansen, and J. Salo, “An interim channel model for beyond-3G systems: extending the 3GPP spatial channel model (SCM),” in 2005 IEEE 61st Vehicular Technology Conference, 2005, vol. 5, p. 3132–3136 Vol. 5.
[29] L. Zhang, Y. Zhu, and S. h Leung, “An Analytical Formula of Spatial Correlation Based on the Hierarchical Angle Structure for 3GPP Spatial Channel Model,” in 2013 IEEE 78th Vehicular Technology Conference (VTC Fall), 2013, pp. 1–5.
[30] S. Ma, D. Duran, H. Sharif, and Y. Yang, “An extension of the 3GPP spatial channel model in outdoor-to-indoor environments,” in 2009 3rd European Conference on Antennas and Propagation, 2009, pp. 1064–1068.
[31] E. A. Ibrahim, E. F. Badran, and M. R. M. Rizk, “An optimized LTE measurement handover procedure for high speed trains using WINNER II channel model,” in 2016 22nd Asia-Pacific Conference on Communications (APCC), 2016, pp. 197–203.
[32] M. Narandzic, C. Schneider, R. Thoma, T. Jamsa, P. Kyosti, and X. Zhao, “Comparison of SCM, SCME, and WINNER Channel Models,” in 2007 IEEE 65th Vehicular Technology Conference - VTC2007-Spring, 2007, pp. 413–417.

[33] C. J. Park, H. W. Moon, W. Kim, and Y. J. Yoon, “WINNER channel model with geometric optics and probability for indoor environment,” in 2014 International Symposium on Antennas and Propagation Conference Proceedings, 2014, pp. 253–254.

[34] C. Telecommunications and I. A. (CTIA), “CTIA test plan for mobile station over the air performance, Revision 2.2,” CTIA, Washington DC, Nov. 2006.

[35] P.-S. Kildal, C. Orlenius, and J. Carlsson, “OTA Testing in Multipath of Antennas and Wireless Devices With MIMO and OFDM,” Proc. IEEE, vol. 100, no. 7, pp. 2145–2157, Jul. 2012.

[36] P. KYÖSTI, J. P. Nuutinen, and J. Malm, Over-the-air test. Google Patents, 2011.

[37] W. Yu, Y. Qi, K. Liu, Y. Xu, and J. Fan, “Radiated Two-Stage Method for LTE MIMO User Equipment Performance Evaluation,” Electromagn. Compat. IEEE Trans. On, vol. 56, no. 6, pp. 1691–1696, Dec. 2014.

[38] 3GPP, “Technical Specification Group Radio Access Network Measurements of radio performances for UMTS terminals in speech mode(Release 7),” Jun. 2006.

[39] T. Sakata et al., “Experimental investigation of a dual-band handset MIMO antenna using a spatial fading emulator,” in Antennas and Propagation Society International Symposium (APSURSI), 2010 IEEE, 2010, pp. 1–4.

[40] 3GPP, “Verification of radiated multi-antenna reception performance of User Equipement,” Sep. 2013.

[41] A. Choumane, M. Mouhamadou, C. Decroze, D. Carsenat, and S. Liebus, “Creation of an isotropic multi-path propagation channel using SATIMO SG24 system,” in Proceedings of the 5th European Conference on Antennas and Propagation (EUCAP), 2011, pp. 1644–1645.

[42] A. Marín-Soler and D. A. Sánchez-Hernández, “New MIMO OTA figures of merit,” In 2012 6th European Conference on Antennas and Propagation (EUCAP), 2012, pp. 2123–2126.

[43] Y. Jing, H. Kong, and M. Rumney, “MIMO OTA test for a mobile station performance evaluation,” IEEE Instrum. Meas. Mag., vol. 19, no. 3, pp. 43–50, Jun. 2016.

[44] X. Carreno, W. Fan, J. Ø. Nielsen, J. S. Ashta, G. F. Pedersen, and M. B. Knudsen, “Test setup for anechoic room based MIMO OTA testing of LTE terminals,” in 2013 7th European Conference on Antennas and Propagation (EuCAP), 2013, pp. 1417–1420.

[45] J.E Hansen , “Spherical near-field antenna measurements”1988 Peter Peregrinus Limited.

[46] T. Laitinen, P. Kyosti, J.-P. Nuutinen, and P. Vainikainen, “On the number of OTA antenna elements for plane-wave synthesis in a MIMO-OTA test system involving a circular antenna array,” in Antennas and Propagation (EuCAP), 2010 Proceedings of the Fourth European Conference on, 2010, pp. 1–5.

[47] A. Khatun et al., “Experimental Verification of a Plane-Wave Field Synthesis Technique for MIMO OTA Antenna Testing,” IEEE Trans. Antennas Propag., vol. 64, no. 7, pp. 3141–3150, Jul. 2016.

[48] W. Fan, X. Carreño, J. Ø. Nielsen, K. Olesen, M. B. Knudsen, and G. F. Pedersen, “Measurement Verification of Plane Wave Synthesis Technique Based on Multi-Probe MIMO-OTA Setup,” in 2012 IEEE Vehicular Technology Conference (VTC Fall), 2012, pp. 1–5.

[49] W. A. T. Kotterman, A. Heuberger, and R. S. Thomä, “On the accuracy of synthesised wave-fields in MIMO-OTA set-ups,” in Proceedings of the 5th European Conference on Antennas and Propagation (EUCAP), 2011, pp. 2560–256.

[50] T. Laitinen, P. Kyösti, J. P. Nuutinen, and P. Vainikainen, “On the number of OTA antenna elements for plane-wave synthesis in a MIMO-OTA test system involving a circular antenna array,” in Proceedings of the Fourth European Conference on Antennas and Propagation, 2010, pp. 1–5.

[51] D. A. Hill, “A circular array for plane-wave synthesis,” IEEE Trans. Electromagn. Compat., vol. 30, no. 1, pp. 3–8, Feb. 1988.

[52] W. Fan, X. Carreño, J. Ø. Nielsen, J. S. Ashta, G. F. Pedersen, and M. B. Knudsen, “Verification of emulated channels in multi-probe based MIMO OTA testing setup,” in 2013 7th European Conference on Antennas and Propagation (EuCAP), 2013, pp. 97–101.

[53] W. Fan et al., “3D Channel Model Emulation in a MIMO OTA Setup,” in Vehicular Technology Conference (VTC Fall), 2013 IEEE 78th, 2013, pp. 1–5

[54] A. Glisson, “Spherical near-field antenna measurements, edited by J.E. Hansen,” Antennas Propag. Soc. Newsl. IEEE, vol. 31, no. 3, pp. 35–36, Jun. 1989.

[55] T. J. P. Kyosti and J.Nuutinen, “Channel Modelling for Multiprobe Over-the-Air MIMO Testing,” Int. J. Antennas Propag., 2012.

[56] W. Fan et al., “Probe Selection in Multiprobe OTA Setups,” Antennas Propag. IEEE Trans. On, vol. 62, no. 4, pp. 2109–2120, Apr. 2014.

[57] C. Schirmer, M. Lorenz, W. A. T. Kotterman, R. Perthold, M. H. Landmann, and G. D. Galdo, “MIMO over-the-air testing for electrically large objects in non-anechoic environments,” in 2016 10th European Conference on Antennas and Propagation(EuCAP), 2016, pp. 1–6.

[58] P. Hallbjörner, Z. Ying, M. Håkansson, C. Wingqvist, T. Anttila, and J. Welinder, “Multipath simulator for mobile terminal antenna characterisation,”Micro., Antennas Propag., vol. 4, no. 6, pp. 743-750, 2010.

[59] A. Khatun, T. Laitinen, V-M. Kolmonen, and P. Vainikainen, “Dependence of Error Level on the Number of Probes in Over-the-Air Multiprobe Test S tems,” International Journal of Antennas and Propagation, vol. 2012, 6 pages, 2012.

[60] P. Kyösti and L. Hentilä, “Criteria for physical dimensions of MIMO OTA multi-Probe test setup,” 6th European Conference on. in Antennas and Propagation (EUCAP), 2012 IEEE, 2012, pp. 2055–2059.

[61] M. Belhabib and R. D'Errico and B. Uguen ,"Effect of finite ring radius and antenna radiation on spatial correlation in multiprobe Over-The-Air Tests", IEEE,Eucap 2016.

[62] I-METRA, D2 (Feb. 1999) IST-1999-11729, MIMO channel characterisation.

[63] W. Dziunikowski, “Channels, propagation and antennas for mobile communications [book review],” Communications Magazine, IEEE,vol. 42, no. 6, pp. 38–38, June 2004

[64] A. Glisson, “Advanced engineering electromagnetics, by constantine a.balanis [book review],” Antennas and Propagation Society Newsletter, IEEE, vol. 31, no. 6, pp. 24–26, December 1989.

[65] W. Fan, F. Sun, J. Nielsen, X. Carreno, J. Ashta, M. Knudsen, and G. Pedersen, “Probe Selection in Multiprobe OTA Setups,” Transaction on Antennas and Propagation, IEEE vol. 62, no. 4, pp. 2109–212- April 2011.

[66] A. Ghosh, R. Ratasuk, B. Mondal, N. Mangalvedhe, and T. Thomas, LTE-Advanced: Next-Generation Wireless Broadband Technology [Invited Paper],” Wireless Communications, IEEE, vol. 17, no. 3, pp. 10–22,June 2010.

[67] D. Baum, J. Hansen, and J. Salo, “An interim channel model for beyond- 3G systems: extending the 3GPP spatial channel model (SCM),” in Vehicular Technology Conference, 2005. VTC 2005-Spring. 2005 IEEE 61st, vol. 5, May 2005, pp. 3132–3136 Vol. 5.

[68] L. Hentila, P. Kyosti, and J. Meinila, “Elevation extension for a geometry- based radio channel model and its influence on MIMO antenna correlation and gain imbalance,” Proceedings of the 5th European Conference in Antennas and Propagation (EUCAP), on April 2011, pp. 2175– 2179.

[69] P. Kyosti and A. Khatun, “Probe configurations for 3D MIMO Over-The Air testing,” 7th European Conference in Antennas and Propagation (EuCAP), 2013 on, April 2013, pp. 1421–1425.

[70] W. Fan, P. Kyosti, S. Fan, J. Nielsen, X. Carreno, G. Pedersen, and M. Knudsen,“3D Channel Model Emulation in a MIMO OTA Setup,” in Vehicular Technology Conference (VTC Fall), 2013 IEEE 78th, Sept 2013, pp. 1–5.

[71] M. Knudsen and G. Pedersen, “Spherical outdoor to indoor power spectrum model at the mobile terminal,” Selected Areas in Communications, IEEE Journal on, vol. 20, no. 6, pp. 1156–1169, Aug 2002.

[72] J. R. Shewchuk, “An introduction to the conjugate gradient method without the agonizing pain,” Tech. Rep., 1994.

[73] P. Kyosti and A. Khatun, “Probe configurations for 3D MIM Over-the- Air testing,” in Antennas and Propagation (EuCAP), 2013 7th European Conference on , April 2013, pp. 1421–1425.

[74] W. Fan, P. Kyosti, S. Fan, J. Nielsen, X. Carreno, G. Pedersen, and M. Knudsen, “3D Channel Model Emulation in a MIMO OTA Setup,” in Vehicular Technology Conference (VTC Fall), 2013 IEEE 78th, Sept 2013, pp. 1–5.

[75] Carreo, W. Fan, J. Nielsen, J. S. Ashta, G. F. Pedersen, and M. B,Knudsen,“Test setup for anechoic room based mimo ota testing of the terminals,” 7th European Conference in Antennas and Propagation (EuCAP), 2013 on , April 2013, pp. 1417–1420

[76] Ripley, B. D. (1981) Spatial Statistics. Wiley, 78-80 pp.41

[77] Le Rest, KÃľvin, David Pinaud, and Vincent Bretagnolle. "Accounting for spatial autocorrelation from model selection to statistical inference: Application to a national survey of a diurnal raptor." Ecological Informatics 14 (2013): 17-24

[78] Patuelli, Roberto, et al. "The use of spatial filtering techniques: the spatial and space-time structure of German unemployment data." Available at SSRN 893540.

[79] R.G. Vaughan, J. Bach Andersen, “Channels, Propagation and Antennas for Mobile Communications”, The institution of Electrical Engineers, Electromagnetic wave series 50, London, United Kingdom, 2003.
[80] CTIA “Test plan for mobile station over the air performance”, rev 2.2.2, December 2008.
[81] WINNER I: “Final Report on Link Level and System Level Channel Models,”Deliverable D5.4, v.1.4, 2005.
[82] WINNER II Channel Model Implementation (Matlab TM). http://projects.celtic Initiative.org/WINNER+
[83] 3D extension of the WIM2 Channel Model Implementation. Esa Kunnari. CWC, University of Oulu. https://bscw-winner.celtic-initiative.org/bscw/bscw.cgi/31264
[84] IST-WINNER II Deliverable 1.1.2 v.1.2, “WINNER II Channel Models”, IST-WINNER2 Tech. ., 2008 (http://projects.celtic-initiative.org/winner+/deliverables.html)
[85] 3GPP, “Measurement of radiated performance for MIMO and multi-antenna reception for HSPA and LTE terminals,” RP-090352, 2011.
[86] 3GPP, “Verification of radiated multi-antenna reception performance of UEs in LTE/UMTS,” RP-120368, 2012.
[87] P. Hallbjorner, J. D. Sanchez-Heredia, and M. Antonio, “Mode-stirred chamber sample selection technique applied to antenna correlation coefficient,” Hindawi IJAP Special Issueon MIMO OTA, 2012.
[88] 3GPP, “MIMO OTA way forward,” R4-122132, March 2012.
[89] A. Marin-Soler, G. Ypina-Garcia, A. Belda-Sanchiz et al.“MIMO throughput effectiveness for basic MIMO OTA complianc e testing,” Hindawi IJAP Special Issue on MIMO OTA,2012.
[90] M. A. Garc´ıa-Fern´andez, C. Decroze, D. Carsenat et al., “On the relationship between the distribution of the field amplitude,its maxima, and field uniformity inside a mode stirred reverberation chamber,” Hindawi IJAP Special Issue onMIMO OTA, 2012.
[91] N. Arsalane, M.Mouhamadou, C. Decroze et al., “3GPP channelmodel emulation with analysis of MIMO-LTE performancesin reverberation chamber,”Hindawi IJAP Special Issue on MIMO OTA, 2012.
[92] T. B. Hansen, “Correlation and capacity calculations with reference antennas in an isotropic environment,” Hindawi IJAP Special Issue on MIMO OTA, 2012.
[93] A. Khatun, T. Laitinen, V. M. Kolmonen et al., “Dependence of error level on the number of probes in over-the-air multi-probe test systems,” Hindawi IJAP Special Issue on MIMO OTA, 2012.
[94] P. Kyosti, T. J¨ams¨a, and J. P. Nuutinen, “Channel modelling for multi-probe over-the-air MIMO testing,” Hindawi IJAP Special Issue on MIMO OTA, 2012.
[95] Wei Fan, Fan Sun, Jesper Ø. Nielsen, Xavier Carreño, Jagjit S. Ashta, Mikael B. Knudsen and Gert F. Pedersen, “Probe Selection in Multi-probe OTA Setups,” IEEE Transactions on Antennas and Propagation, vol. 62, no. 4, pp. 2109–2120,April, 2014.

[96] Wei Fan, Jesper Ø. Nielsen, and Gert F. Pedersen, “Estimating Discrete Power Angular Spectra in Multi-probe OTA Setups,” IEEE Antennas and Wireless Propagation Letters, vol. 13, pp. 349–352, February, 2014.

[97] L. Hentila, P. Kyösti, and J. Meinila, “Elevation Extension for a geometry based radio channel model and its influence on MIMO antenna correlation and gain imbalance,” in Proc. of EuCAP 2011, Rome, Italy, April 2011.

[98] P. Kyösti and A. Khatun, “Probe Configurations for 3D MIMO Over-the-Air Testing,” in Proc. of EuCAP 2013, Gothenburg, Sweden, April,2013

[99] J. Nuckelt, T. Abbas, F. Tufvesson, C. F. Mecklenbr¨auker, L. Bernad´o, and T. Kurner, “Comparison of ray tracing and channel-sounder measurements for vehicular communications,” in Proc. IEEE 77 The Vehicular Technology Conference (VTC2013-Spring), Dresden, Germany, pp. 01–05, June 2013

[100] M. Nilsson, P. Hallbj orner, N. Araback, B. Bergqvist, and F. Tufvesson,“Multipath propagation simulator for V2X communication tests on cars,” in Proceedings of 7th European Conference on Antennas and Propagation (EuCAP), 8-12 April 2013, pp. 1342 – 1346.

[101] R. K. Sharma. W. Kotterman , M. H. Landmann , C. Schirmer , C. Schneider , F. Wollenschläger , G. Del Galdo M. A. Hein and R. S. Thomä, “Over-the-air testing of cognitive radio nodes in a virtual electromagnetic environment,” Int. J. Antennas Propagation. , vol. 2013.article 94528/ p. 16, 2013.

[102] M. Sonkki, V. Hovinen, and E. Salonen, “Probe Configurations for 3D MIMO Over-the-Air Testing,” in Antennas and Propagation (EUCAP), Proceedings of the 7th European Conference on. IEEE, 2013.

[103] O. Franek and G. Pedersen, “Spherical horn array for wideband propagation measurements, «Antennas and Propagation, IEEE Transactions on, vol. 59, no. 7, pp. 2654–2660, July 2011.

[104] IEEE Standard for Definitions of Terms for Antennas," IEEE Std 145-2013 (Revision of IEEE Std. 145-1993), vol., no., pp.1,50, March 6 2014.

[105] Laybros, S., and P. F. Combes. "On radiating-zone boundaries of short lambda/2 and lambda/dipoles." IEEE antennas and propagation magazine, vol. 46, No.5, Oct. 2004: pp. 53 - 64.

[106] A. Forenza, D. Love, and R. W. Heath, Jr., “Simplified spatial correlation models for clustered MIMO channels with different array configurations, IEEE Transactions on Vehicular Technology, vol. 56, no. 4, pp. 1924–1934, 2007.

Publications

- M.Belhabib, R. D'Erricco, B.Uguen « Dimensionnement d'un Banc de Test MIMO OTA et son Effet sur la Corrélation Spatiale, XIXème Journées Nationales Microondes, (JNM 2014), Bordeaux, 2015

- M.Belhabib, R. D'Erricco, B.Uguen « Spatial Correlation in Spherical and Cylindrical 3D MIMO Over-The-Air Tests Setups » 2016 10th European Conference on Antennas and Propagation (EuCAP), Davos, 2016

- M.Belhabib, R. D'Erricco, B.Uguen « « Effect of Finite Ring Radius and Antenna Radiation on Spatial Correlation in Mult-iprobe Over-The-Air Tests **»,** 2016 10th European Conference on Antennas and Propagation (EuCAP), Davos, 2016,
- M.Belhabib, R. D'Erricco, B.Uguen « A 3D Ultra-wide Band OTA test setups »,IEEE European Conferences in Antennas and Propagation **» »** 2017 11th European Conference on Antennas and Propagation (EUCAP), Paris, 2017

VU :
Le Directeur de Thèse
Uguen Bernard

VU
Le Responsable de l'École Doctorale

VU pour autorisation de soutenance

Rennes, le

Le Président de l'Université de Rennes 1

Guy CATHELINEAU

VU après soutenance pour autorisation de publication :

Le President de Jury,